

This is to certify that the

dissertation entitled

Repair of Corrosion-Damaged Columns Using FRP Wraps

presented by

Mohamad Imad Baiyasi

has been accepted towards fulfillment of the requirements for

Ph.D. degree in <u>Civil Engineering</u>

Major professor

Date June 2000

MSU is an Affirmative Action/Equal Opportunity Institution

0-12771



PLACE IN RETURN BOX to remove this checkout from your record.

TO AVOID FINES return on or before date due.

MAY BE RECALLED with earlier due date if requested.

DATE DUE	DATE DUE	DATE DUE
	-	
		-
		-

6/01 c:/CIRC/DateDue.p65-p.15

Repair of Corrosion-Damaged Columns Using FRP Wraps

By

Mohamad Imad Baiyasi

A Dissertation

Submitted to
Michigan State University
In partial fulfillment of the requirement
for the degree of

DOCTOR OF PHILOSOPHY

Department of Civil and Environmental Engineering

2000

Abstract

Repair of Corrosion-Damaged Columns Using FRP Wraps

Ву

Mohamad Imad Baiyasi

Many bridge columns in Michigan are damaged by chloride contamination resulting in the corrosion of the steel reinforcement, and swelling and spalling of the concrete and use of the bridges is typically continued. This in itself may not be a serious problem since most columns in Michigan are over-designed and the loss of strength is not a significant issue. However, the lack of any method to minimize or prevent corrosion of the steel results in continued deterioration and unsightly columns. Polymer composite (also known as fiber-reinforced polymer or FRP) jackets offer a possible remedy to this problem. They offer a rapid repair technique with the potential to enhance the long-term durability and compression strength of damaged columns due to the confinement that is provided when fibers are oriented in the hoop direction. Fibers oriented in the vertical direction can enhance the bending strength.

Experiments were conducted to assess the effects of using FRP wraps with fibers oriented in the hoop direction for rehabilitating corrosion-damaged columns. Issues that were explored are: (1) effect of freeze-thaw and wet-dry cycles on the properties of FRP panels; (2) freeze-thaw durability of concrete square and cylindrical specimens wrapped with glass and carbon FRP and subjected to an internal expansive force; and (3) effect of wrapping on the rate of corrosion in an accelerated corrosion test.

The results of the freeze-thaw experiment indicate that freeze-thaw cycles have no statistically significant effect on the compressive strength of glass and carbon wrapped specimens. For round specimens, glass and carbon wraps increased the strength by a factor of about 2.3 and 2.6, respectively. For square specimens, glass and carbon wraps increased the strength by a factor of 1.4-1.5. Freeze-thaw conditioning generally reduced the longitudinal failure strain of wrapped specimens.

The square wrapped specimens had lower compressive strength compared to the round specimens, even though the cross sectional area of the square prisms is higher than that of the round cylinders. This is due to the reduced confinement provided by the wraps for square cross sections and stress concentrations that develop at the corners. Wrapped square prisms always failed by rupture of the wrap at a corner. A reduction of approximately 30% to 40% in failure stress was noted between round and square wrapped specimens.

The results of the accelerated corrosion experiment indicate that wrapping reduced the corrosion depth in the reinforcing bars by 46% to 59% after 190 days of testing. Both glass and carbon wraps are equally effective in slowing down corrosion. Although unbonded wraps do reduce stress concentrations in the FRP, they are less effective in reducing the corrosion rate than the bonded wraps. It is postulated that this is due to the ingress of water along the unbonded FRP-concrete interface.

Wrap strains for bonded specimens with both types of wraps tend to level off with time indicating that corrosion slows down significantly after some time. One explanation could be that the stress concentration near the anodes in the bonded wraps is more effective in containing the corrosion-induced crack and reducing the corrosion rate. The

slip of unbonded wraps and the resulting redistribution of strain along the entire wrap may be less effective at containing the large corrosion-induced crack near the anodes. Dedicated to

my father, M. Fayez Baiyasi

Acknowledgements

The author would like to thank the following people:

Dr. R. Harichandran (Ron) for his support, guidance, and understanding. I am unable to find the words to express my gratitude. Thank you for everything.

Dr. P. Soroushian (CEE), Dr. L. Segerlind (AGE) and Dr. V. Zeidan (Math) for serving as Ph.D. guidance committee members.

Dr. G. Cloud (MSM Department) for providing the data acquisition system used in this work.

Dr. D. Liu (MSM Department) for allowing use of the impact machine used in this work.

Mr. J. Grove (MSU Radiology Department) for repeatedly taking X-rays of the concrete specimens and not complaining once. Thank you John.

Mr. Roger Till (MDOT) for his invaluable input and guidance.

Mr. John Janiszewski, student helper, (aka LB), I will remember your help and hard work always. Thanks a whole lot.

TABLE OF CONTENTS

CHAPTER 1: INTRODUCTION AND LITERATURE REVIEW

1.1	INTR	ODUCTION	1
1.2	PROJ	ECT OBJECTIVES	4
1.3	LITE	RATURE REVIEW	4
	1.3.1	Fiber Reinforced Polymers (FRP) for Infrastructure	4
		1.3.1.1 Fibers	
		1.3.1.2 Matrices	6
	1.3.2	Durability of Concrete	7
	1.3.3	Environmental Effects on FRP Composites	
	1.3.4	Corrosion of Reinforcing Steel	
		1.3.4.1 Factors Affecting Corrosion	
		1.3.4.2 Volume Expansion Due to Corrosion of Steel	
		1.3.4.3 Localized Corrosion	17
	1.3.5	Mechanical Properties of FRPs	
		1.3.5.1 Stress Corrosion and Stress Rupture	
	1.3.6	Effect of Confinement	
	1.3.7	Repair of Corrosion Damaged Columns Using FRP	
		R 2: DESCRIPTION OF EXPERIMENTS	
2.1		DRATORY TESTING	
	2.1.1	Stiffness and Strength of Glass and Carbon FRPs	
	2.1.2	Strain Expected in Wraps Due to Corrosion	
	2.1.3	Freeze-Thaw Test	
		2.1.3.1 Mold Fabrication	
		2.1.3.2 Bristar Calibration	
		2.1.3.3 Chloride Content	
		2.1.3.4 Strain Gage Placement	
		2.1.3.5 Compression Testing	
	2.1.4	Accelerated Corrosion	
		2.1.4.1 Corrosion Prior to Wrapping	
		2.1.4.2 Construction of the Corrosion Tank and Appurtenances	
		2.1.4.3 Monitoring Progress of Corrosion During Test	
		2.1.4.4 Corrosion Test Matrix	54
CHA	APTEF	R 3: DATA COLLECTION AND ANALYSIS OF RESU	JLTS
3.1		CT OF FREEZE-THAW AND WET-DRY CYCLING ON THE PERTIES OF FRP PANELS	56

3.2	FREEZE-THAW TEST	57
	3.2.1 Strain Gage Readings	57
	3.2.2 Results of Compression Testing	
	3.2.3 Statistical Analysis	
	3.2.4 Effect of Sustained Loads on Freeze-Thaw Durability of Wraps	88
	3.2.5 Comparison of Measured and Predicted Compression Strength	
3.3	ACCELERATED CORROSION	89
	3.3.1 Mass Loss Results	89
	3.3.2 Statistical Analysis	94
	3.3.3 Strain Measurements	96
CHA	APTER 4: SUMMARY, CONCLUSIONS, AND	
	RECOMMENDATIONS	
4.1	FREEZE-THAW TEST	102
4.2	ACCELERATED CORROSION TEST	104
4.3	RECOMMENDATION FOR FIELD INSTALLATION	105
4.4	COST SAVING OF USING FRP WRAPS	106
CH	APTER 5: FIELD INSTALLATION AND FUTURE STUDIES	i
5.1	FIELD INSTRUMENTATION	108
	5.1.1 Corrosion Monitoring of Field Columns	
	5.1.2 Results of Field Monitoring	
	5.1.2.1 Calculation of Corrosion Rate	
REF	FERENCES	114
API	PENDICES	
A DD	ENDIX A: Aerospace Corporation's FRP Panel Environmental Durability Da	to 110
	ENDIX B: Calculation Details	
/ 11 I I	B.1 Strain in Column Wrap After 10 Years	
	B.2 Confining Pressure and Strain in Steel Jacket	
APP	ENDIX C: Specimen, Bar and Gage Numbering	
	ENDIX C. Specificity, Dat and Gage Humbering	

LIST OF TABLES

Table 1.1	Capillary porosity of Portland cement paste as a function of	
	water/cement Ratio and the degree of hydration	8
Table 2.1	Vender recommended and measured wrap properties	31
Table 2.2	Volume expansion for some rust products	31
Table 2.3	Strain in column wrap due to steel corrosion after 10 years	32
Table 2.4	Freeze-thaw laboratory test matrix	34
Table 2.5	Internal pressure generated by corrosion for wrap strain of 0.531%	36
Table 2.6	Corrosion level required in two bars to induce a strain of	
	0.531% in the wrap	46
Table 2.7	Number of wrapped and unwrapped specimens in corrosion groups	48
Table 2.8	Accelerated corrosion laboratory test matrix	55
Table 3.1	Mean properties for FRP panels	57
Table 3.2	Ductility enhancement under compression for wrapped specimens	72
Table 3.3	Freeze-thaw summary data	82
Table 3.4	Results of hypothesis tests (95%) on specimens exposed to	
	freeze-thaw cycles	84
Table 3.5	Comparison of measured and predicted confined compression	
	strength	89
Table 3.6	Mass loss and average corrosion depth for specimens exposed to	
	130 days of accelerated corrosion	92
Table 3.7	Mass loss and average corrosion depth for specimens exposed to	
	190 days of accelerated corrosion	93
Table 3.8	Results of hypothesis tests (95%) on specimens exposed to	
	accelerated corrosion	95
Table 4.1	Estimated material and installation cost for Tyfo-S glass and	
	MBrace carbon wrap systems	
Table 4.2	Estimated total cost of different repair techniques over ten years	
Table 5.1	Initial weight of corrosion bars installed in field columns	109

LIST OF FIGURES

Fig. 1.1	Load vs. deflection curve for glass FRP composite specimens	
	subjected to 300 cycles of freezing and thawing	9
Fig. 1.2	Expansion and cracking of concrete due to corrosion of the embedded steel	16
Fig. 1.3	Reduction of tensile strength of E-glass fibers under sustained loads	18
Fig. 1.4	Stress/strain curves for confined and unconfined concrete	20
Fig. 1.5	Stress-strain curves for A36 steel, E-glass and carbon fibers	21
Fig. 1.6	Illustration of effectively confined area of a rectangular cross section	25
Fig. 2.1	Prism mold used for freeze-thaw test specimens	34
Fig. 2.2	Cylindrical mold used for freeze-thaw test specimens	35
Fig. 2.3	Strain in steel tube for water/Bristar ratio of 400g/1000g	37
Fig. 2.4	Strain in steel tube for water/Bristar ratio of 500g/1000g	37
Fig. 2.5	Strain measurement instrument and switch box	42
Fig. 2.6	Capping fixture	43
Fig. 2.7	New compressometer	43
Fig. 2.8	Wiring diagram for accelerated corrosion specimens	45
Fig. 2.9	Severely corroded specimens prior to patching	48
Fig. 2.10	Patching of the severely corroded specimens	49
Fig. 2.11	Corrosion tank	50
Fig. 2.12	Corrosion specimens in the tank	50
Fig. 2.13	Sample X-ray taken in the beginning of the accelerated corrosion test	52
Fig. 2.14	Sample X-ray taken after 90 days of accelerated corrosion test	53
Fig. 2.15	Sample X-ray taken after 105 days of accelerated corrosion test	53
Fig. 2.16	Reinforcing bars after removal from a corrosion specimen	54
Fig. 3.1	Hoop strains in glass wrap of round control specimen #3 before	
	correcting for thermal contraction of dummy FRP panel	59
Fig. 3.2	Hoop strains in glass wrap of square control specimen #7 before correcting for thermal contraction of dummy FRP panel	60
Fig. 3.3	Hoop strains in carbon wrap of round control specimen #11 before correcting for thermal contraction of dummy FRP panel	60

Fig. 3.4	Hoop strains in carbon wrap of square control specimen #15 before correcting for thermal contraction of dummy FRP panel
Fig. 3.5	Hoop strains in glass wrap of round specimen #1 during freeze-thaw cycles
Fig. 3.6	Hoop strains in glass wrap of round specimen #2 during freeze-thaw cycles
Fig. 3.7	Hoop strains in glass wrap of control round specimen #3
Fig. 3.8	Hoop strains in glass wrap, round specimen #4 during freeze-thaw cycles
Fig. 3.9	Hoop strains in glass wrap, square specimen #5 during freeze-thaw cycles
Fig. 3.10	Hoop strains in glass wrap, square specimen #6 during freeze-thaw cycles
Fig. 3.11	Hoop strains in glass wrap of control square specimen #7
Fig. 3.12	Hoop strains in glass wrap of square specimen #8 during freeze-thaw cycles
Fig. 3.13	Hoop strains in carbon wrap of round specimen #9 during freeze-thaw cycles
Fig. 3.14	Hoop strains in carbon wrap of round specimen #10 during freeze-thaw cycles
Fig. 3.15	Hoop strains in carbon wrap of control round specimen #1166
Fig. 3.16	Hoop strains in carbon wrap of round specimen #12 during freeze-thaw cycles
Fig. 3.17	Hoop strains in carbon wrap of square specimen #13 during freeze-thaw cycles
Fig. 3.18	Hoop strains in carbon wrap of square specimen #14 during freeze-thaw cycles
Fig. 3.19	Hoop strains in carbon wrap of control square specimen #1568
Fig. 3.20	Hoop strains in carbon wrap of square specimen #16 during
	freeze-thaw cycles
Fig. 3.21	Compressive stress-strain curves for plain, round, control specimens 73
Fig. 3.22	Compressive stress-strain curves for plain, round specimens
	subjected to 150 freeze-thaw cycles73
Fig. 3.23	Compressive stress-strain curves for plain, round specimens
	subjected to 300 freeze-thaw cycles74

Fig. 3.24	Compressive stress-strain curves and tensile hoop strain for glass-wrapped, round, control specimens
Fig. 3.25	Compressive stress-strain curves for glass-wrapped, round specimens subjected to 150 freeze-thaw cycles
Fig. 3.26	Compressive stress-strain curves and tensile hoop strain for glass-wrapped, round specimens subjected to 300 freeze-thaw cycles
Fig. 3.27	Compressive stress-strain curves and tensile hoop strain for glass-wrapped, square, control specimens
Fig. 3.28	Compressive stress-strain curves for glass-wrapped, square specimens subjected to 150 freeze-thaw cycles76
Fig. 3.29	Compressive stress-strain curves and tensile hoop strain for glass-wrapped, square specimens subjected to 300 freeze-thaw cycles77
Fig. 3.30	Compressive stress-strain curves and tensile hoop strain for carbon-wrapped, round, control specimens77
Fig. 3.31	Compressive stress-strain curves for carbon-wrapped, round specimens subjected to 150 freeze-thaw cycles
Fig. 3.32	Compressive stress-strain curves and tensile hoop strain for carbon-wrapped, round specimens subjected to 300 freeze-thaw cycles
Fig. 3.33	Compressive stress-strain curves and tensile hoop strain for carbon-wrapped, square, control specimens
Fig. 3.34	Compressive stress-strain curves for carbon-wrapped, square
	specimens subjected to 150 freeze-thaw cycles79
Fig. 3.35	Compressive stress-strain curves and tensile hoop strain for carbon-wrapped, square specimens subjected to 300 freeze-thaw cycles
Fig. 3.36	Failure modes for square specimens under compression testing80
Fig. 3.37	Failure modes for round specimens under compression testing81
Fig. 3.38	Average compressive strength of round glass-wrapped specimens 85
Fig. 3.39	Average compressive strength of round carbon-wrapped specimens 86
Fig. 3.40	Average compressive strength of square glass-wrapped specimens 86
Fig. 3.41	Average compressive strength of square carbon-wrapped specimens 87
Fig. 3.42	Average compressive strength of round plain specimens
Fig. 3.43	Average corrosion depths due to accelerated corrosion91
Fig. 3.44	Hoop strains in bonded, glass-wrapped specimens99
Fig. 3.45	Hoop strains in unbonded, glass-wrapped specimens99
Fig. 3.46	Hoop strains in bonded, carbon-wrapped specimens 100
Fig. 3.47	Hoop strains in unbonded, carbon-wrapped specimens 100

Fig. 3.48	Hoop strains in glass and carbon-wrapped specimens,				
	gages at the anodes	101			
Fig. 5.1	Column condition before surface repairs	110			
Fig. 5.2	Column condition after surface repairs	110			
Fig. 5.3	Corrosion probe and reinforcing bars for monitoring mass loss	111			
Fig. 5.4	Field installation of glass wrap to selected columns	111			
Fig. 5.5	Field installation of carbon wrap to selected columns	112			
Fig. 5.6	Completed installation of glass and carbon wraps	112			

Chapter 1 Introduction and Literature Review

1.1 Introduction

Retrofitting bridge columns with jackets encasing the concrete has been undertaken extensively in the West Coast, primarily for seismic rehabilitation. Steel jackets have been used for the most part, but are expensive to install and require several days for each column. The use of fiber reinforced polymers (FRP) wraps also has been developed and numerous columns have been retrofitted with different kinds of wraps. FRP wraps can be installed quickly (four to six columns per day), with minimal interruption to traffic flow. FRP wraps can be made of low-cost glass fiber, medium-cost aramid (also known as Kevlar) fiber, or high-cost high- performance carbon fiber, and polyester, vinyl ester or epoxy resins can be used as a matrix. Hexcel Fyfe Co. (Del Mar, Calif.) is the first composite fabricator to install a field demonstration with the California Department of Transportation, but other suppliers such as XXsys Technologies Inc., C. C. Myers Inc., Master Builders Inc., Mitsubishi Corporation, and Hardcore DuPont Composites L.L.C. also are performing field installations now.

The Pennsylvania Department of Transportation selected the Tyfo-S fiber wrap system (by Fyfe Company) for a concrete-column repair project on Interstate 84 in Scranton (Tarricone 1995). The New York State Department of Transportation used FRP wraps on six severely deteriorated concrete columns of the Court Street Bridge (Tioga County) in the summer of 1998 to protect against failures and to improve their durability in a cost effective manner. Six suppliers of FRP column wraps participated in this project

(Alampalli et al. 1999). In California numerous columns have been wrapped with the Tyfo-S fiber wrap system, and XXsys Technologies' filament winding for the bridges under the jurisdiction of the California Department of Transportation. This was done mainly for seismic strengthening. XXsys Technologies in conjunction with the Utah Department of Transportation used its composite wrapping system in 1996 to strengthen and extend the useful life of an existing bridge. The bridge has deteriorated from the effects of more than thirty years of corrosion of the steel reinforcing bars. Structural Preservation Systems of Baltimore, Maryland has used carbon wraps in 1997 to strengthen parking garage columns in Charleston, South Carolina.

While advanced composite materials are relatively expensive, labor costs are approximately 30% less than for conventional strengthening methods primarily because of the light weight of the materials. The quick turnaround and the reduced labor costs associated with FRP have reduced the overall cost making its use attractive for rehabilitation and strengthening of concrete infrastructure.

Four types of FRP jackets are currently available:

- Composite fabrics: The fabrics must be thoroughly saturated usually with two-part resin during installation and are cured at room temperature. The mechanical properties of the final product are somewhat variable. The Tyfo™ S Fiberwrap System by Fyfe Company is of this type.
- Prepregnated composite fabrics (Prepregs): Prepregs are pre-impregnated, usually with an epoxy resin, which results in good control over the mechanical properties of the final product. However, most prepregs must be stored in cold storage before installation, and need to be thermally cured after installation. For column

- applications, thermal curing can be achieved using heating blankets. There are few commercial carbon fiber prepregs, such as MBrace and REPLARK marketed by Master Builders and Mitsubishi respectively, that may be air cured.
- <u>Filament winding:</u> Jackets are produced by winding a continuous composite fiber
 onto the resin coated column. Typically automated winding equipment is used and the
 jacket is heat cured. XXsys Technolgies has retrofitted several columns in the West
 Coast using this technology.
- Precured shells: Precured jackets are formed around a mandrel of the diameter matching the column to be jacketed, typically using a multi-axial, stitched, nonwoven E-glass fiber fabric. The jackets have an axial slit that allows them to be opened and placed around a column for installation. Field crews install the jacket by first spraying a urethane adhesive onto the column. Two workers can then snap on a 132 kg, 1.2 m tall by 1.2 m diameter jacket segment. The adhesive and jacket installations are repeated to obtain three to five plies of composite, with the axial slit in each additional ply being staggered from that of the previous ply to avoid overlap. The whole multi-layer jacket system is bound to the column while the adhesive cures, creating an efficient, labor-saving system. As an alternative to the 360° bands, smaller arc segments can be installed by gluing each segment around the column with sufficient overlap. The smaller arc segments are easier to package and ship.

All of the jacketing systems described above are acceptable, and the advantage of one over another would depend on their performance in Michigan's harsh climate, their cost and their availability. Precured shells are presently available only for circular columns.

1.2 Project Objectives

The main objective of this project was to investigate the suitability of using glass and carbon FRP wraps to repair concrete columns damaged by corrosion in Michigan. The following issues were investigated:

- Strength loss of wrapped columns subjected to expansive forces, due to freezing and thawing.
- Strains in FRP wraps during freeze-thaw conditioning.
- Increased strength due to confinement provided by wraps.
- Magnitude of confining pressure generated by wraps due to corrosion.
- Localization of strains near reinforcing bars in wraps bonded to the concrete and the merit of using unbonded wraps.
- Reduction in corrosion rate due to the use of FRP wraps.

1.3 Literature Review

1.3.1 Fiber Reinforced Polymers (FRP) for Infrastructure

Newly developed composite materials have been used recently in civil engineering structures because of their superior mechanical properties as well as their resistance to aggressive environmental conditions. In general composites can be defined as a combination of two or more materials, that are insoluble into one another, without chemical interaction such that the properties of the combination is better than the individual constituents (De Wilde 1988). Fiber reinforced polymers are made of two constituent materials: polymer fibers and polymer matrices.

1.3.1.1 Fibers

Fibers have the largest volume and are the load-carrying element of FRP composites. Proper selection of the amount, type and orientation results in a composite with the desired mechanical properties.

- Glass fibers: These are widely used. Molten glass can be drawn into fine continuous filaments. These can be fabricated into continuous fibers, chopped strands, woven fabrics and milled fibers. The strength of glass fiber is highly dependent on the form in which the fibers are used. Continuous fibers have the highest strength and chopped fibers have the lowest strength. The average tensile strength for freshly drawn glass fibers may exceed 3500 MPa. Surface flaws tend to reduce this value to between 1750-2100 MPa. The internal structure of a glass fiber is a three dimensional network of different atoms. They behave in a linearly elastic manner until failure (Mallik 1993). Glass fibers are available in a variety of forms suited for different applications. The most common type is E-glass (which was initially developed for use in electrical applications). Other types of glass fibers that are used include S-glass (which has approximately 25% greater tensile strength than E-glass but is more expensive), Cglass (which was developed for application in corrosive environments), D-glass (which has lower density and dielectric constant than the other types of glass fibers), AR-glass (alkali resistant), and ECR-glass (modified E-glass which provides improved acid resistance).
- <u>Carbon and graphite fibers</u>: The difference between carbon and graphite is in the
 molecular structure. In carbon, the bonding between layers is weak, so it has twodimensional ordering. Graphite is formed from carbon atoms, which are arranged in

crystallographical parallel planes of regular hexagons. Carbon fibers are commercially available in three basic forms: long and continuous tow, chopped (6-50 mm long), and milled (30-300mm long). Carbon fiber can also be woven into two-dimensional fabrics of various styles. Graphite fibers are mainly considered in high strength composite applications. They show very high specific strength and stiffness. Graphite has a higher tensile modulus than carbon. Generally, as the modulus of elasticity increases, ultimate load and elongation decreases. Therefore, high modulus graphite fibers exhibit a lower strain at failure than high strength carbon. The tensile strength and the modulus of elasticity of graphite and carbon are not temperature dependent. These fibers behave elastically to failure and are highly resistant to aggressive environment. Their diameter is in the range of 5 to 10 microns.

Aramid fibers: Made from aromatic polyamides, these have the lowest specific
gravity and highest specific tensile strength among all type of fibers (Mallik 1993).
 Due to its high tensile strength and modulus of elasticity, aramid was the first organic
fiber to be used as a reinforcing fiber.

1.3.1.2 Matrices

The matrix is considered the secondary material in FRPs. Its major roles are transferring stresses between the fibers and protecting fibers against the environmental and mechanical conditions. The importance of the matrix in a composite is its effect on interlaminar and in-plane shear strengths. It also provides support against buckling of the fibers under compressive loads.

Polymer matrices are divided into two categories:

- Thermoplastic Polymers: Individual molecules are in a linear structural form. Weak secondary bond holds these molecules together. Heat or pressure temporarily breaks the bonds, which causes movement between the molecules. After cooling, the molecules set into their new position. Thermoplastics have higher impact strength, fracture and microcracking resistance compared to thermosetting polymers. Examples of thermoplastic polymers include nylon and polyethylene.
- Thermosetting Polymers: Also known as resin. The molecules are joined together by cross-links which leads to a more stable three-dimensional form that can not be reshaped by heat or pressure. Epoxy, polyester, and vinyl ester are the most common types of thermosetting polymers (Malek and Saadatmanesh 1996).

1.3.2 Durability of Concrete

Concrete is a porous material consisting of cement, water, fine and coarse aggregates and, possibly, admixtures. Cement and water react to form a hardened paste binding together the coarse and the fine aggregates. Voids are left in the originally waterfilled space between the cement grains, which are not filled with the hydration products of the chemical reactions. These voids are known as capillary pores. They range in size from approximately 5 nm to 1 mm. Capillary forces in such small volumes play an important role in the durability characteristics of concrete.

The capillary pore volume is a function of two parameters: the water/cement ratio of the paste, and degree of hydration of the cement (Pigeon and Pleau 1988). Table 1.1 gives the approximate capillary porosity of Portland cement paste as a function of the water/cement ratio and the degree of

hydration also have an influence on the average size of capillary pores. The average size decreases significantly with the degree of hydration, and the number of very large pores decreases significantly with lower water/cement ratios.

Table 1.1. Capillary porosity of Portland cement paste as a function of the water/cement ratio and the degree of hydration

the water/cement	ratio	and	tne	aegree	or n	yaration.
		\neg				

Water/cement ratio	Capillary Porosity (% volume)				
(by mass)	At 50% hydration	At 75% hydration			
0.4	31	18			
0.5	39	28			
0.6	46	36			

Cement paste also contains a significant volume of smaller pores that are called gel pores. The hydrants have a very large specific surface area, which is covered with a few layers of absorbed water. The gel pores correspond to the surface occupied by this absorbed water. Unless the temperature is high or the relative humidity is very low, the gel pores are always filled with water because the forces that bind water to the surfaces of the hydrates are strong.

When ice forms in the pores, a 9% increase in the volume of water takes place when water changes from liquid to solid. This volume expansion and the flow of water, as it is forced out of the pores, cause tensile stress to be generated in the paste. This is the basic cause of damage to concrete due to freezing.

When concrete is air entrained, which is achieved by adding admixtures to the mix, a very large number of closely spaced air voids develop. If these air voids are sufficiently close, the pressure generated by the flow of water out of the pores does not

cause any damage and water can freeze in these voids without generating internal pressures in the concrete (Pigeon and Pleau 1988).

1.3.3 Environmental Effects on FRP Composites

Environmental factors such as extreme temperature fluctuation and water absorption can adversely affect the behavior of some polymer composite material. Water absorption reduces the strength and stiffness of some polymeric composites by as much as 30%, compared to dry material. Water absorption breaks down the interface between the reinforcing fiber and resin matrix leading to loss of strength and rigidity. Cycles of freezing and thawing tend to magnify the effect of water absorption (Gomez and Casto 1996). The strength loss in glass FRP due to 300 cycles of freezing and thawing is depicted in Figure 1.1

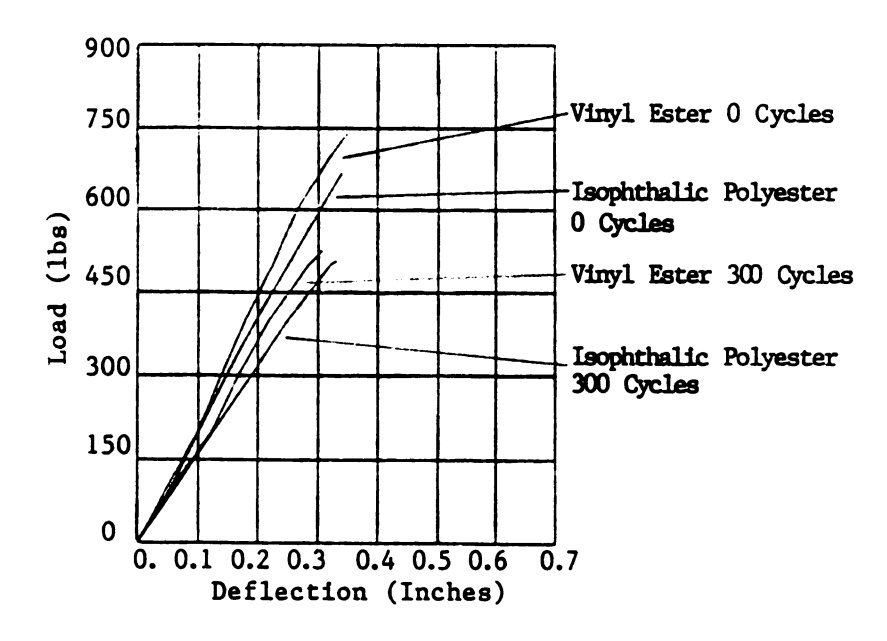


Figure 1.1 Load vs. deflection curve for glass FRP composite specimens subjected to 300 cycles of freezing and thawing (reproduced from Gomez and Casto 1996)

While several studies have been conducted on the strength of columns wrapped with FRPs, studies on durability under harsh environmental conditions such as freeze-thaw, exposure to chloride, and degradation from exposure to ultraviolet light are much fewer. Questions related to durability under harsh environmental conditions are extremely important in Michigan, and it is important to provide answers to these questions based on laboratory research prior to field installation.

Chajes et al. (1994) investigated the durability of several composite systems externally attached to concrete beams. One set of beams was exposed to cycles of freezing and thawing, the second set was exposed to cycles of wetting and drying, while the third set was unconditioned. Their results indicated that flexural strength was lost due to a degradation of the bond between the concrete and the external reinforcement.

Degradation of the composite material was not reported.

Sen et al. (1993) investigated the durability concrete beams pretensioned with glass/epoxy FRP subjected to cycles of wetting and drying. Several specimens were initially cracked to simulate pile-driving damage. Their results indicated extensive damage in the glass FRP, leading to an unacceptable level of strength loss.

Gomez and Casto (1996) studied the effect of chloride and freeze-thaw on two pultruded fiberglass all-composite systems. Both systems used glass fibers, but one used a vinyl ester resin while the other used a polyester resin. Samples were exposed to freeze-thaw cycles while immersed in a 2% sodium chloride and water solution. Their results indicated a loss of 22-32% in the flexural strength and stiffness of the composite materials.

Fyfe et al. (1996) studied the effect of prolonged (1000 hours) exposure of the Tyfo™ S System to ozone, salt water immersion, fresh water immersion, alkaline soil burial, high temperature, low temperature, and Weatherometer aging. All tests were performed according to ASTM standards, but only on the composite material, not on wrapped concrete specimens. In general, no serious degradation was observed due to prolonged exposure. However, a fundamental limitation of this study is that the environmental conditions were not cycled, and hence durability against cyclic freezethaw and chloride immersion cannot be assessed.

Toutanji and Balaguru (1998) studied the effect of wet-dry and freeze-thaw conditions on the performance of concrete columns wrapped with two layers of carbon and two layers of glass FRP composites. Three types of FRP wraps were used; two types of carbon and one glass. Twenty four concrete specimens (76 mm diameter and 305 mm long cylinders) were divided into three groups. Each goup consisted of eight specimens: six confined (two with each type of the FRP sheets) and two unconfined. The first group was used as virgin samples and the second was exposed to wet-dry cycling and the third group was exposed to freeze-thaw cycling. Three hundred wet-dry and freeze-thaw cycles were performed in a salt water solution. CFRP experienced no reduction in strength or ductility due to wet-dry exposure, whereas samples with GFRP experienced reduction of 10% and 20% in strength and ductility, respectively. In the case of freeze-thaw exposure, both CFRP and GFRP wrapped specimens experienced reductions in strength and ductility. Strength losses were 28% and 19% for glass and carbon, respectively. The specimens

subjected to freeze-thaw cycling also exihibited more catastrophic brittle failure as compared with the unconditioned and the wet-dry conditioned specimens.

Rivera and Karbhari (1999) conducted tests on concrete cylinders wrapped with glass and carbon FRP after subjecting them to 201 freeze-thaw cycles (between 22.5° C and -20° C). Three layers of carbon fabric and seven layers of glass fabric were used. Wrapped specimens subjected to freeze-thaw cycling showed increased stiffness and strength and more catastrophic failure compared to control specimens under ambient temperature. In order to isolate the effects of temperature from those of excessive moisture absorption, thawing was in air.

Murphy et al. (1999) investigated the effects of alkali exposure on the performance of glass fiber reinforced composites. Glass fiber reinforced vinylester coupons (two, four and six layers) were placed in solutions with pH and salt content predicted by leaching out the concrete itself, new concrete (28 days) and old concrete (ten years). In addition, a cementitious extract was prepared by collecting the solution that formed after settling of the aggregates (while preparing the new concrete). The starting pH level was approximately 12 and dropped to 8.5 in about 60-80 days for the new and old concrete solutions. For the cementitious extract solution, the pH dropped to 8.5 in about 250 days. The strength was degraded by 17 to 32% over a period of one year. The coupons placed in the cementitious extract was degraded the most (32%) indicating that reduction in strength cannot be attributed to pH levels alone, but rather to a combination of alkaline salts from concrete and the pH levels present.

Almusallam et al. (2000) conducted tests on concrete specimens wrapped with three layers of bi-directional glass FRP. Each group of specimens contained three GFRP

wrapped specimens and three unwrapped specimens. It was concluded that the compressive strength of wrapped cylinders subjected to alkaline solution and alkaline solution at elevated temperature (60 °C) exhibited lower increase in strength than the other groups. The increase in strength was about 23% compared to 54% for wrapped specimens at room temperature.

The Aerospace Corporation (Los Angeles, California) conducted extensive FRP panel durability testing on various wrap systems (Steckel 2000). For the glass and carbon systems used in this research study, they concluded that carbon panels are not affected by conditioning while glass panels showed strength and strain reduction of up to 35% and 15% - 20% under 10,000 hours of humidity and salt water (or alkaline solution) exposures, respectively. It should be noted that these conditions were not cycled. Only 20 freeze-thaw cycles were conducted and those had no effect on the FRP panels was noted. Appendix A shows the results obtained by of the Aerospace Corporation for glass and carbon FRP panels, respectively.

1.3.4 Corrosion of Reinforcing Steel

Corrosion is a natural process and is a result of the inherent tendency of metals to revert to their more stable compounds, usually oxides. Most metals are found in nature in the form of various chemical compounds called ores. In the refining process, energy is added to the ore, to produce the metal. It is this same energy that provides the driving force causing the metal to revert back to the more stable compound.

Corrosion of the reinforcement reduces strength, durability, and service life of the reinforced concrete structure. As the reinforcement corrodes, it expands causing cracking of concrete and spalling.

An ASTM-sponsored study (Guttman and Sereda 1968) found the corrosion rate in steel exposed to air at various locations varied from 0.033 to 0.058 mm per year in Cleveland to 0.030 to 0.043 mm per year in Ottawa. For a #25 bar, these translate to 5.3% to 9.1% in Cleveland and 5.0% to 6.7% in Ottawa in 10 years. Similar rates have been observed in Michigan steel bridges (McCrum 1994).

1.3.4.1 Factors Affecting Corrosion

The presence of chlorides, temperature, relative humidity, cover depth, and concrete quality are the major factors affecting the rate of corrosion.

Chlorides can come from several sources. They can be cast into the concrete to promote rapid hardening or they can diffuse from the outside. Chlorides can diffuse into concrete as a result of sea salt spray and deicing salt. Chloride contamination of bridge columns resulting from winter maintenance chloride (deicing salt) applications results in the continuing deterioration of the steel reinforcement, which in turn causes bursting forces emanating from the steel location outward to the periphery of the columns.

Minimum concrete cover and low quality of concrete (high water/cement ratio) decrease the time needed for chlorides to reach the reinforcement. The time for corrosion to start will therefore be decreased and the rate of corrosion will increase (Allen 1995).

Environmental conditions such as ambient temperature and relative humidity also affect corrosion. The concentration of free chloride ions in the pore water increases with

temperature. In addition, corrosion reactions occur at a much faster rate with an increase in temperature. The corrosion rate of steel was found to vary linearly with temperature. The corrosion rates at 40°C was found to be almost double that at 0°C (Lopez et al 1993).

Concrete is alkaline. It contains microscopic pores with high concentrations of soluble calcium, sodium and potassium oxides. These oxides form hydroxides, which are highly alkaline when water is added. This alkaline condition leads to a passive layer forming on the steel surface in the form of a dense, impenetrable film, which if fully established and maintained, prevents further corrosion of the steel. Chlorides act as catalysts to promote corrosion. When there is sufficent chloride concentration at the reinforcing bar surface to break down the passive layer of oxide on the steel, the corrosion process proceeds quickly.

Brockenbrough et al. (1985) conducted tests on stacks of Cor-Ten A steel and carbon steel compressed together with spring washers and exposed (to the atmosphere) at Monroeville, Pennsylvania and Kure Beach, North Carolina. The stacks clamped at low pressures (21.5 and 43.5 kPa) showed large increase in thickness because of corrosion product pressure after five and a half years of exposure. In addition, it was concluded that there is an initial pressure threshold of about 1035 to 1380 kPa above which the rate of corrosion is extremely small and no significant expansion due to corrosion product pressure takes place.

1.3.4.2 Volume Expansion Due to Corrosion of Steel

Corrosion of steel is an electrochemical process. The electrochemical potentials to form the corrosion cells may be generated when cells are formed due to differences in concentration of dissolved ion in the vicinity of steel, such as alkalies, chlorides, and oxygen. As a result, some parts of the metal become anodic and the others cathodic. The fundamental chemical changes occurring at the anodic and cathodic areas are as follows (see Fig. 1.2-a).

Anode: Fe \rightarrow 2e $\dot{}$ + Fe $^{2+}$

Cathode: $\frac{1}{2} O_2 + H_2 O + 2 e^- \rightarrow 2 (OH)^-$

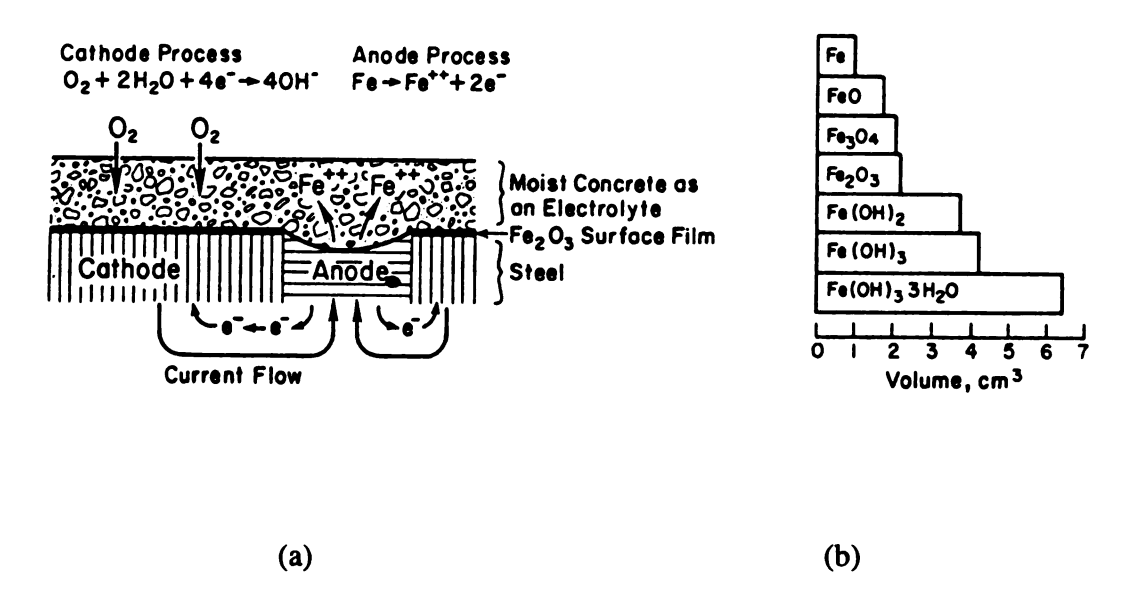


Figure 1.2. Expansion and cracking of concrete due to corrosion of the embedded steel (reproduced from Mehta 1996)

The transformation of metallic iron to rust can result in increases in volume of up to 600% (Mehta 1996), depending on the final rust form (see Fig. 1.2-b). Since the presence of both air and water is required for the corrosion activity to continue, column wrapping may provide adequate confinement that would minimize the entry of air and water, thereby slowing down the continuation of corrosion.

1.3.4.3 Localized Corrosion

Corrosion of steel reinforcement inside bridge columns is not uniform. It is dependent on the location of cracks and surface exposure (i.e. salt contact due to deicing of roads). Further, the volume expansion due to corrosion is localized near the reinforcement bars. This may exert strains on the wrap at localized areas. All or most of the metal loss occurs at discrete areas (www.Corrosionsource.com 2000).

Pitting corrosion is highly localized corrosion occurring on a metal surface.

Pitting is commonly observed on surfaces with little or no general corrosion.

Pitting typically occurs as a process of local anodic dissolution where metal loss is exacerbated by the presence of a small anode and a large cathode.

Crevice corrosion is another form of localized corrosion which may occur in small areas of stagnant solution in crevices, joints and under corrosion deposits. Crevice corrosion is the localized corrosive attack that occurs as a result of the occluded cell that forms under a crevice on the metal surface. To prevent this type of corrosion, it is recommended that crevices be closed with non-absorbent materials or a barrier to prevent moisture penetration into the crevice be incorporated.

1.3.5 Mechanical Properties of FRPs

Many FRPs have tensile strengths that exceed the strength of steel, but their stiffness is generally lower than that of steel. When loaded along the fiber direction they behave essentially linearly until fracture, and are therefore brittle by nature.

1.3.5.1 Stress Corrosion and Stress Rupture

The average ultimate tensile strength of freshly drawn glass fibers may exceed 3500 MPa. However, surface flaws tend to reduce the tensile strength to values in the range of 1750 to 2100 MPa. Strength degradation is increased as the surface flaws grow under cyclic loads. This is one of the major disadvantages of using glass fibers in applications where fatigue may be an issue. Sustained loads also cause surface flaws to grow, resulting in reduced tensile strength. Figure 1.3 shows reduction of strength with time for E-glass fiber under different temperatures.

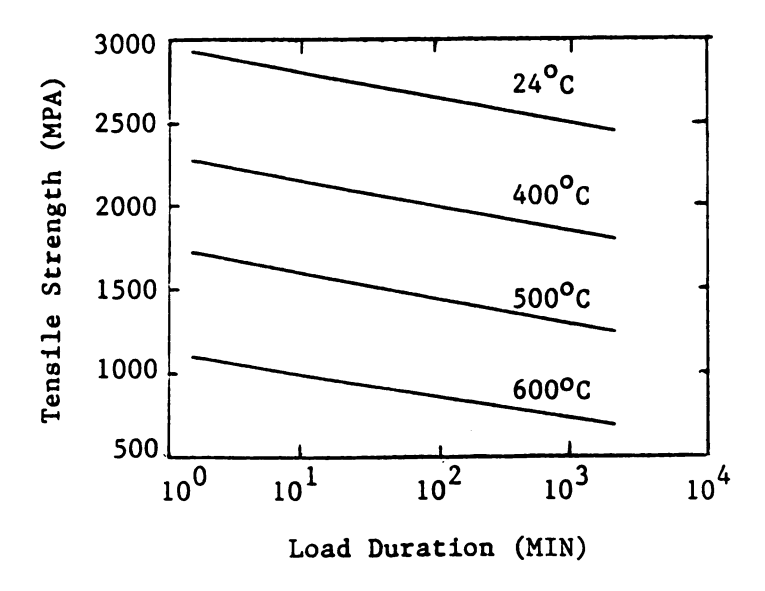


Figure 1.3 Reduction of tensile strength of E-glass fibers under sustained loads (taken from Mallick 1993)

Stress corrosion refers to the characteristic property of FRPs in which the failure strength under long term sustained loads in a chemical environment is lower than its short term tensile strength. In air, this phenomenon is referred to as "stress rupture" (Sen et al. 1993). Stress rupture tests are usually performed by applying a constant tensile stress to a specimen until it fractures completely. The time at which fracture occurs is termed the "lifetime". Creep, on the other hand, is defined as the increase in strain with time at a constant load level (Mallick 1993).

Glass, Aramid, and Boron fibers and their composites exhibit failure by stress rupture. Carbon fibers, on the other hand, are relatively less prone to stress rupture failure. In order to prevent stress rupture in glass FRP for a period of 10, 30, and 50 years, the sustained strains in the GFRP should be less than about $0.35 \, \varepsilon_u$, $0.32 \, \varepsilon_u$, $0.30 \, \varepsilon_u$, respectively (Sen et al.1993, ACI 2000).

The relationship between the sustained stress (or strain) and the logarithm of time is approximately linear as shown in figure xx. ACI Committee 440R recommends the use of a safety factor of 1.67 and hence a safe level of sustained strain to prevent stress rupture is about $0.2 \, \epsilon_u$.

1.3.6 Effect of Confinement

Lateral confining pressure increases the strength and ductility of concrete in the axial direction. The stress-strain curves of confined concrete show a remarkable energy dissipation characteristic. Such behavior is of great importance as it can prevent catastrophic failure of highway bridges or high-rise buildings under overload conditions. Figure 1.4 shows stress-strain curves for confined and unconfined concrete.

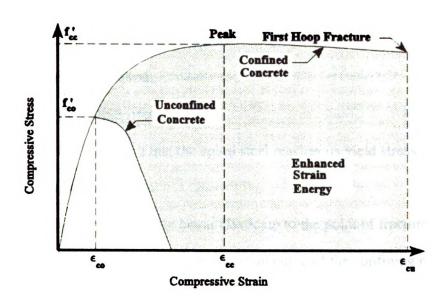


Figure 1.4 Stress/strain curves for confined and unconfined concrete (Mander, et al.1988)

The relationship between confined compressive strength (f_{cc}) , unconfined compressive strength (f_{cc}) , and the lateral stress in core concrete produced by confining pressure (f_t) is

$$f_{cc} = f_c + k f_r \tag{1.1}$$

The average value of the confinement effectiveness coefficient k was found to be equal to 4.1 (Richart, et al. 1928).

For circular column with spiral steel, the confining pressure f_r is given by (Nilson and Winter 1991)

$$f_r = \frac{2A_{xp}f_y}{d.S} \tag{1.2}$$

where

 A_{sp} = the cross-sectional area of the spiral steel

 d_c = the outside diameter of the spiral

S = the pitch of the spiral.

 f_y = spiral steel yield stress

Eq. (1.2) is calculated assuming that the spiral steel reaches its yield stress f_y before the column eventually fails.

FRP materials are essentially linear elastic up to the point of fracture, while steel shows an elastic-plastic behavior. The stress-strain curve of the confining materials affects the failure mode of the confined core. Figure 1.5 shows stress-strain curves for A36 steel, E-glass and carbon fibers.

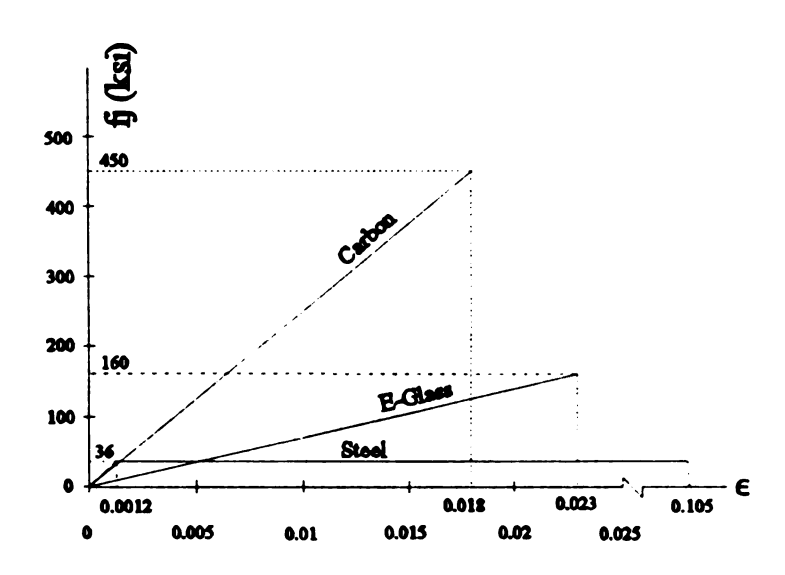


Figure 1.5 Stress-strain curves for A36 steel, E-glass and carbon fibers

Confinement of concrete columns with FRP wraps offers many advantages in comparison to other confinement methods. Composite material with their high strength and high stiffness to density ratios allow for field installation with minimal workforce and disruptions to traffic. Preliminary testing of concrete columns wrapped with FRPs has shown that the confinement provided results in improved compressive strength and ductility. Picher at el. (1996) conducted a series of tests on confined circular, square and rectangular concrete specimens. Axial loads were applied to concrete specimens wrapped with different orientation of carbon FRP wraps. It was concluded that confinement of concrete cylinders with CFRP wraps improves their compressive strength and ductility (up to 41% axial strength increase and about 500% axial strain increase for cylinders confined with three layers of carbon sheets with fibers oriented in the hoop direction) compared to unconfined specimens. Although axial stiffness decreases with the increase of fiber angle orientation, ductility and modes of failure remain the same. Wrapping of square and rectangular specimens improves ductility but to a lesser degree than that observed for cylindrical specimens. In the case of square and rectangular specimens, it was found that rounding the corners greatly improved the compressive strength.

Tests on round and rectangular specimens and full scale columns wrapped with glass and carbon FRPs was conducted by Kestner at el. (1997). They found that enhancement in axial strength and deformation are proportional to jacket strength and stiffness. It was found that due to the ineffectively confined concrete region in the square cross sections, the jackets provided to square cross sections were not as effective as those provided to circular cross sections. A shape factor, κ_s , was used to account for the

ineffectively confined regions of concrete within the rectangular and square cross sections.

From mechanics of thin walled cylinders, the confining pressure in a confined column can be determined to be

$$f_r = 2 (f_t t n) / D$$
 (1.3)

where

t = the thickness of the wrap per layer

 f_t = the circumferential stress of wrap

n =number of wrap layers

D = the diameter of the concrete cylindrical column

The maximum confining pressure, f_{ru} is determined by the ultimate tensile strength of the wrap f_{tu} given by

$$f_{ru} = 2 (f_{tu} t n) / D = 2 (E \varepsilon_{tu} t n) / D$$
 (1.4)

where

E =modulus of elasticity of the wrap

 ε_{tu} = wrap ultimate strain

Substituting f_{ru} from Eq. (1.4) into Eq. (1.1) yields the maximum compressive strength due to confinement with FRP wraps.

More generally, for round and rectangular cross sections, the maximum confining pressure may be expressed as (Restrepol and DeVino 1996)

$$f_{ru} = 0.5 \kappa_s \rho_i E \varepsilon_{tu} t \tag{1.5}$$

where

 $\rho_i = 4n/D$ for circular columns

 $\rho_i = 2n(d+b)/db$ for rectangular columns

n = number of layers of wrap

D =overall diameter of circular column

b =overall width of rectangular column

d =overall depth of rectangular column

 κ_s = shape factor determined as the ratio of effectively confined concrete to the gross area of the section

The shape factors for circular and rectangular are

Circular: $\kappa_s = 1$

Rectangular: $\kappa_s = \frac{1 - [(b - 2r)^2 + (d - 2r)^2] - \rho}{1 - \rho}$

where

r = radius of rounded corners

 ρ = longitudinal reinforcement ratio of cross section

Fig. 1.6 shows the effectively confined area of a rectangular cross section.

For circular columns, substituting $\kappa_s = 1$ in Eq. (1.5) will yield Equation (1.4), while for rectangular columns

$$f_{ru} = \kappa_s n E \varepsilon_{ru} t (d+b)/db$$
 (1.6)

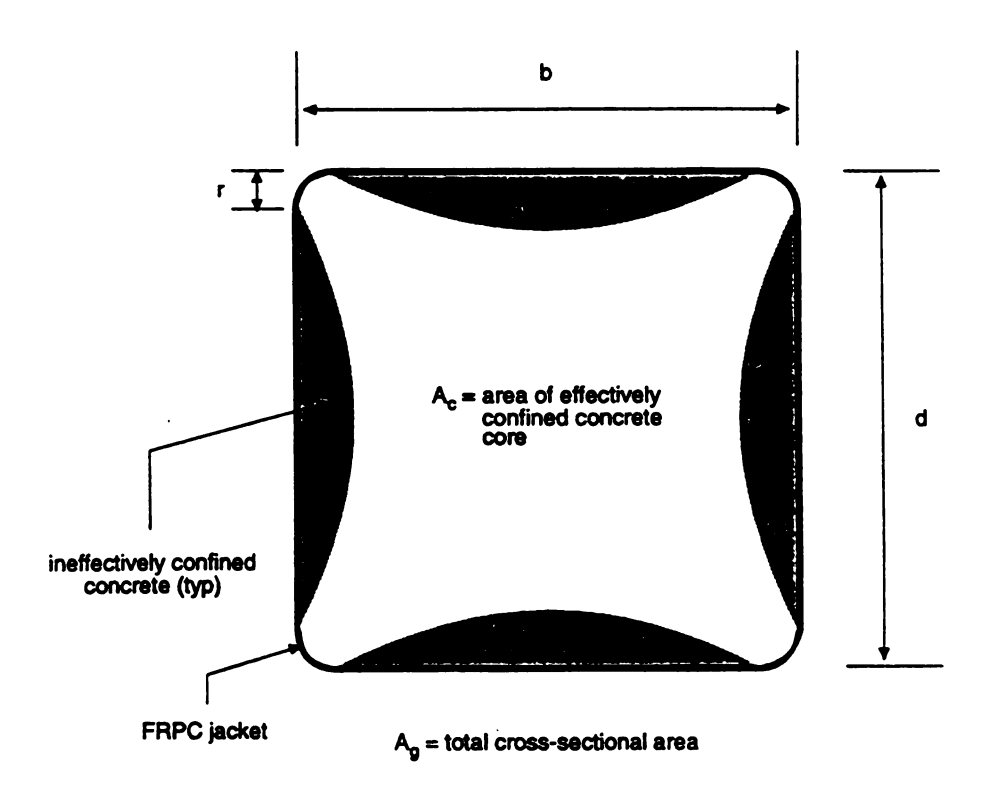


Fig. 1.6 Illustration of effectively confined area of a rectangular cross section

1.3.7 Repair of Corrosion-Damaged Columns Using FRP

A review of research conducted to study the effectiveness of FRP wraps in repairing corrosion-damaged columns indicates that FRP wraps have the following advantages:

- They provide a barrier to oxygen, moisture and chlorides.
- They have high strength and stiffness and provide confinement and ductility to the concrete structure.

Debaiky and Green (1999) are investigating the suitability of using FRP wrap to rehabilitate corroded concrete structures. The focus of the experiment is to assess what

happens to the corrosion process after the structure has been rehabilitated with FRP wraps. The experiment consists of 12 reinforced concrete columns (300x 1200 mm) with chlorides cast in the concrete cover. The columns are placed in a water bath to initiate corrosion. After the initial corrosion phase, the columns will be wrapped with FRP sheets. The "natural" accelerated corrosion environment will then be continued. Monitoring corrosion will be through the use of a half-cell potential. This project is still underway.

Pantazopoulou et al. (1996), Michniewicz (1996), and Lee (1998) from the University of Toronto conducted several projects using FRP for repair of corrosion damaged columns since 1993.

Two concrete mixes were used to construct the 150x300 mm cylinders. High density concrete was used for the end caps, and high porosity concrete contaminated with 2.6% NaCl by weight of cement was used for the middle 210 mm of the cylinder height. The corrosion was electrically accelerated using a 6 volt potential while the cylinders were placed in 50 mm of 2% chloride solution. Damage was significant after 150 days. Several repair techniques were considered such as conventional patching, epoxy coating and wrapping with plastic foil. In addition, glass FRP wrap also was used. The most effective repair method was the use of a conventional patch with two layers of glass FRP (GFRP) wrap. The strength was fully restored and ductility was doubled compared with an undamaged specimen.

Ten large-scale circular columns also were built and corrosion was accelerated in a similar manner (voltage ranged from 3 to 15V). The columns were repaired using different methods ranging from:

- Surface cleaning, non shrinkage grout, epoxy coat, and 2 layers of GFRP wrap to
- Epoxy coat and 2 layers of GFRP wrap only.

Compression tests results showed only columns that were repaired using the first method, surface cleaning, non shrinkage grout, epoxy coat, and 2 layers of GFRP wrap, had the capacity of an undamaged column.

Another project was also conducted at the University of Toronto. Seven large scale columns were corroded using a 12 V fixed potential and wet-dry cycles consisting of one day wet and 2.5 days dry. After significant corrosion, they were wrapped with one layer of carbon FRP (CFRP) sheet. The results showed that using the CFRP wrap increased the strength of the corroded specimens by 28% compared to the unwrapped specimens. The axial deformation at failure was six times that of corroded unrepaired specimens.

It should mentioned that the above research projects conducted at the University of Toronto did not investigate the effect of continuing corrosion on the FRP rehabilitation.

At the University of Sherbrooke, the following field applications have been conducted (Rochette et al. 1996, Demers et al. 1996, and Kenneth et al. 1998):

- Corrosion-damaged circular building columns were repaired with GFRP after the
 column section was restored with cement grout. The repair took place in November
 1995, the resin cured properly despite the cold temperature.
- Eighteen (18) circular bridge columns were repaired in August 1996. Five columns were wrapped with GFRP, four with CFRP, and three were repaired using

conventional material. Axial deformation and circumferential expansion were monitored.

• The concrete pier on the Champlain bridge in Montreal was repaired in 1997. The pier received nine layers of GRFP wrap in the four meters above its base.

The University of Minnesota is currently monitoring the rehabilitation of corrosion-damaged columns for a bridge near Minneapolis (Debaiky and Green 1999).

The set up is as follows:

- Electrochemical chloride extraction (ECE) was used on three columns and then one
 column was wrapped with CFRP sheets (supplied by Hexcel-Fyfe Company), the
 second was wrapped with CFRP sheets (supplied by Tonen Corporation), and the
 third was wrapped with chopped glass sheets.
- ECE was used on three columns and were then sealed without wrapping.
- Three columns were wrapped similar to the first group without the ECE.
- Three columns were left as control specimens.

Corrosion will be monitored for five years. Chloride sampling will be conducted once a year. This project started in 1997 and is still underway.

In order to study the deterioration and evaluate different repair techniques, an FRP column wrap project was initiated by the New York State Department of Transportation in 1998 (Halstead et al. 2000). Six severely deteriorated concrete columns of the Court Street Bridge (Tioga County) were wrapped using six different wrap systems (by different suppliers). A comprehensive testing program to evaluate the effectiveness of FRP column wrapping was implemented. Prior to installation of the FRP wraps, three corrosion probes were embedded in each column. Additional monitoring equipment was

installed on each column and data collection started in September 1998. Strain sensors were installed on the surface to measure the effect of continued corrosion on the wraps. Concrete humidity and temperature are also being monitored. The corrosion probes use linear polarization to monitor instantaneous corrosion rates. Data is being collected at three month intervals. This non-destructive testing is scheduled to continue for five years.

.

Chapter 2 Description of Experiments

2.1 Laboratory Testing

2.1.1 Stiffness and Strength of Glass and Carbon FRPs

A 4-ply composite Tyfo-S fiber glass/epoxy sheet and a 2-ply Tonen carbon/epoxy sheet were fabricated at MSU on 9/30/97 and 10/21/97 under the supervision of the respective composite vendors. After the vendor-recommended curing periods of five to seven days, these specimens were tested under direct tension at the MSU Composite Material and Structures Center to check the moduli against the vendor-recommended values. Table 2.1 shows a comparison between actual tested and recommended moduli, thickness, effective axial stiffness per unit width (equal to modulus x thickness) and ultimate strain. Although the thickness and the moduli varied from the vender recommended values, especially for carbon, the effective axial stiffnesses which control confinement and behavior were within 96% and 88% of the recommended values for glass and carbon FRPs, respectively. Master Builders specify the thickness and modulus of their carbon FRP based on the fiber properties only which is why their values differ significantly from the measured values.

Table 2.1 Vendor recommended and measured wrap properties

Wrap Type	Thickness (mm)	Modulus (MPa)	Effective Stiffness (N/mm)	Ultimate Strain		
		Vendor Recommendations				
Glass	1.016	27600	28042	.02		
Carbon	0.165	227700	37590	.015		
	As Measured					
Glass	1.227	22011	27000	.020		
Carbon	0.625	53061	33150	.014		

2.1.2 Strain Expected in Wraps Due to Corrosion

The transformation of metallic iron to rust can result in increases in volume of up to 600% (Mehta 1996), depending on the final rust form. (Table 2.2 shows sample calculations for the volume expansion for some rust products.)

Rust Forms: FeO, Fe₃O₄, Fe₂O₃, Fe(OH)₂, Fe(OH)₃, Fe(OH)₃ 3H₂O

Table 2.2. Volume expansion for some rust products

Rust Form	Density (D)	Mol.Wt.	Volume(MW/D)	Vol.Rust/Vol.Fe
Fe	7.86	56	7.12	
FeO	5.7	71.85	12.6	12.6/7.12=1.7
Fe ₃ O ₄	5.18	231.54	44.70	44.7/(3x7.12) = 2
Fe(OH) ₂	3.4	89.86	26.43	26.43/7.12=3.71

Table 2.3 shows the strain developed in the wrap due to corrosion in a 915 mm diameter column with longitudinal steel ratios of 3%, 2%, and 1%, and ties spaced at 152 mm and 305 mm. Corrosion rates by cross section of 5% in the longitudinal reinforcement and 20% in the lateral reinforcement over a 10 year period are assumed (Martin and Schieles 1969). For cases one and two it is assumed that the volume of rust is three times and six times, respectively, the volume of the corroded steel. The table shows

that the strain in the wrap is within 0.30 $\varepsilon_u = 0.6\%$ for GFRP (which is the sustained strain limit in order to prevent stress rupture in glass FRP for a period of 50 years) for all situations considered, indicating that stress rupture should not be a problem. If carbon FRP is used, then stress rupture is not an issue and the strains in Table 2.3 are below the rupture strain of $\varepsilon_u = 1.5\%$. Hence the use of CFRP is also feasible.

Table 2.3 Strain in column wrap due to steel corrosion after 10 years

Column	Spacing of	Steel ratio of	Strain in wrap			
dia. (mm)	tie (mm)	cross section	Case 1	Case 2		
#13 tie						
915		3%	0.394%	0.450%		
	305	2%	0.260%	0.327%*		
		1%	0.145%	0.203%		
		3%	0.414%	0.530%		
	152	2%	0.290%	0.410%		
		1%	0.160%	0.284%		

Sample calculation for this row is shown in Appendix B.1.

2.1.3 Freeze-Thaw Test

Strength and durability tests were carried out on wrapped circular (diameter of 152 mm by 305 mm high) and square cylinders (152 mm by 152 mm by 305 mm high). The primary purpose of the tests was to determine the endurance of the jackets under simulated cyclic environmental conditions, with strength considerations being secondary. An internal bursting force similar to that produced by corroding steel was induced. This was done by fabricating cylinders with a hole in the longitudinal direction and filling it with an expanding cement known as Bristar (used for silent demolition). Chloride was impregnated into the cylinders during casting in order to simulate deteriorated concrete

(11 kg of NaCl/m² was used). Strength tests were carried out on plain control cylinders as well as wrapped test specimens before and after freeze-thaw conditioning.

Climate data for Lansing, Michigan indicates that there were 58 days in the 1993/1994 year when the temperature cycled above and below 32° F and 78 days for the 1992/1993 year. Based on this and ASTM C666 specifications, 150 and 300 freeze/thaw cycles were used in the freeze-thaw conditioning. Subsequent to freeze/thaw cycles, the compressive strengths were compared against those of wrapped control specimens that were not subjected to freeze-thaw cycles. In addition, unwrapped plain concrete specimens also were exposed to freeze-thaw cycles to establish loss of strength in concrete alone due to freeze/thaw conditioning.

Table 2.4 shows the test matrix used for the freeze/thaw laboratory testing. A total of 60 specimens were involved in the testing, of which 30 were subjected to freeze/thaw. Specimen and gage numbering is shown in Table C.1 in Appendix C. A water/cement ratio of 0.4 was used; the 28-day strength for the freeze-thaw specimens was 37700 kPa.

A half bridge configuration was used for reading the strain gages, and temperature correction was done by using dummy gages mounted on glass and carbon FRP panels which also were located in the freeze-thaw machine. However, thermal contraction and expansion of the FRP panels on which the dummy gages were mounted had to be determined and compensated for. The dummy gages also were used when reading strains on control specimens not subjected to freeze-thaw.

Table 2.4 Freeze-thaw laboratory testing matrix

		No. of Specimens		
Specimen Type	Conditioning	ditioning Unwrapped		Carbon Wrap
Round	None	3	3	3
Square	None		3	3
Round	None	3	3	3
Square	None		3	3
Round	150 cycles of freeze-thaw	3	3	3
Square	150 cycles of freeze-thaw		3	3
Round	300 cycles of freeze-thaw	3	3	3
Square	300 cycles of freeze-thaw		3	3

2.1.3.1 Mold Fabrication

Prism molds

Nine 152 mm x 152 mm x 305 mm PVC molds were fabricated. Each is composed of five panels (four sides and one bottom). The short side panels were fabricated with a center hole that was 38 mm in diameter. A 38 mm steel rod was placed in the hole during casting. Dow Corning release agent was applied to the steel rod and a plastic sheet was then wrapped around it to aid removal after the concrete sets. The center hole was later filled with Bristar (a form of an expanding grout). Fig. 2.1 provides a picture of the prism mold.



Fig. 2.1 Prism mold used for freeze-thaw test specimens

Cylindrical Molds

Nine 152 mm x 305 mm steel cylindrical molds were fabricated. Steel base plates and wooden top plates with a 38 mm diameter center hole were used. As with the prism molds, a steel rod was inserted at the middle of each cylinder to create a hole in which Bristar was later inserted. Fig. 2.2 provides a picture of the cylindrical mold.



Fig. 2.2 Cylindrical mold used for freeze-thaw test specimens

2.1.3.2 Bristar Calibration

The Bristar mix used to create an internal bursting force in cylinders had to be calibrated to yield the appropriate pressure when set. Nine 152 mm x 305 mm steel tubes were filled with concrete and a 38 mm diameter hole was fabricated in the center of each. Each steel tube was mounted with two strain gages located diametrically opposite each other at mid-height on the exterior surface.

After the concrete was allowed to set, Bristar mixes with different water/Bristar ratios were poured into the center hole. The intent was to calibrate the water/Bristar ratio so that a confining pressure in the steel tube similar to that developed by corrosion-

induced expansion could be generated. The desired confining pressure was based on the strains in composite wraps due to the expected volume expansion in a bridge column caused by corrosion (see Table 2.3).

Table 2.5 shows the strains that would be induced in the steel tube used for calibration by confining pressures expected to be generated by corrosion in composite wrapped columns (for a wrap strain of 0.531%). These strain, selected from Table 2.3, corresponds to a wrap strain that would be generated in a 915 mm diameter column due to steel corrosion after 10 years when the steel ratio by cross section and tie spacing are 3% and 152 mm, respectively. A steel ratio of 3% and tie spacing of 152 mm are conservative. Sample calculations on how the values in Table 2.5 were obtained are shown in Appendix B.2.

Table 2.5 Internal pressure generated by corrosion for wrap strain of 0.531%

Wrap	Number	Pressure	Strain in
	of layers	kPa	steel jacket
	2	3763.6	0.029%
Glass	3	5644.9*	0.045%
	4	7527.2	0.060%
	1	2310.4	0.018%
Carbon	2	4620.8	0.037%
	3	6931.2	0.055%

Sample calculation for this row is shown in Appendix B.2.

Figs. 2.3 and 2.4 show the strain generated in the steel jacket when the water/Bristar weight ratio was 400g/1000g and 500g/1000g, respectively. The maximum strain of over 0.062% generated in the steel calibration jacket by the 400g/1000g water/Bristar ratio corresponds to an internal pressure of over 7600 kPa, which is larger than all the pressures shown in Table 2.5. However, the maximum strain of about 0.038%

generated in the steel calibration jacket by the 500g/1000g water/Bristar ratio corresponds to an internal pressure of about 4830 kPa. This is closer to the pressures expected due to corrosion in columns (with wrap strain of 0.531%) wrapped with 3 layers of fiberglass and 2 layers of carbon. The 500g/1000g water/Bristar ratio is quite dilute and a higher water content is not feasible. Therefore, a water/Bristar ratio of 500g/1000g was used for all specimens requiring Bristar.

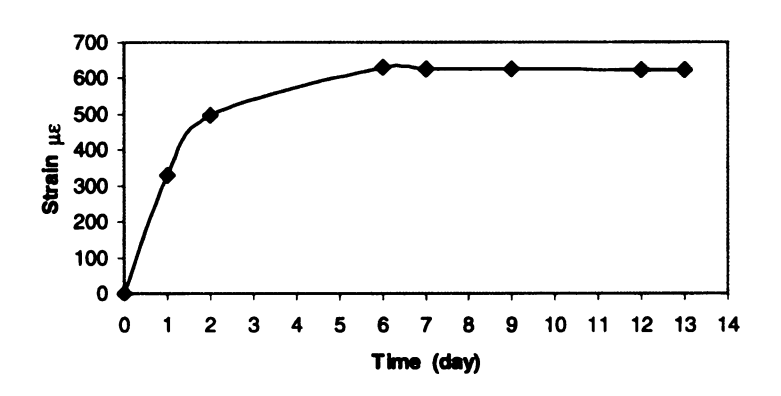


Fig.2.3 Strain in steel tube for water/Bristar ratio of 400g/1000g

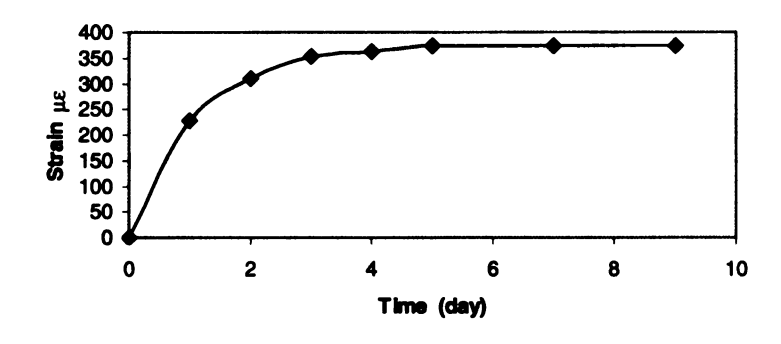


Fig. 2.4 Strain in steel tube for water/Bristar ratio of 500g/1000g

It was decided that three layers of glass and two layers of carbon would be used in the freeze/thaw tests, and that the Bristar would be prepared to generate a pressure of about 4830 kPa. The strain in the glass wrap would then be about 0.45% while that in the

carbon wrap would be about 0.55%. Variations in these values occurred because it was not possible to control the Bristar pressure precisely. It was felt that using more than three layers of glass and two layers of carbon would unnecessarily increase the cost of the wraps.

Since Bristar is highly porous, and water absorption with subsequent freezing and thawing within the hole containing Bristar was undesirable, the ends of the specimens were coated with epoxy prior to the freeze/thaw tests.

2.1.3.3 Chloride Content

Sodium chloride (NaCl) was used exclusively in freeze/thaw and accelerated corrosion tests to contaminate concrete with chloride ions. Some examples of NaCl concentrations found in the literature are:

- Arya and Sa'id-Shawaqi (1996) conducted tests on concrete prisms. Concrete was
 dosed throughout by either 2%, 3% or 4% Cl⁻ ions by weight of cement.
 For concrete mix data used by the Michigan Department of Transportation (MDOT)
 and 4% Cl⁻ ions by weight, this translates to 22.12 kg NaCl/m³ of concrete:
 - 336 kg cement/m³ of concrete \times 0.04 = 13.44 kg Cl⁻/m³ of concrete
 - 13.44 kg Cl⁻/ m³ of concrete × (58.5 NaCl/35.5 Cl⁻) = 22.12 kg NaCl/m³ of concrete.

For 3%Cl⁻ and 2%Cl⁻ this translates to 16.59 and 11.06 kg NaCl/m³ of concrete respectively.

2. Yamato, et al. (1987) found that the chloride content investigated in an off-shore concrete bridge was about 3.0% NaCl by weight of cement at a point 2 cm in from the

vertical sides of a girder. Following calculations as in item 1, this translates to 22.69 kg NaCl/m³ of concrete.

A 2% Cl⁻ ion by weight of cement was used in the freeze/thaw and accelerated corrosion tests. This translates to 11 kg NaCl/m³ of concrete.

2.1.3.4 Strain Gage Placement

Strain gages were used to monitor wrap hoop strains during freeze/thaw tests on six round specimens and six square specimens (three specimens for each type of wrap), and four control specimens (one for each type of wrap and specimen shape). Each specimen was fitted with two strain gages oriented in the circumferential direction and placed opposite each other at mid-height.

Half of the specimens were wrapped with three layers of Tyfo-SEH Glass composite and the other half were wrapped with two layers of MBrace (Tonen) Carbon composite. A total of 16 specimens (eight with each type of wrap system) that were to undergo 300 cycles of freeze-thaw were fitted with strain gages (two strain gages per specimen). The gages were coated with wax and silicon for moisture and mechanical protection.

The expansive nature of Bristar caused the specimens to expand in the hoop direction as desired. An undesirable side effect was simultaneous expansion in the longitudinal direction. This caused the specimens with the carbon wrap to split across the cross sectional area since the carbon wrap contained no longitudinal fibers. The glass wrap had Kevlar strands embedded in the longitudinal direction, which prevents these specimens from splitting.

Considerable effort was devoted to devising a system for releasing the vertical expansion of Bristar using a greased aluminum tube. However, after several unsuccessful trials it was determined that the vertical stresses caused by Bristar could not be totally eliminated. In order not to risk having the carbon-wrapped specimens fail while in the freeze-thaw machine, additional longitudinal reinforcement was provided to the carbon-wrapped specimens. This was done by strengthening with strips of carbon in the longitudinal direction. The strain gage reading should not be affected since the strips are placed adjacent to the gages but not above them, and the longitudinal strips should not provide any additional confinement. Carbon-wrapped specimens subjected to freeze-thaw as well as carbon-wrapped control specimens were fitted with vertical strips.

Initial strain gage readings were taken prior to pouring Bristar in the center hole of each specimen. After the initial expansion period of the Bristar, which is about one week, an epoxy compound was used to cap the top and the bottom of the center hole. It was not possible to control the Bristar pressure precisely. The average strain in the wraps after the addition of Bristar to the specimens measured before starting the freeze/thaw testing varied from:

- 0.31% to 0.60% for Glass with an average of 0.47%
- 0.24% to 0.68% for Carbon with an average of 0.48%

The freeze/thaw machine was set to subject the specimens to freeze/thaw cycles according to ASTM C666 Procedure B, with freezing in air and thawing in water. Strains were monitored during the freeze/thaw tests. A half bridge configuration was used for strain measurements, with dummy gages mounted on FRP panels located inside the freeze/thaw machine so that strains due to temperature variations were eliminated.

Considerable effort was required to properly adjust the freeze/thaw machine. Since some of the specimens were wrapped with composite wrap systems and others were not, careful and precise calibration was needed to control the freeze and thaw temperatures. The wrapped specimens took longer to reach -17.8°C (end set point for the freeze cycle) and 4.4°C (end set point for the thaw cycle) than the unwrapped specimens. A plus or minus 1.7° tolerance is allowed at the upper and lower set points by ASTM C666. After a few trials, it was established that an ideal sump water temperature of 7.2°C would ensure that all specimens attain temperatures of -17.78±1.7°C at the end of the freeze cycle and 4.4±1.7°C at the end of the thaw cycle according to ASTM C666. Temperatures at the center of control specimens were

Specimens prepared as mentioned above were then placed in the freeze/thaw chamber for 150 and 300 freeze-thaw cycles. The strains were measured throughout this period. Two switch boxes were fabricated to facilitate reading of the strain gages during the freeze/thaw and accelerated corrosion tests. A switch box is shown in Fig. 2.5.

monitored for both unwrapped and wrapped specimens.



Fig. 2.5 Strain measurement instrument (left) and switch box (right) used for strain gage reading

2.1.3.5 Compression Testing

Considerable preparation was required prior to compression testing of the freezethaw specimens. Two special fixtures were manufactured to facilitate the testing.

Both end surfaces of each specimen had to be capped in order to provide two perfectly parallel contact surfaces for load application. Sulphur is commonly used for capping. The standard fixture used to align specimens vertically and cap the ends is not effective for wrapped specimens. The standard fixture requires specimens with smooth sides, but FRP wraps make the sides of wrapped specimens uneven. The standard fixture, therefore, does not assure parallel end surfaces after capping. A special fixture was fabricated to enable capping of wrapped specimens. The new fixture could be used with cylinders and square prisms, and minimized the physical labor required to lift up a specimen, pour melted sulphur on a plate, and lower the specimen onto the plate to install the end cap. This fixture is shown in Fig. 2.6.

The standard ASTM compressometer (fixture used to measure the axial strain during compression testing) cannot be used with square prisms. A new compressometer was fabricated for use with the square prisms. This new compressometer is shown in Fig. 2.7.





Fig. 2.6 Capping Fixture

Fig. 2.7 New Compressometer

The following data was gathered every six seconds using a data acquisition system:

- The compressive load and axial strain on all specimens using a load cell and a compressometer fitted with an LVDT, respectively.
- The hoop strain in wraps for specimens fitted with strain gages

2.1.4 Accelerated Corrosion

Accelerated corrosion tests using an electrochemical cell were conducted to study the effect of confinment on the progression of corrosion in the reinforcing steel within a reasonable time frame. In addition, the hypothesis that FRP wraps slow down corrosion by reducing permeability of water and oxygen or that they inhibit corrosion by developing sufficient confining pressure (Brockenbrough at el. 1985) was to be evaluated. The confining pressure was monitored using the strain readings of the wraps during the accelerated corrosion tests. In addition, the rate of corrosion was indirectly measured to determine if confinement had any effect on corrosion activity.

The test used by Detwiler (1991) on lollipop specimens was adopted for use with four #13 steel reinforcing bars cast in 152 mm diameter by 305 mm high concrete cylinders. The specimens were initially immersed in salt water (with 3% NaCl) at room temperature (approximately 20 °C) and connected to a power source so that two of the steel rods became anodic and the other two became cathodic. Figure 2.8 shows the wiring diagram used for connecting specimens to the power supply in order to accelerate corrosion of the reinforcement. The exposed ends of the steel bars were protected against crevice corrosion by using a Teflon tube tightened with a nut and by covering the exposed end with silicon rubber. This forms a barrier to prevent moisture penetration into the crevice (the interface between the steel bars and the concrete surface).

Two bars were used as anodes and two bars were used as cathodes to keep the corrosion products within the specimens as in natural corrosion. When an external cathode is used, the corrosion products tend to migrate out of the cylinder. In addition, since a conductive medium must be provided during accelerated corrosion testing, the

cathodes must be placed inside the wraps, because the specimens were not continually immersed in water. Corrosion was induced on only two of the four bars in each specimen (i.e., at the anodes). Table 2.6 shows the corrosion level required in two bars for various volume ratios (i.e., vol. of rust/vol. of corroded steel) to induce a hoop strain of 0.531%, which is the anticipated strain in the wrap due to steel corrosion after 10 years (see Table 2.3). Two layers of carbon and three layers of glass were used for the accelerated corrosion test. This was the same number used for the freeze-thaw test.

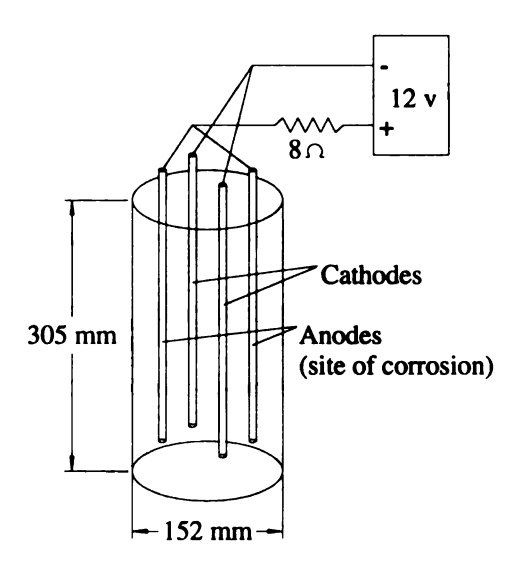


Figure 2.8 Wiring diagram for accelerated corrosion specimens

In order to simulate road column exposure to rain and water spray due to passing traffic, the concrete specimens were subjected to cycles of wetting and drying. The specimens were soaked in salt water for one hour each day and the water was then drained.

Table 2.6 Corrosion level required in two bars to induce a strain of 0.531% in the wrap*

Wrap	Strain %	Vol. Ratio	Percent Corrosion %
		3	38.1
Any number of layers	0.531	4	25.4
Carbon or glass		5	19.1
		6	15.3

^{*}Two #13 bars in 6" (152 mm) diameter cylinder

The rate of corrosion was measured to determine if confinement has any effect on corrosion activity. The corrosion rate was measured using the ASTM G1 (ASTM 1990) test. The hoop strain generated in the wraps due to corrosion induced expansion was monitored using strain gages oriented in the circumferential direction.

A water/cement ratio of 0.6 was used for the accelerated corrosion specimens to promote capillary porosity, which in turn would aid the corrosion process (see Table 1.1). The 28-day strength for the corrosion specimens was 20353 kPa.

Four unwrapped dummy specimens were subjected to accelerated corrosion using different resistors to vary the current intensities. These specimens were closely monitored to determine when cracking initiated. Based on these trials, resistors of 8 Ω were used with a 12 V power supply.

2.1.4.1 Corrosion Prior to Wrapping

Samples were exposed to accelerated corrosion while submerged in salt water prior to applying the composite wrap. This simulated initial corrosion in field columns before wrapping is applied. The initial corrosion period was closely monitored. When cracking started to develop, the specimens were taken out of the water and dried thoroughly before wrapping them with the two types of wrap systems (glass and carbon).

One approach to prevent stress concentrations on FRP wraps due to localized volume expansion is not to bond the wrap directly on the column but only provide bond between the different layers of the wrap. Thus localized volume expansion is contained by the entire wrap system. As with bonded wraps, volume expansion due to corrosion will strain the wrap inducing confining pressure. About half of the wrapped specimens contained a plastic sheet between the concrete and the wrap in order to prevent the wrap from bonding to the concrete.

A total of 24 specimens were subjected to the initial phase of accelerated corrosion for 13 days. Although subjected to the same conditions, the specimens had significant variation in corrosion level as observed from concrete cracking. The specimens were divided into three groups based on the severity of cracking — severe, moderate and light.

A total of five severely corroded specimens, in which some concrete had spalled off, were patched. Patching was done using a sand/cement mortar (that was contaminated with 2% Cl⁻ ion by weight of cement. Specimens for which spalls occurred at an edge were placed in a mold and mortar was placed within the mold. These severely corroded specimens before and after patching are shown in Figs. 2.9 and 2.10, respectively.

Specimens were selected systematically from the three groups for wrapping as shown in Table 2.7. Three layers of glass wrap and two layers of carbon wrap were used to be consistent with the number of layers used in the freeze-thaw test. A total of 16 specimens were fitted with strain gages oriented in the circumferential direction (two gages per specimen located diametrically opposite each other at mid-height). All specimens were then ready for the next phase of accelerated corrosion.

Table 2.7 Number of wrapped and unwrapped specimens in corrosion groups

Corrosion Group	Wasan Adhanian	Number Wrapped with			
	Wrap Adhesion	Glass	Carbon	Nothing	
Severe	Bonded	1	1	,	
	Unbonded	1	1	1	
Moderate	Bonded	1	1		
	Unbonded	1	1	1	
Light	Bonded	2+2	2	2+2	
	Unbonded	2	2	2+2	



Fig. 2.9 Severely corroded specimens prior to patching



Fig. 2.10 Patching of the severely corroded speciemns

2.1.4.2 Construction of the Corrosion Tank and Appurtenances

A special wood tank coated with fiberglass to accommodate the corrosion specimens was constructed. The tank was fitted with a marine pump, a float shut-off mechanism, ball valves, and a timer control. In automatic mode, the pump was activated once a day to fill the tank with salt water (3% NaCl) from a holding tank located below the fiberglass tank. The float shut-off mechanism would turn the pump off when the water level covered the top of the specimens. After one hour of soaking, the timer opened the ball valve and the water was drained into the holding tank. Photographs of the corrosion tank and the corrosion specimens placed in the tank are shown in Figs. 2.11 and 2.12, respectively.



Fig. 2.11 Corrosion tank



Fig. 2.12 Corrosion specimens in the tank

2.1.4.3 Monitoring Progress of Corrosion During Test

Monitoring corrosion levels during the accelerated corrosion test was important in order to know when to remove specimens. Unwrapped specimens were expected to corrode faster than wrapped specimens. Also, some specimens were to be removed

approximately mid-way through testing when the anodic reinforcement in unwrapped specimens lost about half their cross sectional area. The total length of time for the corrosion test could not be predicted in advance. A method was needed to monitor corrosion levels during the test.

Two dummy specimens were originally fabricated to monitor corrosion levels through destructive means. The plan was to cut off sections of the dummy specimens at regular intervals and visually examine the cross section of corroded bars. This approach was error prone because corrosion occurs unevenly and the dummy specimen size would be altered each time a section was sliced off.

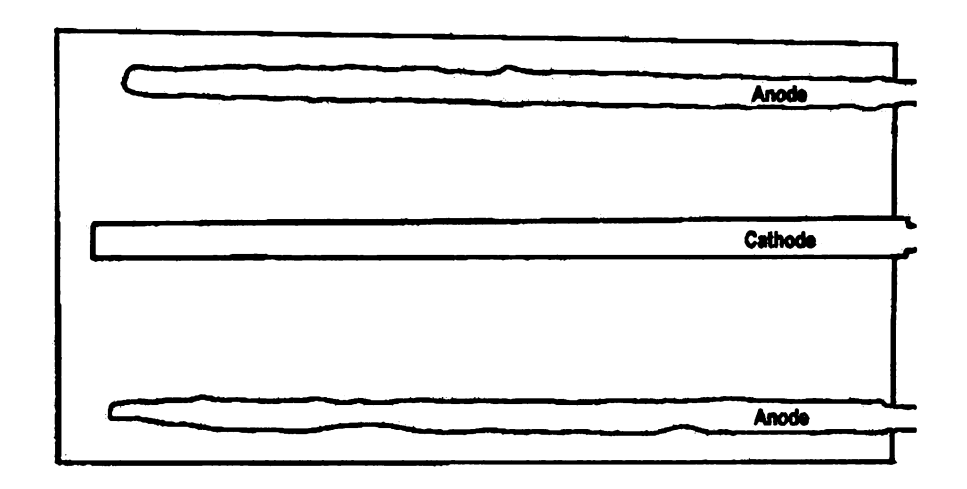
A non-destructive method of monitoring corrosion levels was sought, and an approach utilizing X-rays was identified. Some unwrapped and wrapped pre-corroded specimens were subjected to X-rays in a standard radiology laboratory. The X-ray negatives clearly show the uncorroded parts of the anodic steel reinforcement.

Prior to beginning the accelerated corrosion process after specimens were wrapped, representative specimens were subjected to X-rays to ascertain the level of corrosion during the pre-corrosion phase. The X-ray images showed the reinforcing bars inside the specimen and the approximate level of corrosion in them. This was necessary to establish a reference point and assess the progress of corrosion.

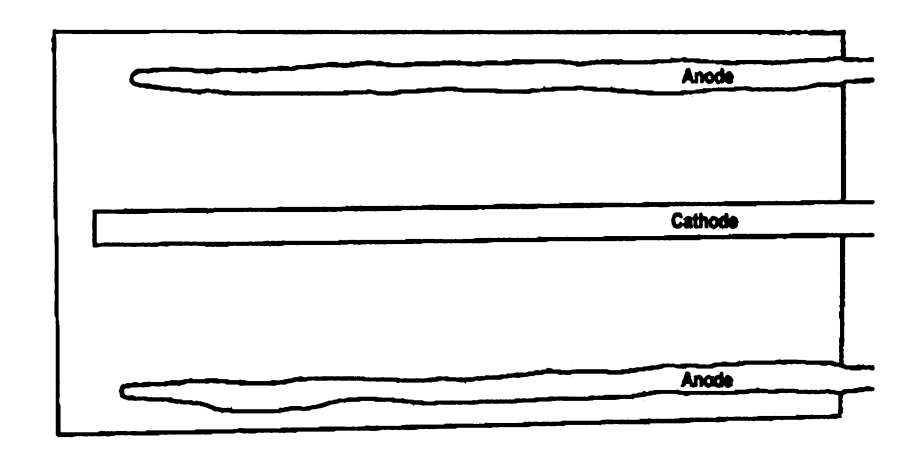
Periodically, the specimens selected for observation were transported to the radiology laboratory and subjected to X-rays. By comparing the state of corrosion in the wrapped and unwrapped specimens, it was evident that the corrosion rate in wrapped specimens was significantly lower than that in unwrapped specimens. Fig. 2.11, 2.12, and 2.13 show views of the X-rays of a typical unwrapped specimen taken after 0, 90 and 105

days of accelerated corrosion after the precorrosion stage, respectively. To facilitate reproduction, the X-ray images were outlined to clearly show the edges of the reinforcing bars and the specimen, and the photographic image was reduced to create the line drawings shown in the figures. Fig. 2.16 shows typical reinforcing bars removed from a specimen. The middle two bars are the cathodes while the outer two bars are the anodes (the site of corrosion).

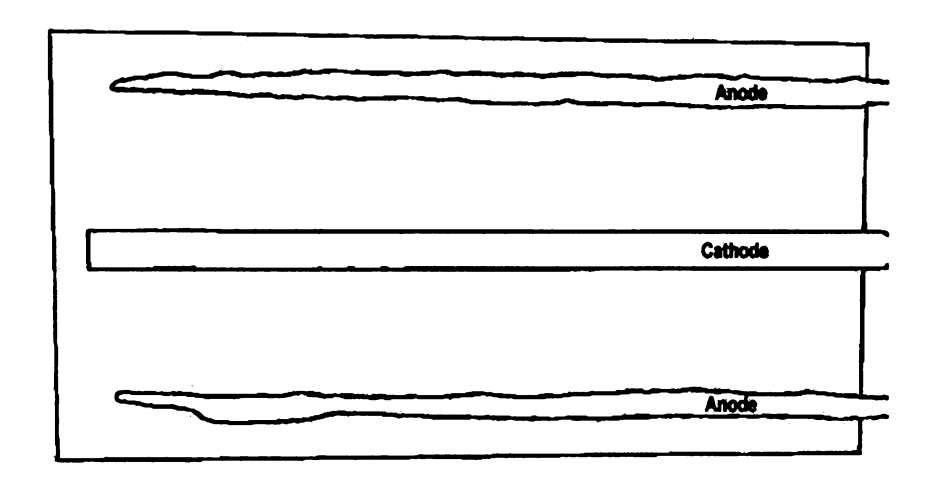
Specimens were removed for X-ray exposure when there was no water in the tank. The current used to accelerate corrosion was shut-off while the specimens were removed and transported to the radiology laboratory, and turned back on when the specimens were returned to the corrosion tank approximately two hours later.



Figs. 2.13 Sample X-ray taken in the beginning of the accelerated corrosion test



Figs. 2.14 Sample X-ray taken after 90 days of accelerated corrosion test



Figs. 2.15 Sample X-ray taken after 105 days of accelerated corrosion test

53

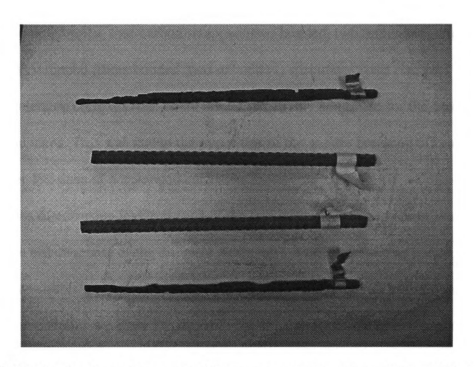


Fig. 2.16 Reinforcing bars after removal from a corrosion specimen. The middle two bars are the cathodes while the outer two bars are the anodes (the site of corrosion)

2.1.4.4 Corrosion Test Matrix

The total number of specimens was 24, including the two extra specimens originally planned for corrosion monitoring through destructive means. The numbers of samples of the various types of specimens used are given in Table 2.8. Specimen, bar and strain gage numbering is shown in Table B.2 in Appendix B. Specimens were removed from the corrosion process and the amount of corrosion was measured as follows:

Four unwrapped, four carbon wrapped (two bonded, two unbonded), and five
glass wrapped (three bonded, two unbonded) specimens were removed when the
X-ray technique indicated that the diameter of corroded bars in unwrapped
specimens was reduced to about 70% of the initial diameter (which corresponds to
about 50% reduction in the cross sectional area). This corresponded to 130 days
of accelerated corrosion

2. Two unwrapped, four carbon wrapped (two bonded, two unbonded), and five glass wrapped (three bonded, two unbonded) specimens were removed when the accelerated corrosion test could not be effectively continued for the unwrapped specimens. This was due to the upper tips of the anodes breaking off and occurred after 190 days of accelerated corrosion.

Comparisons of corrosion levels at each of the two stages mentioned above was used evaluate the effectiveness of the different wrapping systems in reducing corrosion.

Wrap strains were monitored until specimens were removed from the corrosion process. These strains were used to estimate the amount of confining pressure built up due to corrosion.

Table 2.8 Accelerated corrosion laboratory test matrix

Wrap	No. of Specimens Tested for 130 days	No. of Specimens Tested for 190 days
None (control)	4	2
Carbon bonded Glass bonded	2 3	2 3
Carbon unbonded Glass unbonded	2 2	2 2

Chapter 3 Data Collection and Analysis of Results

3.1 Effect of Freeze-Thaw and Wet-Dry Cycling on the Properties of FRP Panels

Table 3.1 provides the mean mechanical properties of FRP panels after 300 freeze-thaw cycles and 190 wet-dry cycles with 3% NaCl solution. By comparing these results to the unconditioned panels tested (see Table 2.1), the following observations are made:

- The freeze-thaw conditioning had little effect on the effective stiffness of glass panels while carbon panels' effective stiffness was increased by 21%. (Note that effective stiffness = modulus x thickness.) The ultimate strains were reduced by approximately 20% and 28% for glass and carbon panels, respectively.
- The wet-dry cycles with 3% NaCl solution had no effect on the effective stiffness of glass panels while the effective stiffness for carbon panels was increased by approximately 39%. The ultimate strains were reduced by approximately 20% and 36% for glass and carbon panels, respectively.

The results in Table 3.1 are based on samples cut from one glass panel and one carbon panel. Investigations involving several panels may yield more reliable results.

Table 3.1 Mean properties for FRP panels

Wrap Type	Thickness (mm.)	Modulus (MPa)	Effective Stiffness (N/mm)	Ultimate Strain
**		300 Freeze-	Thaw Cycles	
Glass	1.092	23805	26000	0.016
Carbon	0.508	79012	40138	0.010
		190 Wet-	Dry Cycles	
Glass	0.914	29539	27000	0.016
Carbon	0.571	81109	46313	0.009

3.2 Freeze-Thaw Test

3.2.1 Strain Gage Readings

Specimens subjected to 300 freeze-thaw cycles were equipped with strain gages, while those subjected to 150 freeze-thaw cycles were not equipped with strain gages. The FRP hoop strains were monitored about once a day during the entire testing period for specimens fitted with strain gages. Two readings were made each day, one during the freeze phase and the other during the thaw phase. All strain gages survived the freeze-thaw test.

By observing the difference in the strain reading of the control specimens (wrapped, no F/T conditioning) between freeze and thaw cycles, the thermal contraction of the FRP panels from thaw to freeze cycles could be determined. Figures 3.1-3.4 show the uncorrected strain readings on round and square control specimens that were not subjected to freeze-thaw. On any given day, the reading of a gage during a freeze or thaw cycle should be approximately the same, since the control specimens were not subjected to freeze-thaw. The difference in gages readings from the thaw to freeze curves observed in Figures 3.1-3.4 is therefore due to contraction of the dummy FRP panel. The

compensation strains for glass and carbon were determined by the average difference between the thaw and freeze readings for control specimens from day 15 onward, when the strains were stable. Note that for carbon (Figures 3.3-3.4), there is only a slight difference between thaw and freeze readings since its coefficient of thermal expansion is close to zero. The compensation strains computed in this manner are 372 micro-strain for glass FRP and -37 micro-strain for carbon FRP. Figures 3.7, 3.11, 3.15 and 3.19 show the compensated strains on the same four control specimens, respectively. The strains during the thaw and freeze cycles are now approximately the same from day 10 onward as expected.

The compensated FRP strains on round and square specimens wrapped with glass and subjected to freeze-thaw are shown in Figures 3.5. 3.6, 3.8, 3.9, 3.10 and 3.12. In general, the strain during the freeze cycle is 100-200 micro-strain higher than that during the thaw cycle. This is most likely due to the thermal contraction of the glass wrap during freezing. Since the concrete specimens prevent the contraction, the tensile strain in the glass wraps increase. An exception is Figure 3.6, in which the strains during the thaw cycle is slightly but consistently higher than that during the freeze cycle.

The compensated FRP strains on round and square specimens wrapped with carbon and subjected to freeze-thaw are shown in Figures 3.13, 3.14, 3.16-3.18 and 3.20. The results are much less consistent for carbon than for glass. In Figures 3.13 and 3.15-3.17 the thaw strains are slightly higher than the freeze strains, while the freeze strains are higher than the thaw strains in Figures 3.14 and 3.20.

A reason for some of the variability in the wrap strains could be the ingestion of water into the Bristar. Although epoxy caps were used on both ends of each specimen to

prevent water penetration, during freeze-thaw cycling the caps of several specimens ruptured due to expansive pressure from Bristar. The loss of strain with time in Figure 3.17 also is likely to be due to the loss of pressure in the Bristar.

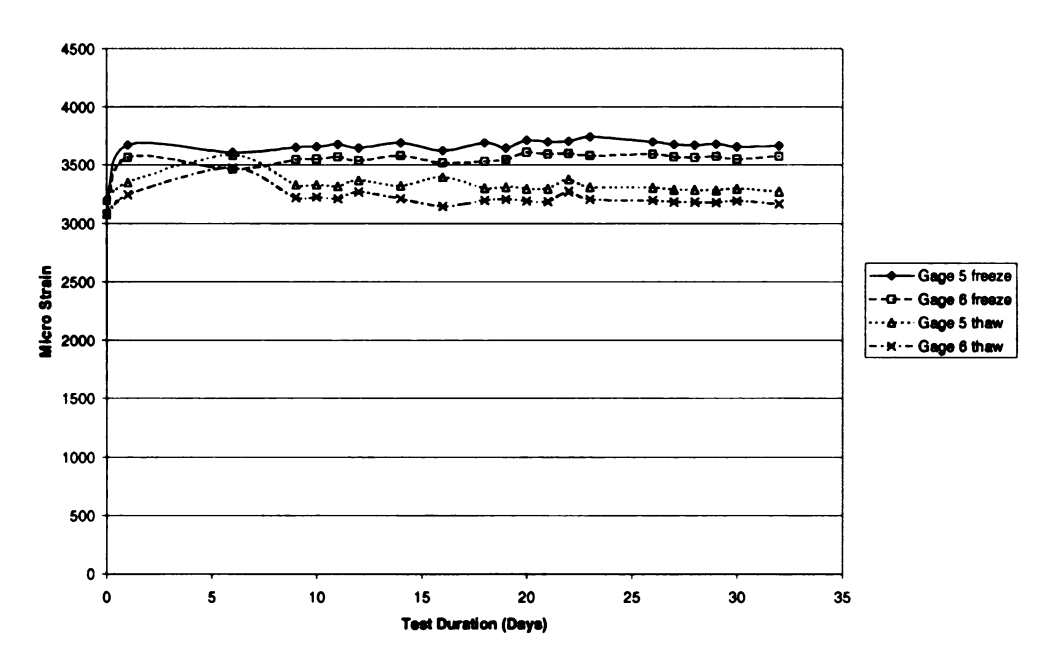


Fig. 3.1 Hoop strains in glass wrap of round control specimen #3 before correcting for thermal contraction of dummy FRP panel

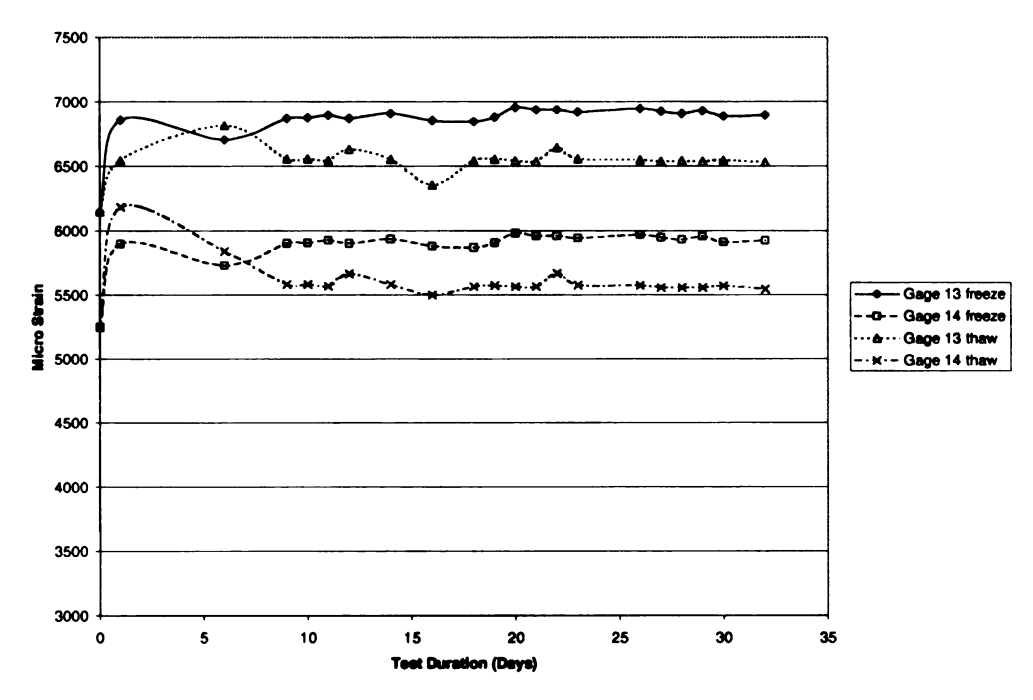


Fig. 3.2 Hoop strains in glass wrap of square control specimen #7 before correcting for thermal contraction of dummy FRP panel

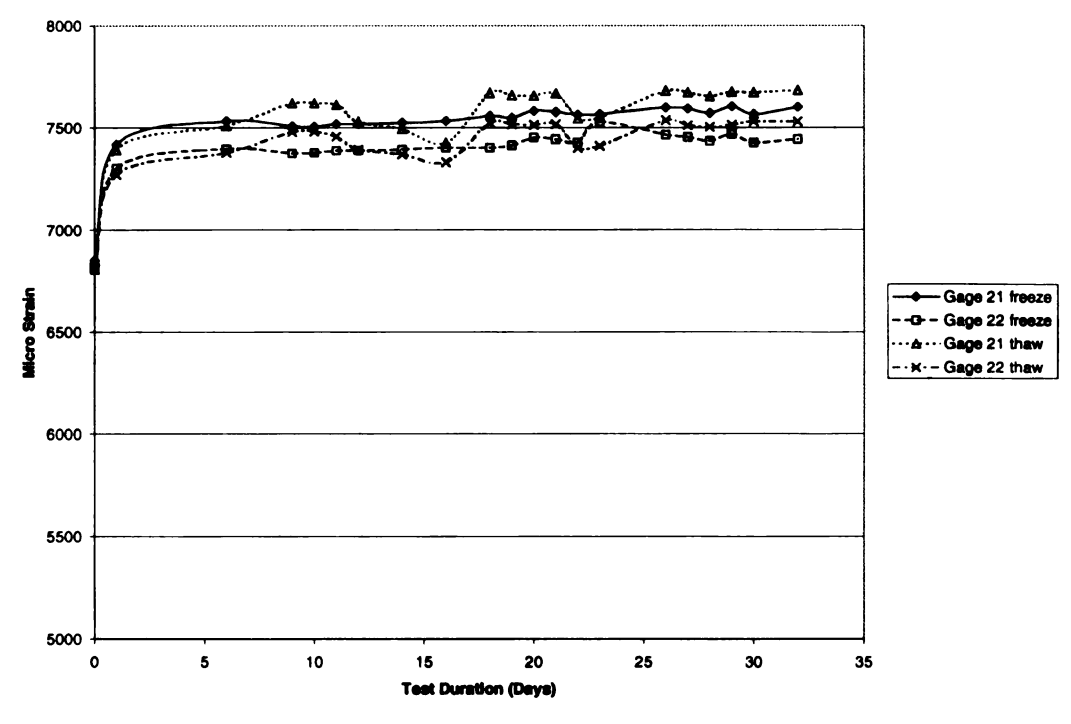


Fig. 3.3 Hoop strains in carbon wrap of round control specimen #11 before correcting for thermal contraction of dummy FRP panel

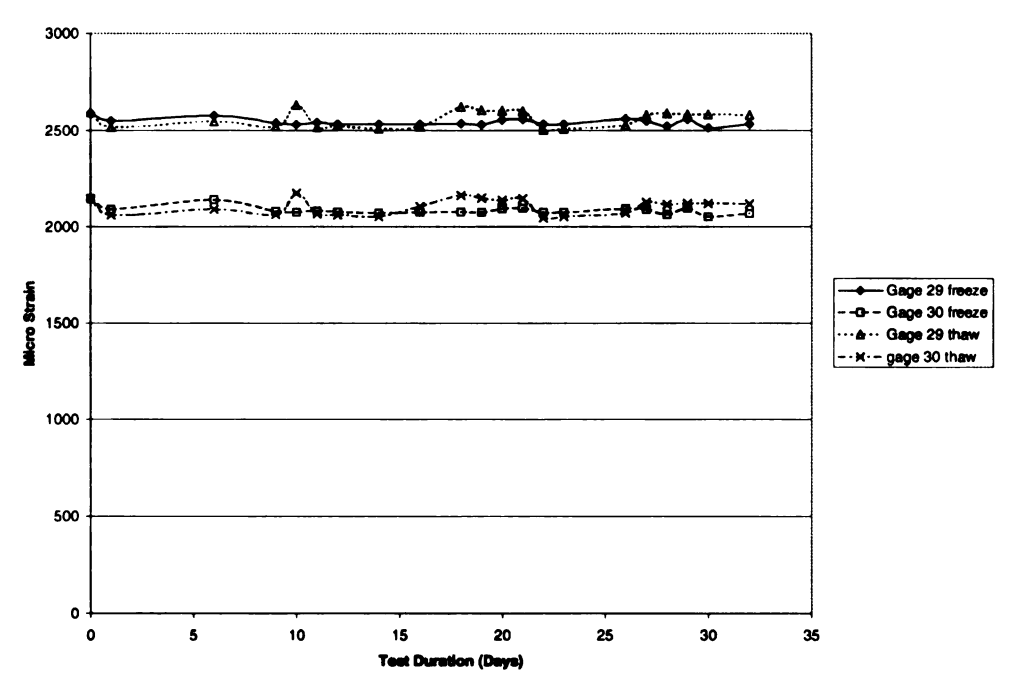


Fig. 3.4 Hoop strains in carbon wrap of square control specimen #15 before correcting for thermal contraction of dummy FRP panel

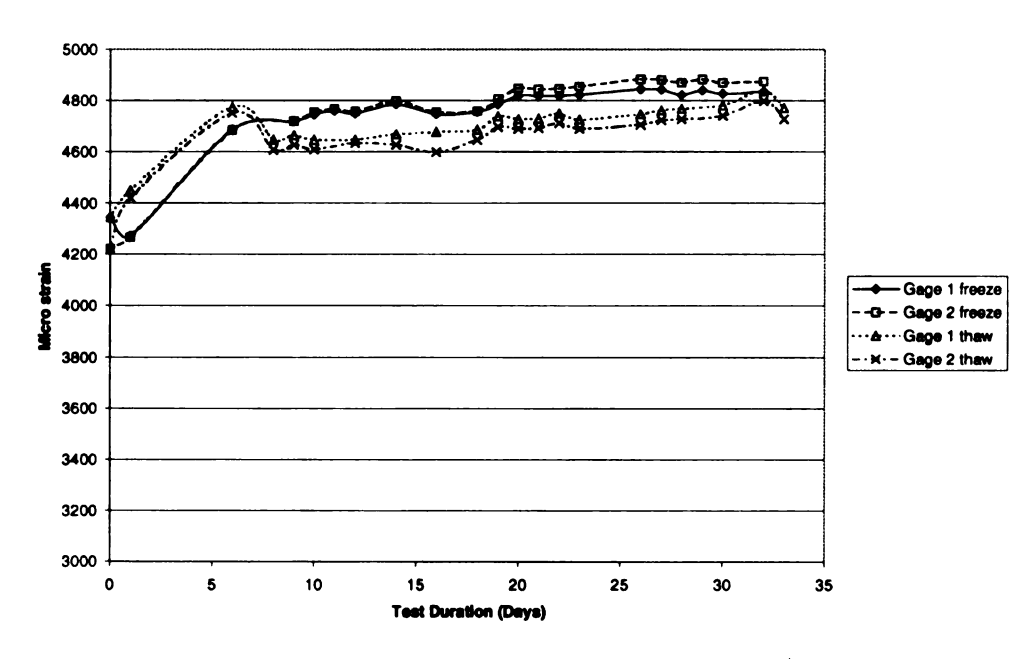


Fig. 3.5 Hoop strains in glass wrap of round specimen #1 during freeze-thaw cycles

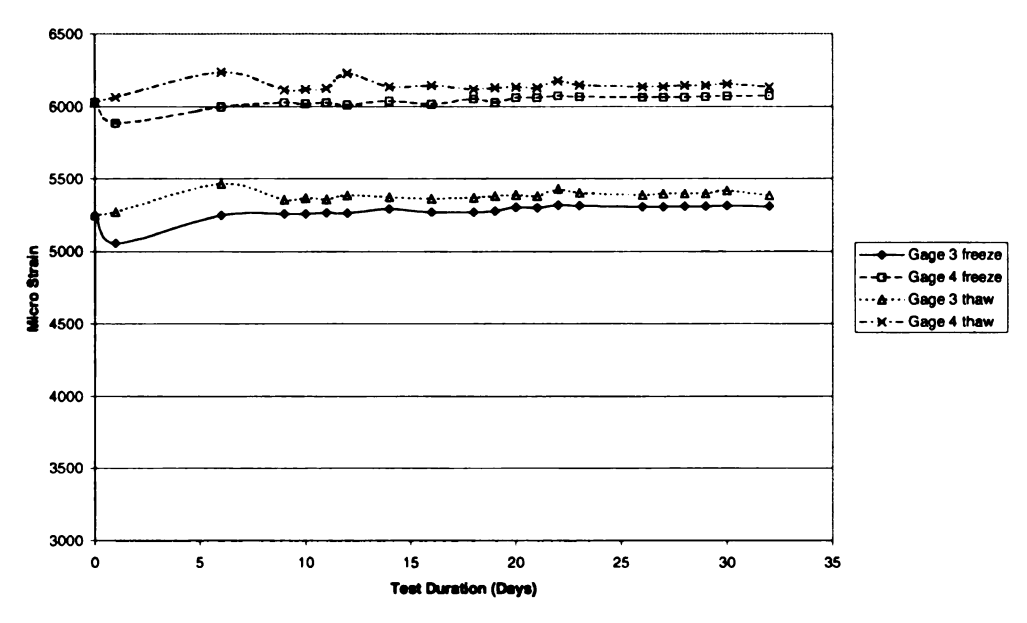


Fig. 3.6 Hoop strains in glass wrap of round specimen #2 during freeze-thaw cycles

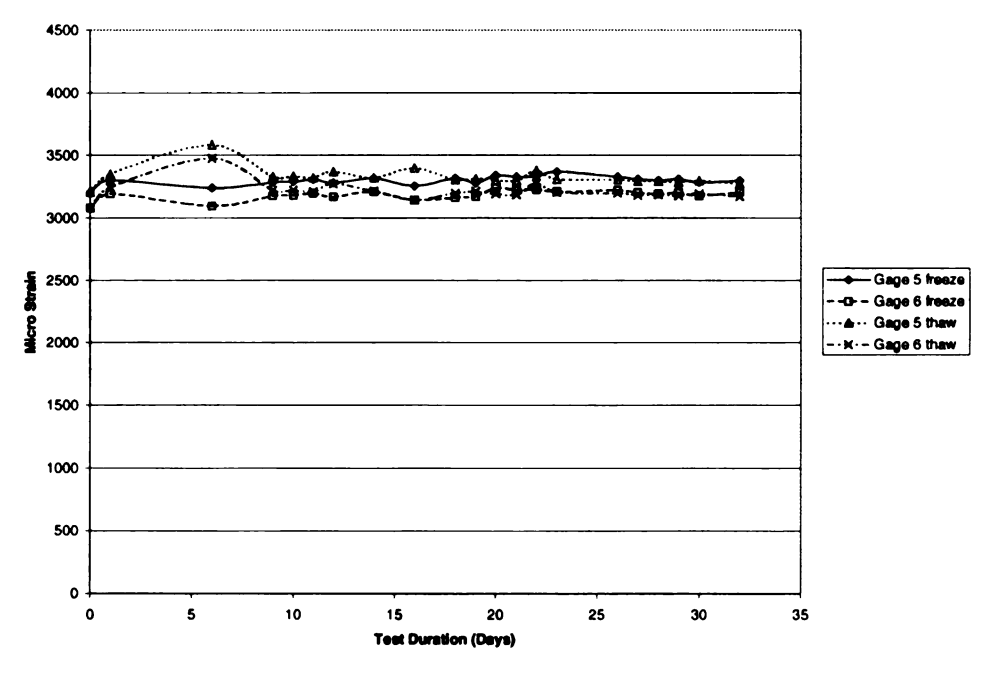


Fig. 3.7 Hoop strains in glass wrap of control round specimen #3

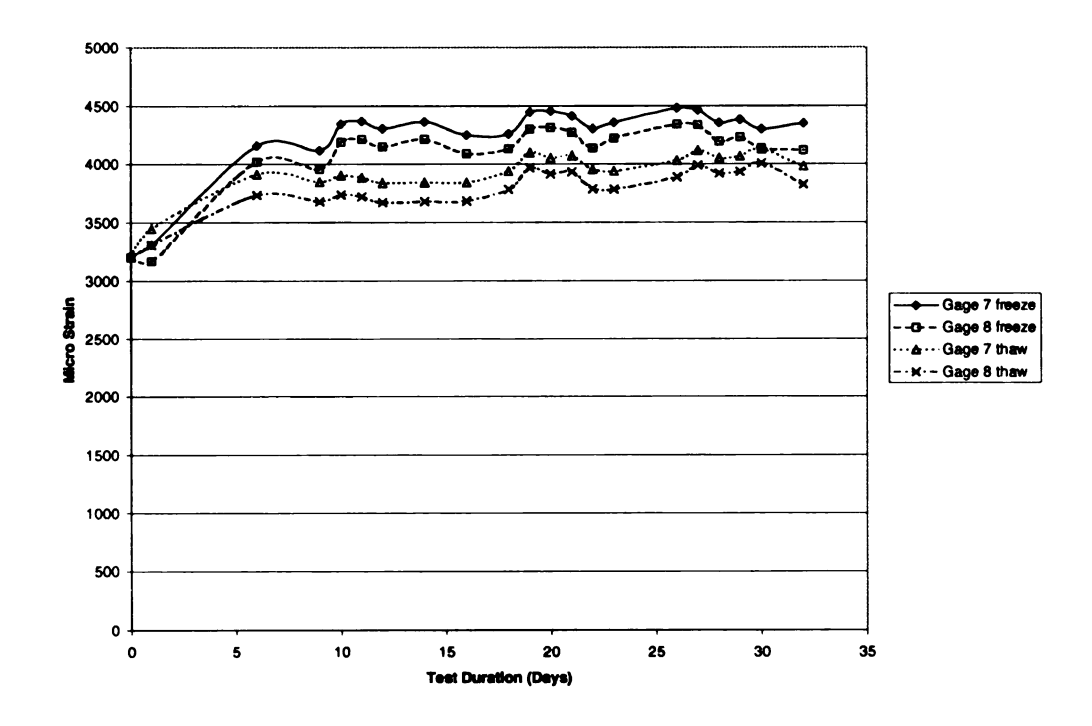


Fig. 3.8 Hoop strains in glass wrap, round specimen #4 during freeze-thaw cycles

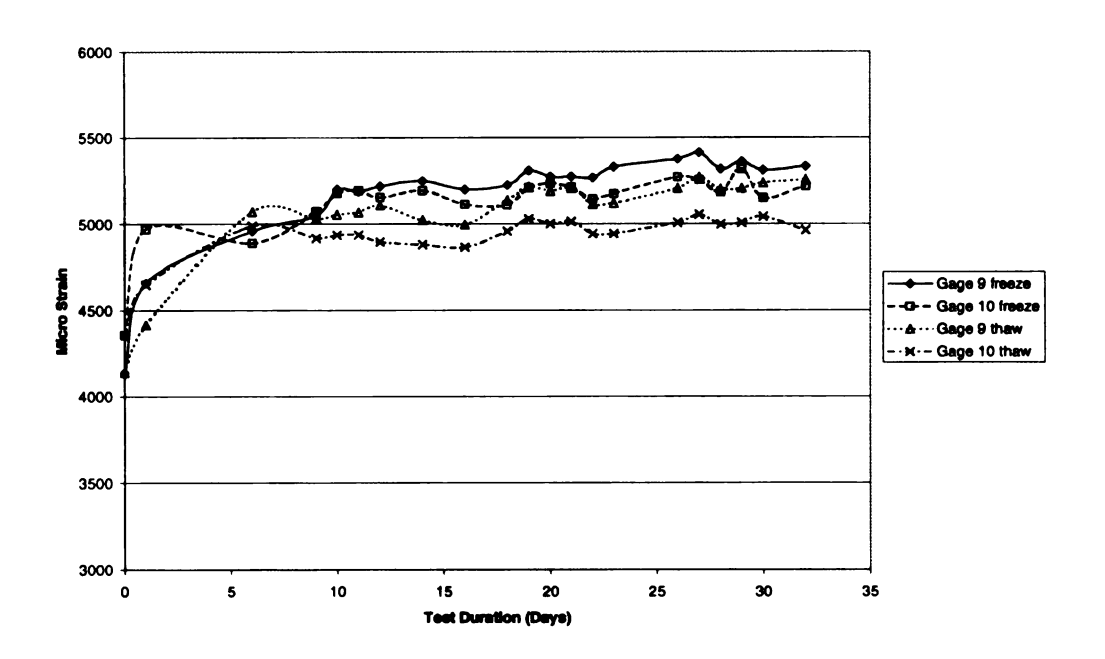


Fig. 3.9 Hoop strains in glass wrap, square specimen #5 during freeze-thaw cycles

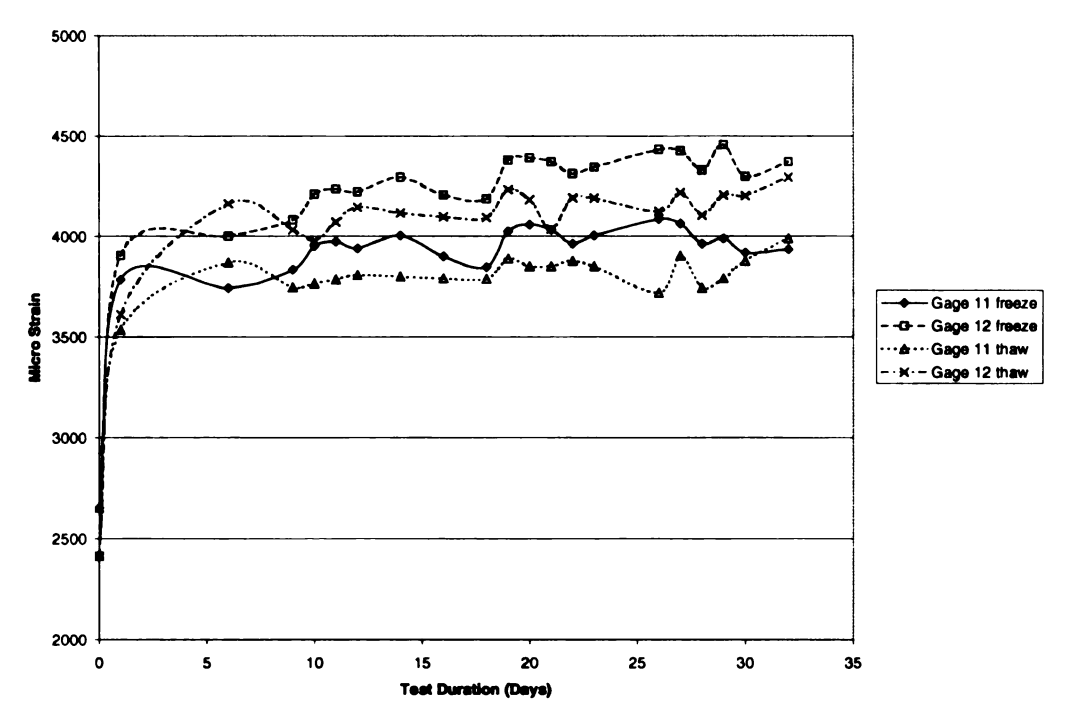


Fig. 3.10 Hoop strains in glass wrap, square specimen #6 during freeze-thaw cycles

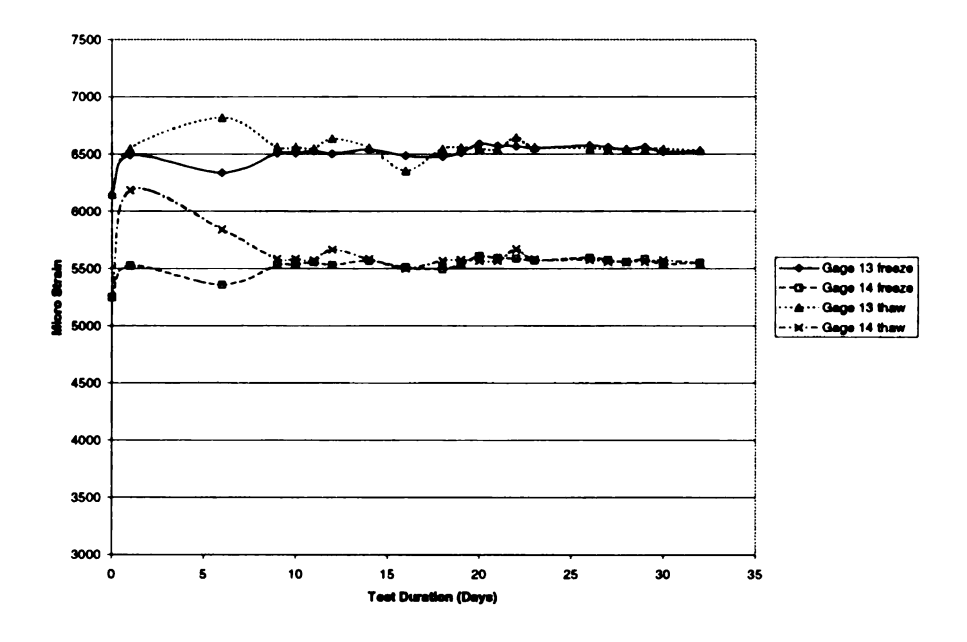


Fig. 3.11 Hoop strains in glass wrap of cotrol square specimen #7

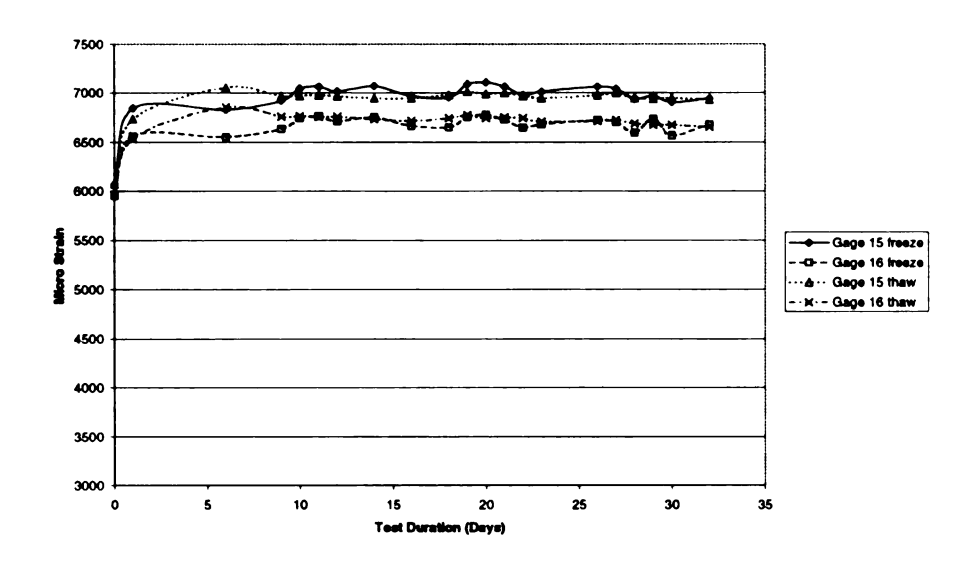


Fig. 3.12 Hoop strains in glass wrap of square specimen #8 during freeze-thaw cycles

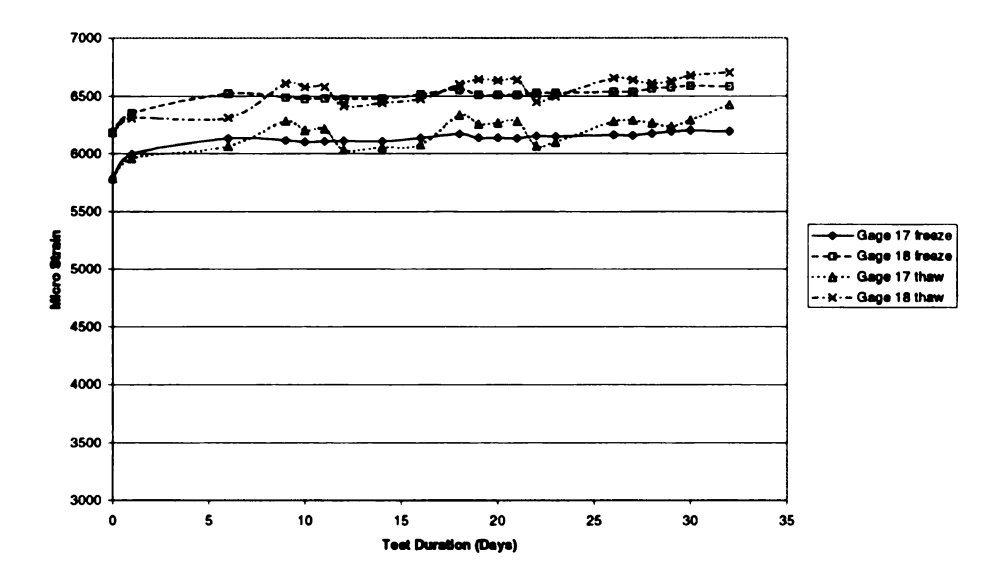


Fig. 3.13 Hoop strains in carbon wrap of round specimen #9 during freeze-thaw cycles

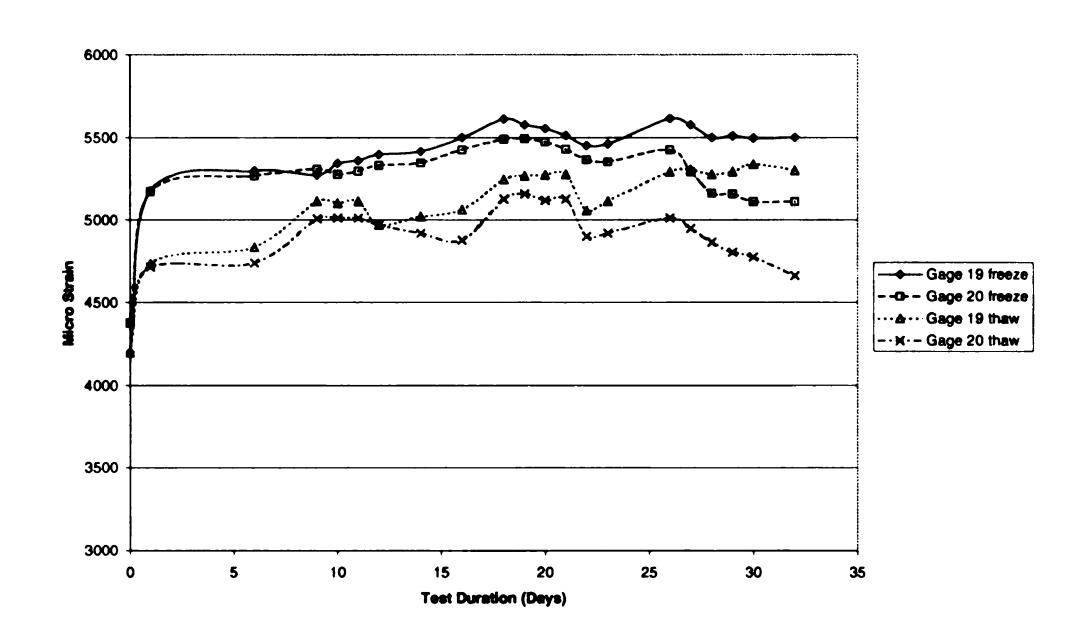


Fig. 3.14 Hoop strains in carbon wrap of round specimen #10 during freeze-thaw cycles

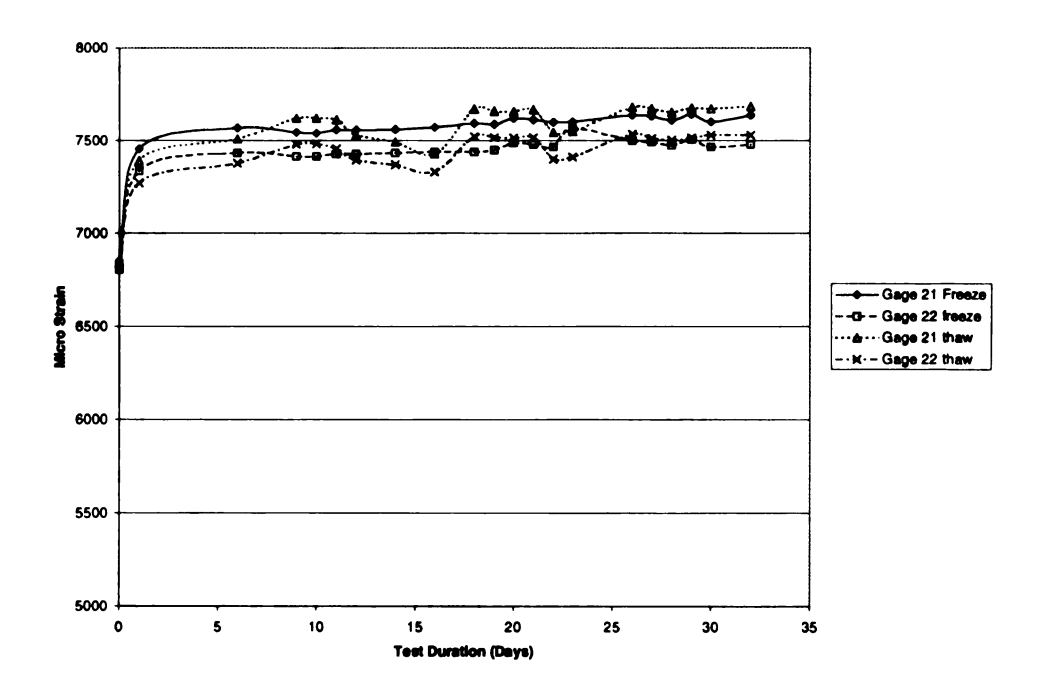


Fig. 3.15 Hoop strains in carbon wrap of control round specimen #11

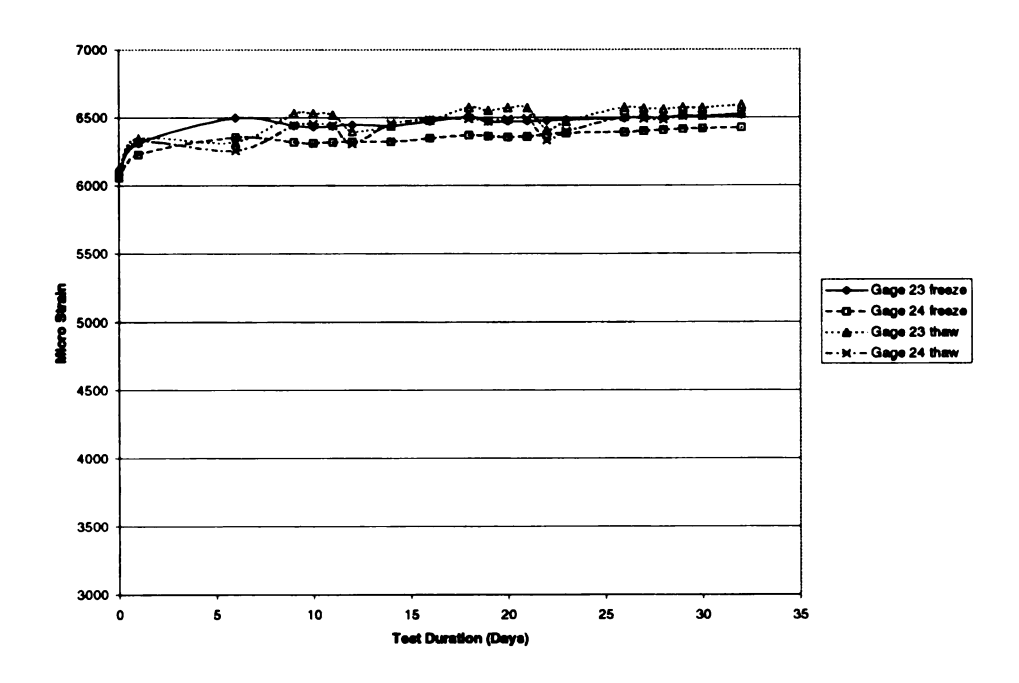


Fig. 3.16 Hoop strains in carbon wrap of round specimen #12 during freeze-thaw cycles

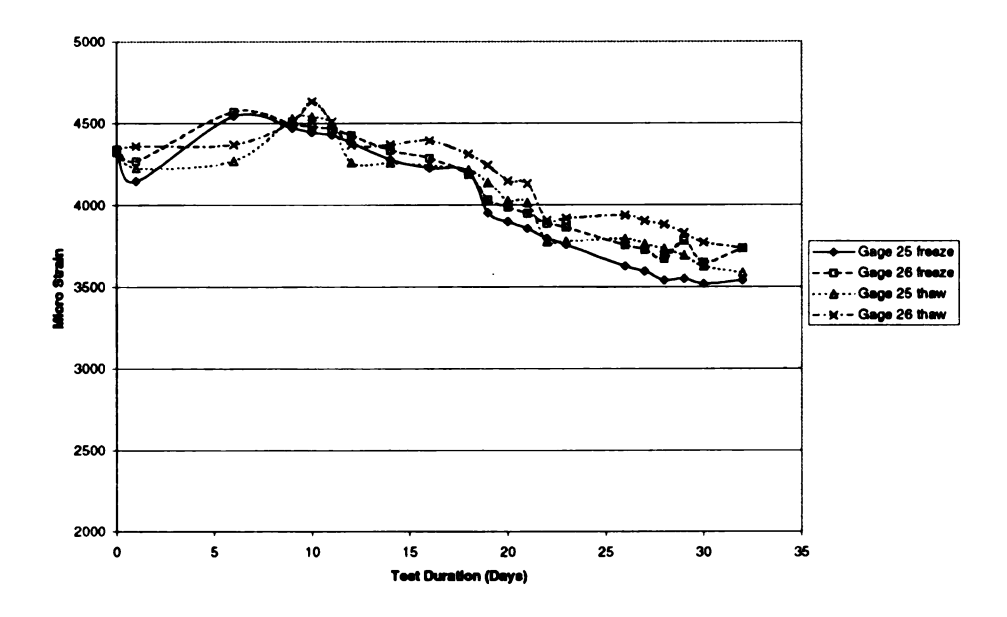


Fig. 3.17 Hoop strains in carbon wrap of square specimen #13 during freeze-thaw cycles

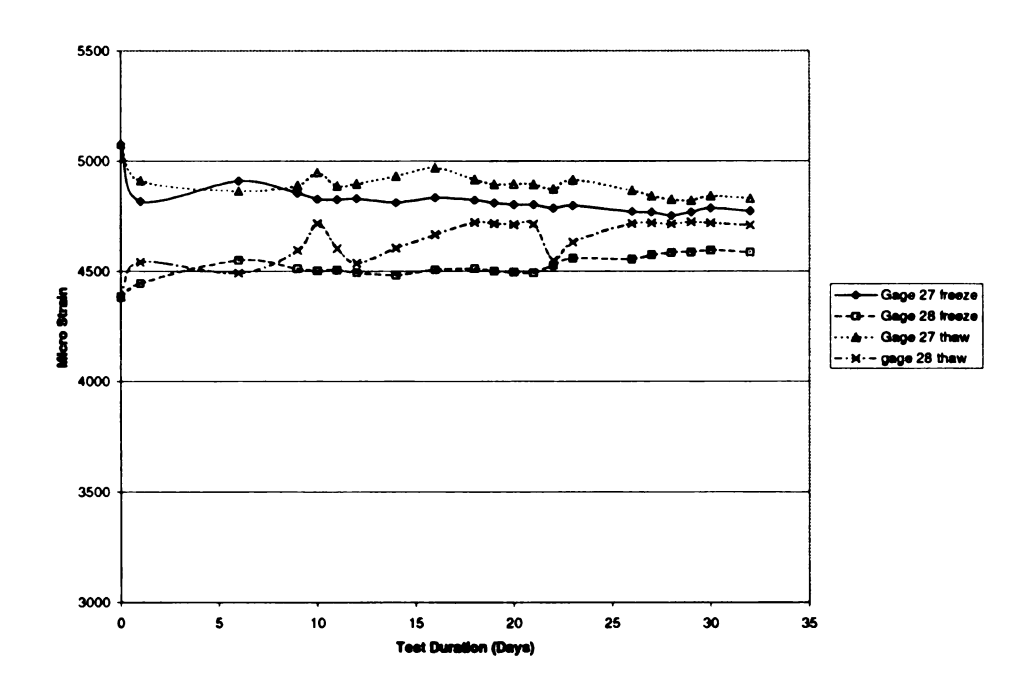


Fig. 3.18 Hoop strains in carbon wrap of square specimen #14 during freeze-thaw cycles

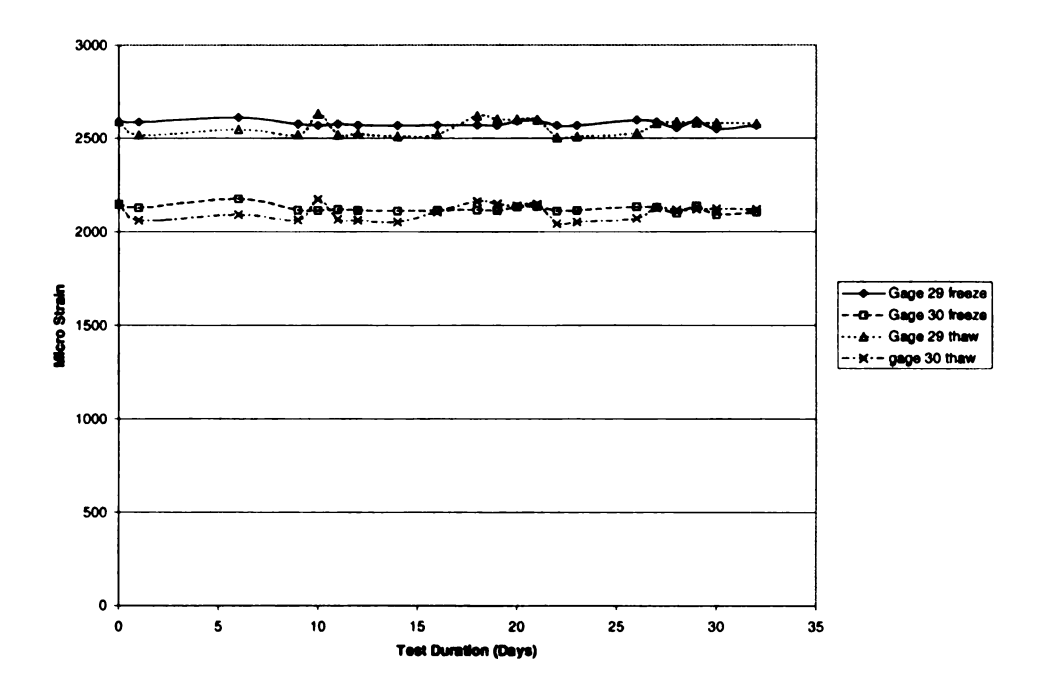


Fig. 3.19 Hoop strains in carbon wrap of control square specimen #15

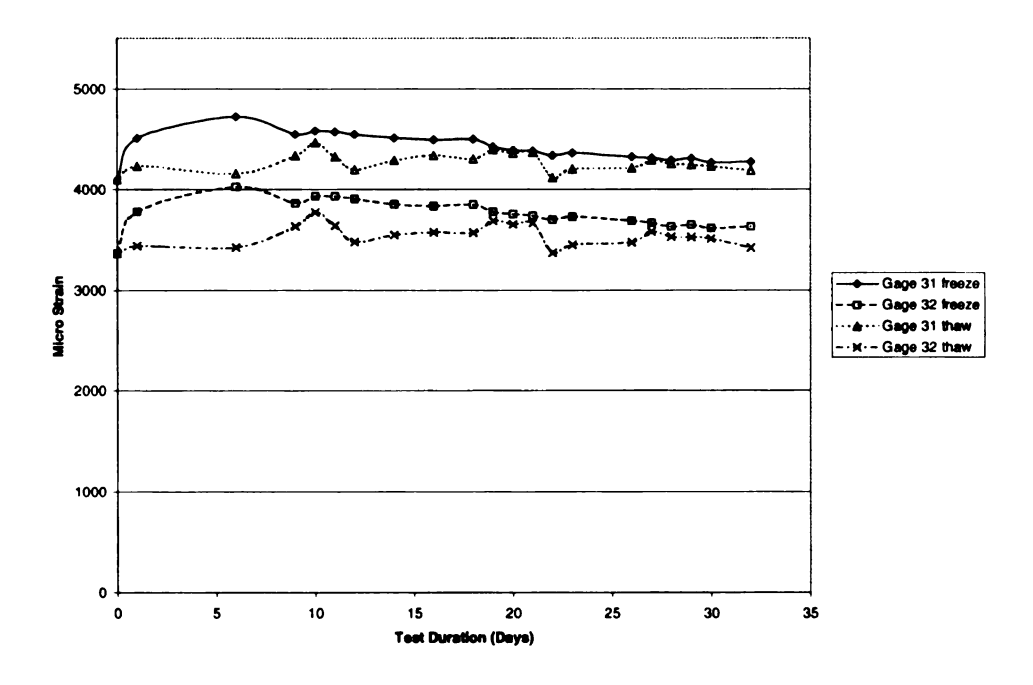


Fig. 3.20 Hoop strains in carbon wrap of square specimen #16 during freeze-thaw cycles

3.2.2 Results of Compression Testing

Figures 3.21 to 3.35 show results of the compression tests for plain and wrapped control specimens and those subjected to 150 and 300 cycles of freeze-thaw. For wrapped specimens fitted with strain gages in the hoop direction, longitudinal compression strains are given along the positive x-axis while the average tensile hoop strain is shown along the negative x-axis. The compression stress for wrapped specimens was computed by excluding the concrete cross sectional area lost due to the presence of the hole in which Bristar was inserted. The following observations are made:

• Plain round specimens (Figures 3.21-3.23): Only one of three specimens survived freeze-thaw conditioning for 300 cycles. This specimen had approximately the same compression strength as the control specimens (~35000-45000 kPa). One of the specimens subjected to 150 freeze-thaw cycles displayed low stiffness and strength,

- and a progressively hardening behavior— it is not apparent what contributed to this behavior. There is no significant reduction in strength due to freeze-thaw conditioning except for the anomalous specimen.
- Round glass-wrapped specimens (Figures 3.24-3.26): The ultimate strength values for two of the six control specimens were unreliable because these specimens could not be crushed in the MSU compression testing machine and were retested at MDOT. In general, conditioning had little effect and compression strength and failure strains were approximately the same for control and conditioned specimens. Strength of wrapped specimens (~105000-114000 kPa) was approximately 2.6 times larger than the strength of unwrapped specimens.
- Square glass-wrapped specimens (Figures 3.27-3.29): Again conditioning had little effect on the compressive strength (~62000-66000 kPa), but it reduced the longitudinal strain at failure from about 0.01-0.017 to ~0.007. Strength of wrapped specimens was approximately 1.5 times larger than the strength of unwrapped specimens.
- Round carbon-wrapped specimens (Figures 3.30-3.32): Conditioning reduced compression strengths from about 92000 kPa (unconditioned) to about 80000 kPa (300 cycles) representing about a 15% strength loss. One specimen each in the 150 and 300 cycle batches had unusually high strengths, indicating that one batch of specimens prepared might have had a different strength level. Longitudinal failure strains reduced from about 0.015 to 0.01 (~33%). Strength of wrapped specimens (~95000 kPa) is approximately 2.3 times larger than the strength of unwrapped specimens.

• Square carbon-wrapped specimens (Figures 3.33-3.35): Conditioning reduced compression strengths slightly from about 58000-65000 kPa to about 55000-63000 kPa. Longitudinal failure strains reduced from about 0.007-0.01 to about 0.005. Strength of wrapped specimens (~60000 kPa) is approximately 1.4 times larger than the strength of unwrapped specimens. Note that for square specimens, glass and carbon wraps increased the strength by about the same amount.

The square wrapped specimens had lower compressive strength compared to the round specimens, even though the cross sectional area of the square prisms is higher than that of the round cylinders. This is due to the reduced confinement provided by the wraps for square cross sections and stress concentrations that develop at the corners. Wrapped square prisms always failed by rupture of the wrap at a corner (see Figure 3.36). Note that a reduction of approximately 30% to 40% in failure stress exists between the round and the square specimens. Figures 3.36–3.37 show the failure modes under compression testing.

It was also noted that the square wrapped specimens demonstrated a sudden loss of strength after the peak stress was reached. However, the wraps were undamaged during this loss of strength. The loss of strength is most likely due to the failure of the ineffectively confined regions of concrete. These regions do not experience capacity enhancement resulting from confinement.

A measure of ductility enhancement under compression is the ratio of the mean longitudinal failure strain of wrapped specimens ($\varepsilon_{u, wrapped}$) to the mean longitudinal failure strain of unwrapped specimens ($\varepsilon_{u, unwrapped}$).

The mean failure strains and strain ratios are given in Table 3.2. The ultimate strain for unwrapped specimens is difficult to determine accurately because of the rapid unloading near failure. Therefore, for unwrapped specimens, the strain at peak stress is used. As expected, ductility under compression is enhanced more for round specimens than for square specimens. In general F/T conditioning reduces the ductility. Glass wrapped specimens are more ductile than the carbon wrapped specimens because the ultimate failure strain of glass is higher than that of carbon.

Table 3.2 Ductility enhancement under compression for wrapped specimens

Shape	Wrap	No. of F/T Cycles	Mean Longitudinal Failure Strain (%)	ε _{u, wrapped} /ε _{u, unwrapped}
		0	0.2	1.0
	None	150	0.2	1.0
		300	0.2	1.0
Dawad		0	1.8	9.0
Round	Glass	150	1.2	6.0
		300	1.7	8.5
		0	1.3	6.5
	Carbon	150	1.0	5.0
		300	0.9	4.5
		0	0.2*	1.0
	None	150	0.2*	1.0
		300	0.2*	1.0
Square		0	1.3	6.5
•	Glass	150	1.2	6.0
		300	0.7	3.5
		0	0.8	4.0
	Carbon	150	0.5	2.5
		300	0.5	2.5

^{*} Unwrapped square specimens were not used. It is assumed that the failure strain for unwrapped square specimens is approximately the same as that for unwrapped round specimens

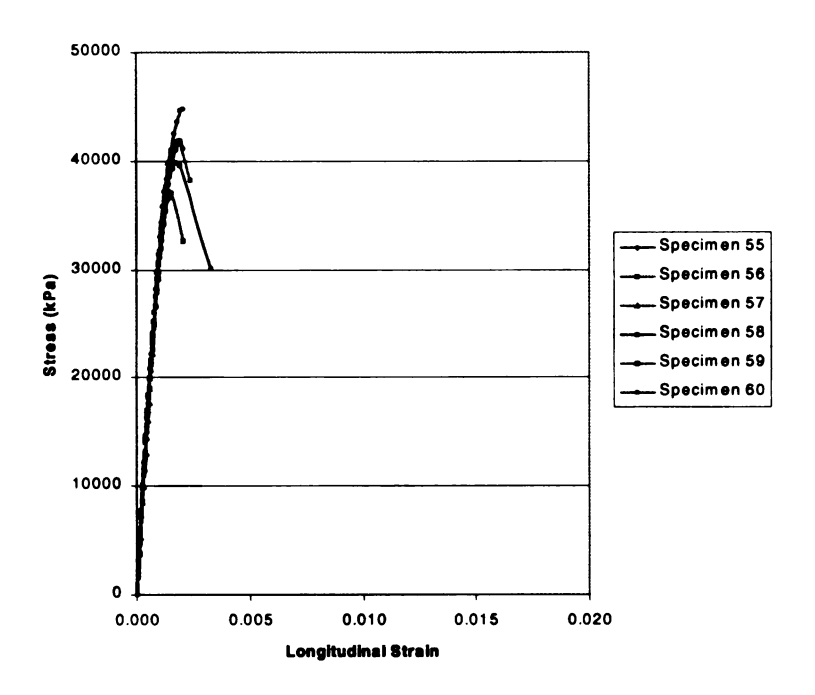


Fig. 3.21 Compressive stress-strain curves for plain, round, control specimens

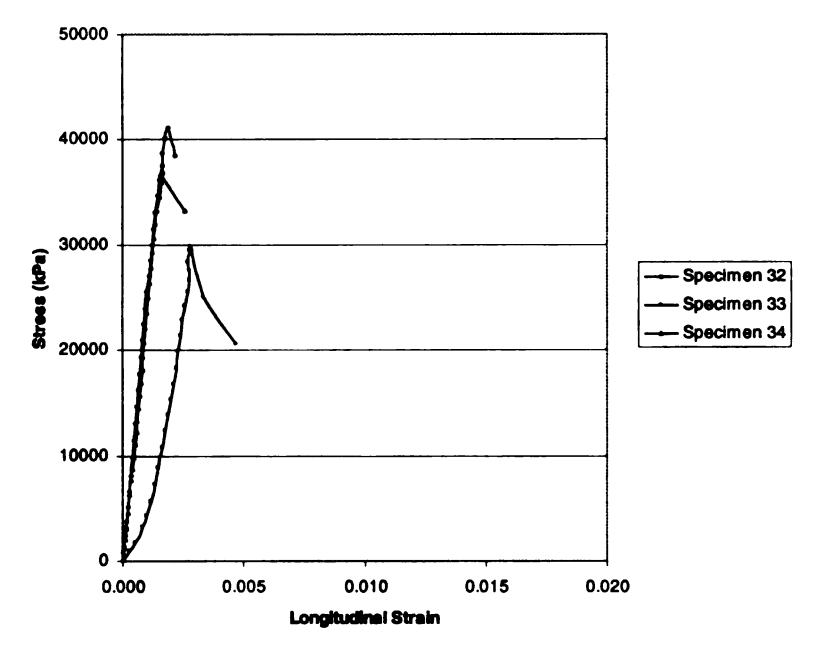


Fig. 3.22 Compressive stress-strain curves for plain, round specimens subjected to 150 freeze-thaw cycles

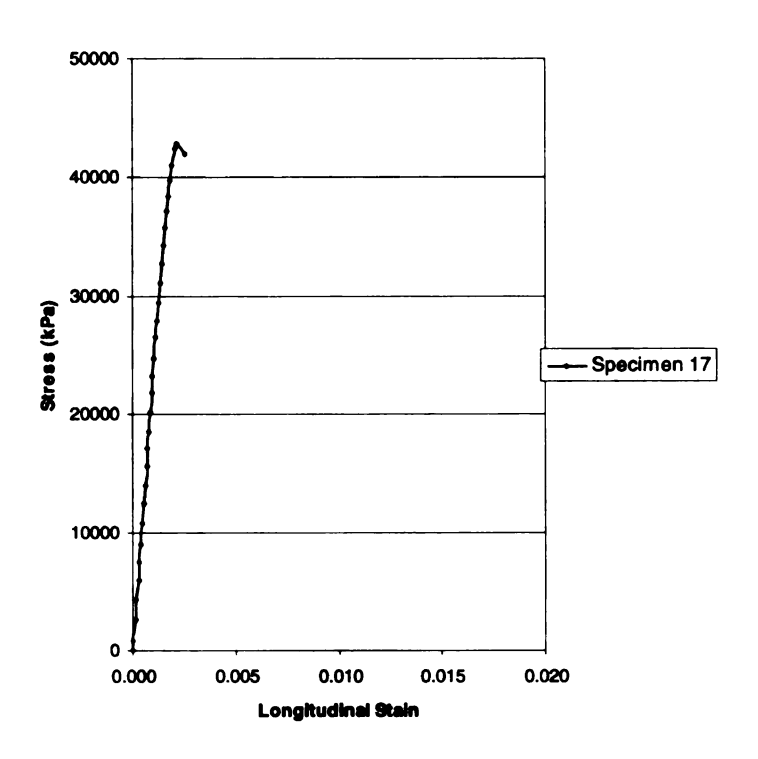


Fig. 3.23 Compressive stress-strain curves for plain, round specimens subjected to 300 freeze-thaw cycles

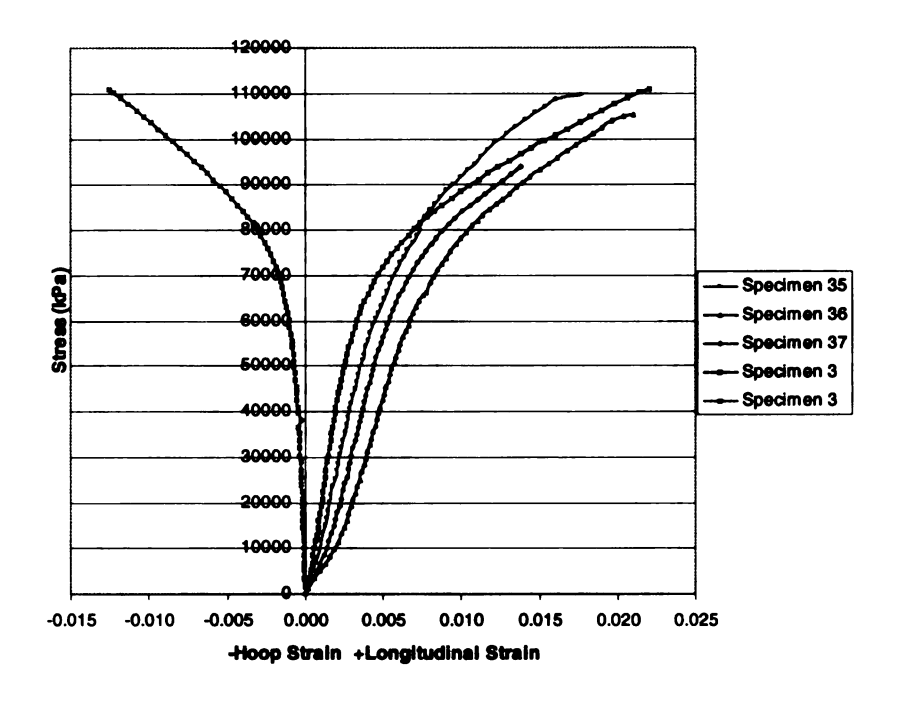


Fig. 3.24 Compressive stress-strain curves and tensile hoop strain for glass-wrapped, round, control specimens

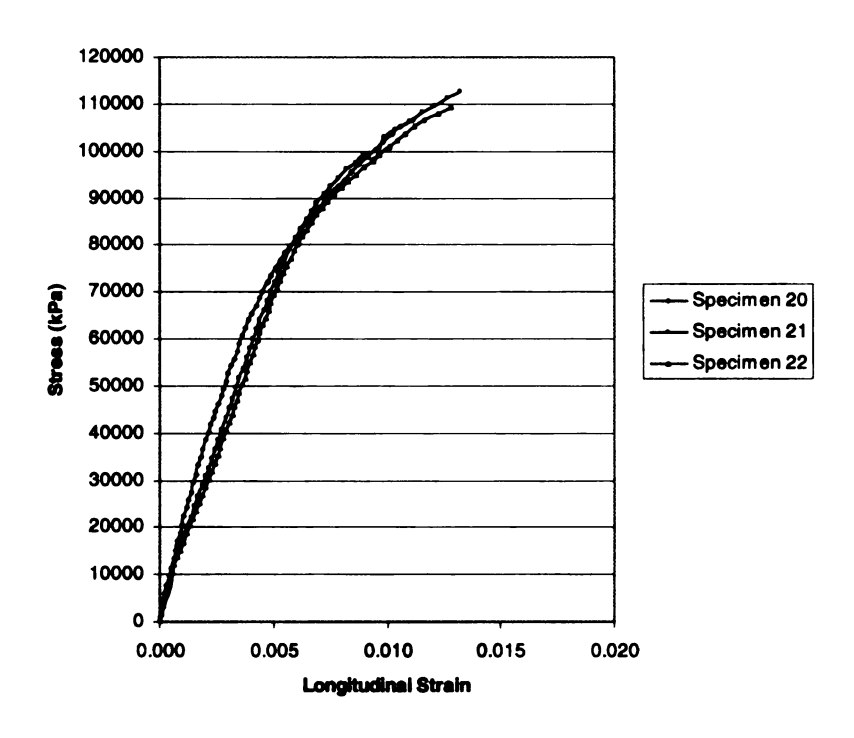


Fig. 3.25 Compressive stress-strain curves for glass-wrapped, round specimens subjected to 150 freeze-thaw cycles

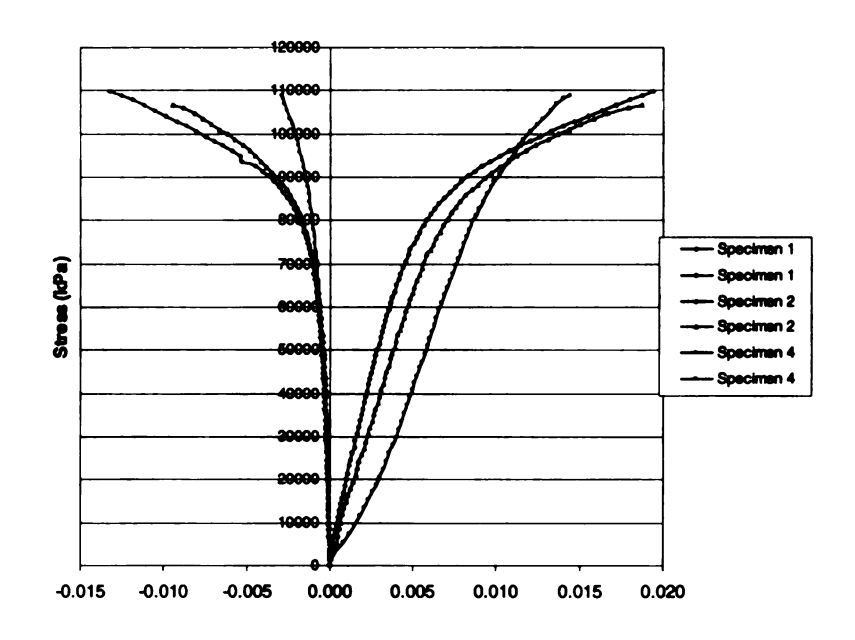


Fig. 3.26 Compressive stress-strain curves and tensile hoop strain for glass-wrapped, round specimens subjected to 300 freeze-thaw cycles

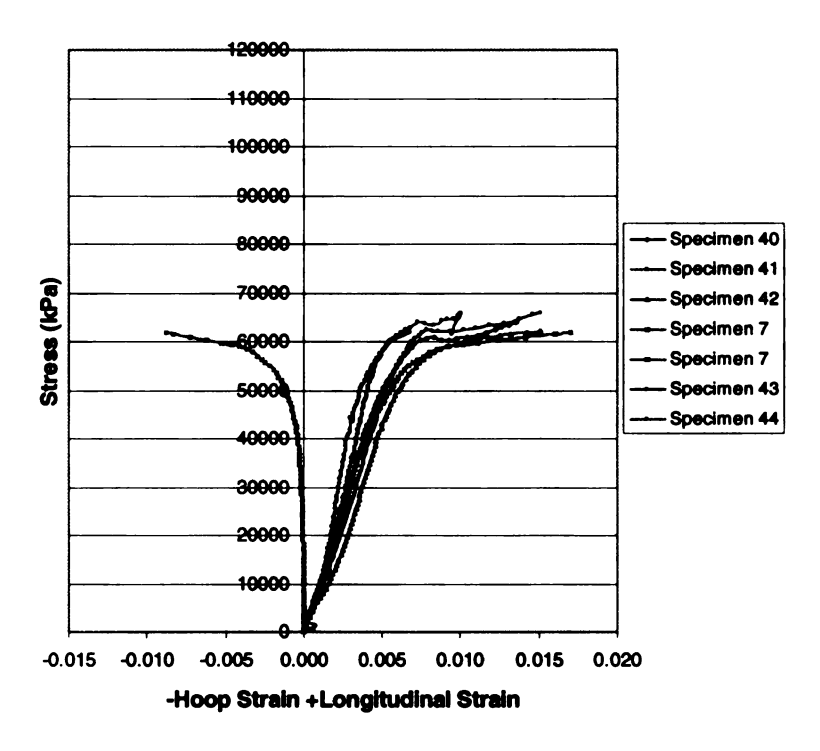


Fig. 3.27 Compressive stress-strain curves and tensile hoop strain for glass-wrapped, square, control specimens

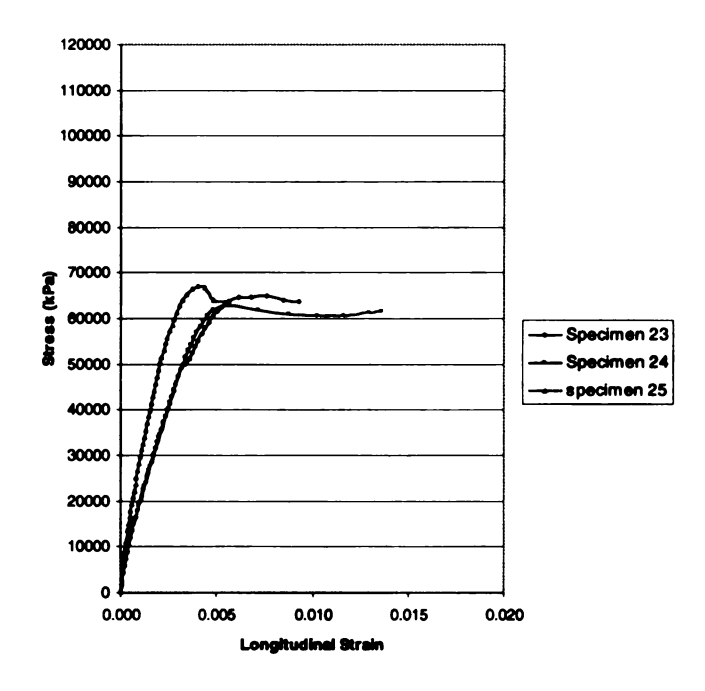


Fig. 3.28 Compressive stress-strain curves for glass-wrapped, square specimens subjected to 150 freeze-thaw cycles

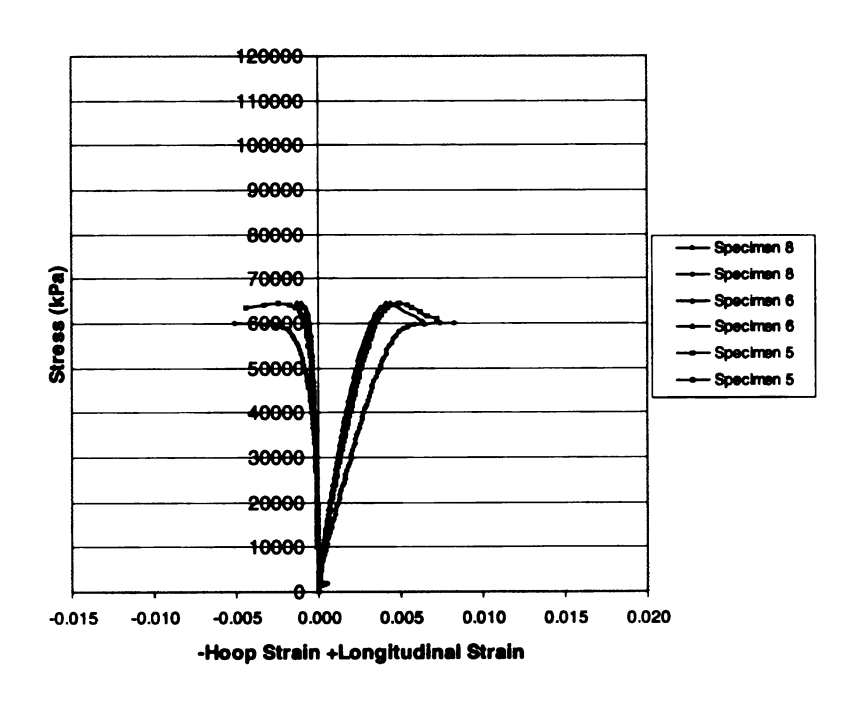


Fig. 3.29 Compressive stress-strain curves and tensile hoop strain for glass-wrapped, square specimens subjected to 300 freeze-thaw cycles

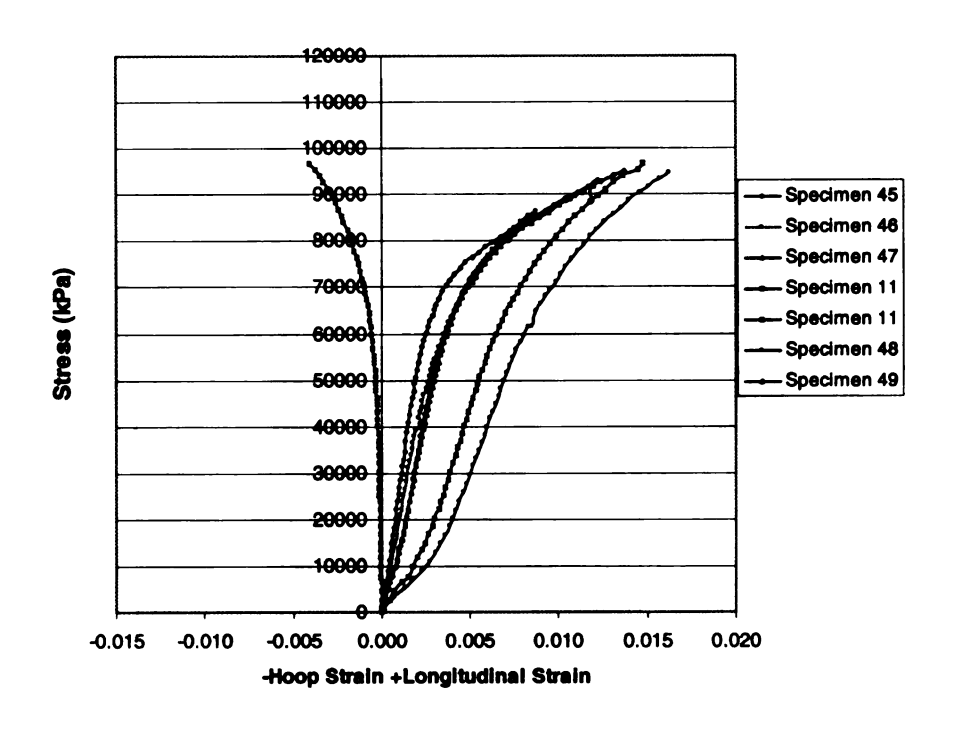


Fig. 3.30 Compressive stress-strain curves and tensile hoop strain for carbon-wrapped, round, control specimens

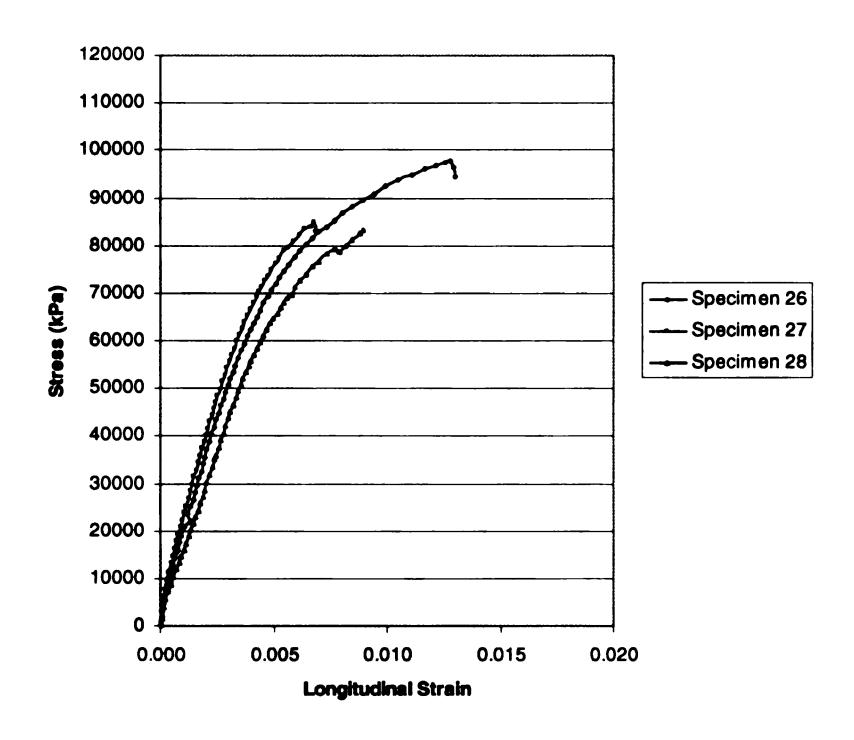


Fig. 3.31 Compressive stress-strain curves for carbon-wrapped, round specimens subjected to 150 freeze-thaw cycles

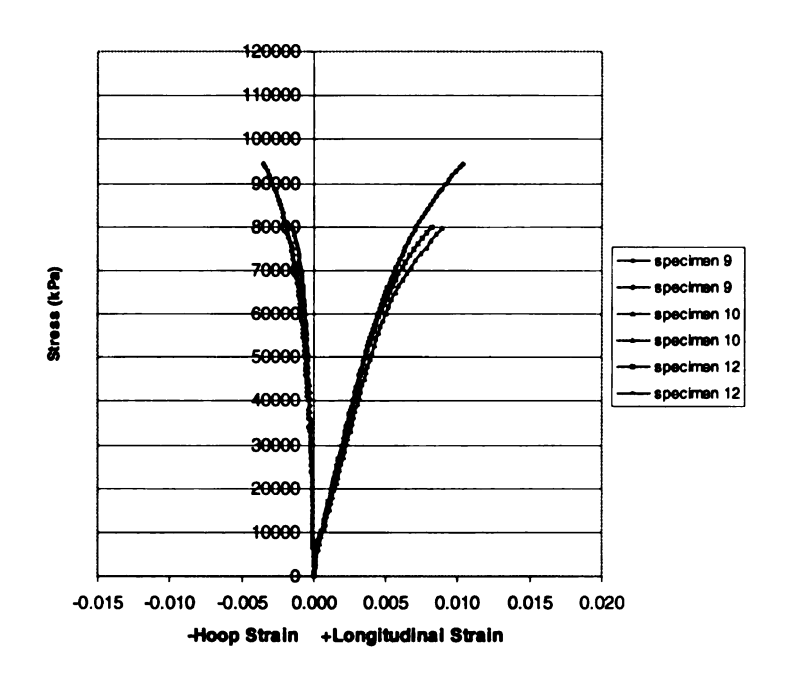


Fig. 3.32 Compressive stress-strain curves and tensile hoop strain for carbon-wrapped, round specimens subjected to 300 freeze-thaw cycles

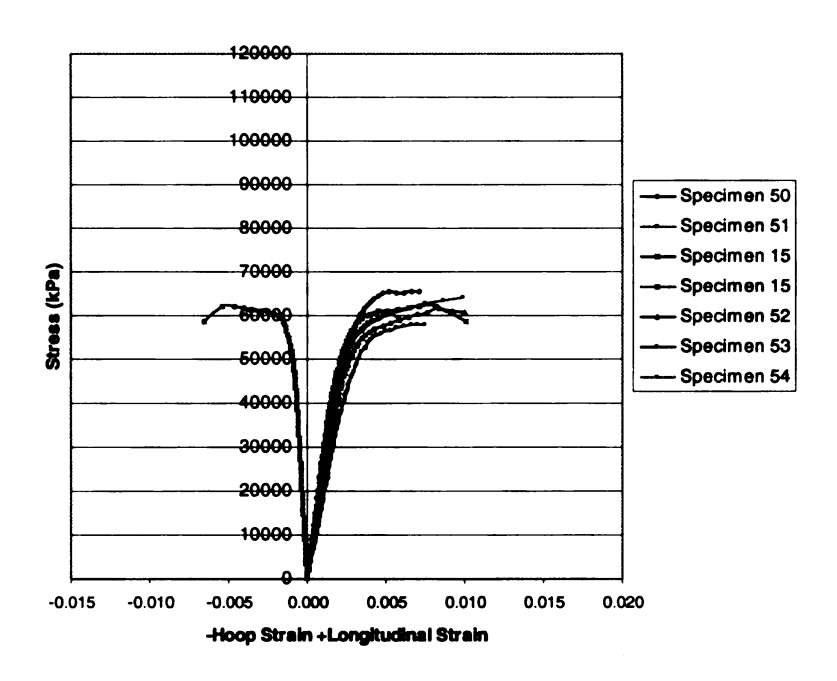


Fig. 3.33 Compressive stress-strain curves and tensile hoop strain for carbon-wrapped, square, control specimens

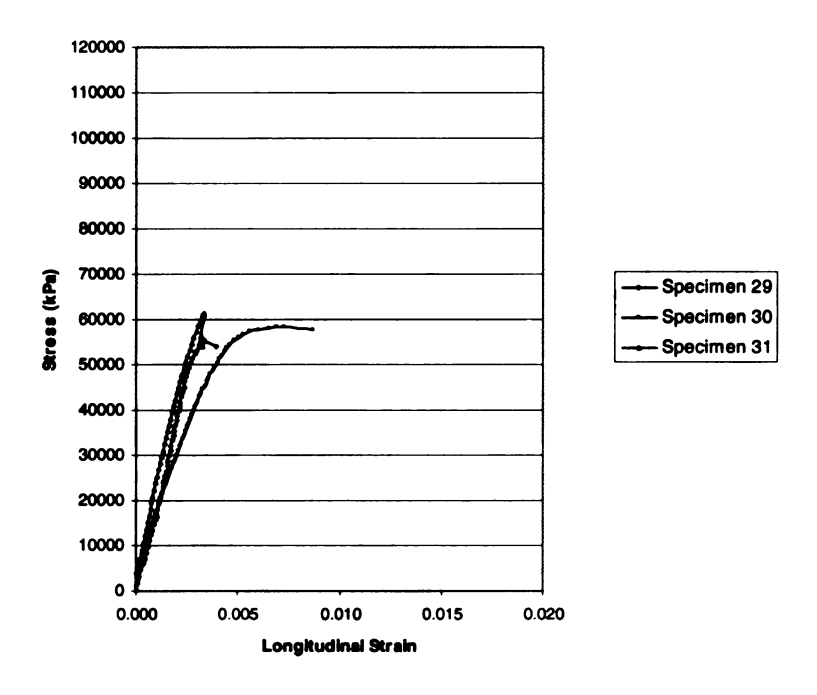


Fig. 3.34 Compressive stress-strain curves for carbon-wrapped, square specimens subjected to 150 freeze-thaw cycles

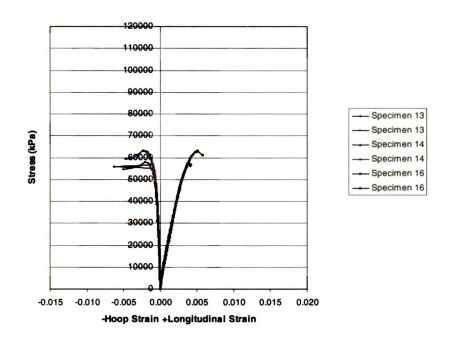


Fig. 3.35 Compressive stress-strain curves and tensile hoop strain for carbon-wrapped, square specimens subjected to 300 freeze-thaw cycles



Fig. 3.36 Failure modes for square specimens under compression testing



(a) Glass wrap



(b) Carbon wrap

Fig. 3.37 Failure modes for round specimens under compression testing

81

3.2.3 Statistical Analysis

Table 3.3 provides the ultimate compression strength, mean, standard deviation and 95% confidence margin for each category of specimens. The cross sectional area lost by the cavity containing Bristar was deducted when calculating the stresses.

Table 3.3 Freeze-thaw summary data

No. of		en Type	w summary data	mpressive S	Strength (kPa)	
F/T Cycles	Shape	Wrap	Individual Specimens	Mean	Standard Deviation	95% Conf. Margin
		Glass	109801, 106451 108858	108370	1727	±4291
	Round	Carbon	94459, 79721 79962	84714	8440	±20967
300		Plain	42875, *, * *	42875	0	NA
	6	Glass	62370, 64362 64551	63761	1208	±3002
	Square	Carbon	57870, 57279 63004	59384	3149	±7822
		Glass	106575, 112621 109316	109504	3027	±7520
	Round	Carbon	97675, 84705 83178	88519	7966	±19788
150		Plain	41080, 29825 36926	35944	5691	±14138
	C	Glass	64881, 61500 66988	64456	2769	±6877
	Square	Carbon	55332, 58231 61421	58328	3046	±7566
		Glass	109504, 104977 114289, 110873 92200 ^b , 89000 ^b	109911	3856	±6136
	Round	Carbon	93254, 90494, 95130 86555, 93174, 96738	92558	3612	±3791
0		Plain	41911, 41696, 40932 39973, 37114, 44818	41074	2531	±2656
	Saves	Glass	65820, 65776, 64148 61856, 62216, 61792	63601	1907	±2002
	Square	Carbon	61623, 58034, 60294 65542, 63967, 62082	61924	2652	±2783

^{*}Specimens that did not survive 300 F/T cycles are denoted with *

^b Data unreliable because specimens did not fail when tested at MSU and were retested at MDOT

The 95% confidence margin is calculated as

 $t^* \frac{s}{\sqrt{n}}$ where s is sample standard deviation and n is sample size

The average compressive strength for the control, 150 freeze-thaw cycle, and 300 freeze-thaw cycle specimens is displayed in Figures 3.38-3.42. A 95% confidence interval is also provided. Due to the small sample sizes and unknown population variances, the t-distribution was used for all hypotheses tests in this report.

The null and alternate hypotheses are:

- Null hypothesis (H_o): There is no significant difference between the means of control and freeze-thaw specimens, i.e., $\mu_{control} = \mu_{F/T}$
- Alternate hypothesis (H_a): There is a significant difference in means of control and freeze-thaw specimens, i.e., μ_{control} ≠ μ_{F/T}

Sample calculations

Comparing results for carbon wrapped, control, round specimens and carbon wrapped, 300 F/T cycle, round specimens, for the former

$$\bar{x}_1 = 92558 \text{ kPa}, S_1 = 3612 \text{ kPa}, n_1 = 6, \text{ and for the latter}$$

$$\bar{x}_2 = 84714 \text{ kPa}, S_2 = 8440 \text{ kPa}, n_2 = 3$$

where \bar{x} , S, and n are sample average, standard deviation, and size, respectively.

A conservative degree-of-freedom is (Neter at el. 1992)

d.o.f.= smaller of
$$n_1$$
 - 1 or n_2 - 1 = 3-1=2 \Rightarrow t* = 4.303 (2 tail test)

The 95% confidence interval for μ control - μ F/T (difference between the mean strength of control specimens not subjected to F/T and the mean strength of specimens subjected to F/T) is

$$\mu_{control} - \mu_{F/T} = \bar{x}_1 - \bar{x}_2 \pm t^* \sqrt{\frac{s_1^2}{n_1} + \frac{s_2^2}{n_2}}$$
 where μ is population mean (Neter at el. 1992)

$$=7844 \pm 4.303 (5091) = (-14063, 29751)$$

Since this confidence interval spans zero, the means are not significantly different and H_o is not rejected.

The results of the hypothesis tests for the various comparisons are given in Table 3.4. The standard deviations and number of samples for each case are given in Table 3.1. The value of t* was 4.303 for all comparisons.

Table 3.4 Results of hypothesis tests (95%) on specimens exposed to freeze-thaw cycles

		No. of F/T	C.I. (kPa) for	Outcome of
Shape	Wrap	Cycles	$\mu_{control} - \mu_{F/T}$	Test
	Plain	150	(-9692, 19952)	Don't Reject Ho
	Fiaili	300	NA	
Round	Glass	150	(-10789, 11603)	Don't Reject Ho
Koulia	Glass	300	(-7799, 10881)	Don't Reject Ho
	Carbon	150	(-16745, 24821)	Don't Reject H _o
	Carbon	300	(-14064, 29751)	Don't Reject H _o
	Glass	150	(-8506, 6796)	Don't Reject H _o
Sauara	Glass	300	(-4339, 4659)	Don't Reject H _o
Square	Carbon	150	(-5290, 12482)	Don't Reject Ho
	Carbon	300	(-6565, 11645)	Don't Reject H _o

At the 95% confidence, means of the compressive strength of freeze thaw specimens are not significantly different from those of control specimens. Similarly, the freeze thaw cycles have no statistically significant effect on the compressive strength of round specimens.

At the 95% confidence level, means of the compressive strength of freeze thaw specimens are not significantly different from those of control specimens. Similarly, the

freeze-thaw cycles have no statistically significant effect on the compressive strength of square specimens.

It should be noted that a reduction in mean compressive strength was observed for carbon-wrapped specimens after freeze-thaw conditioning. This difference is not statistically significant for the sample size used in this study.

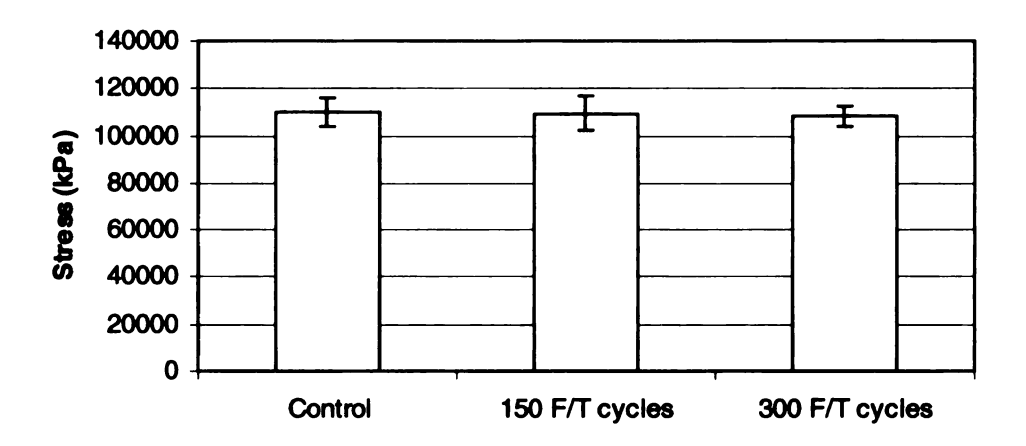


Fig 3.38 Average compressive strength of round glass-wrapped specimens

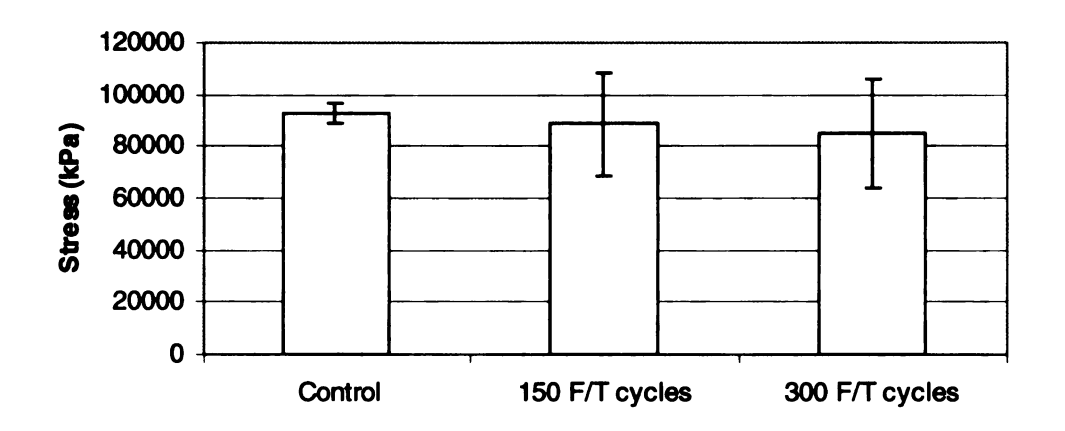


Fig 3.39 Average compressive strength of round carbon-wrapped specimens

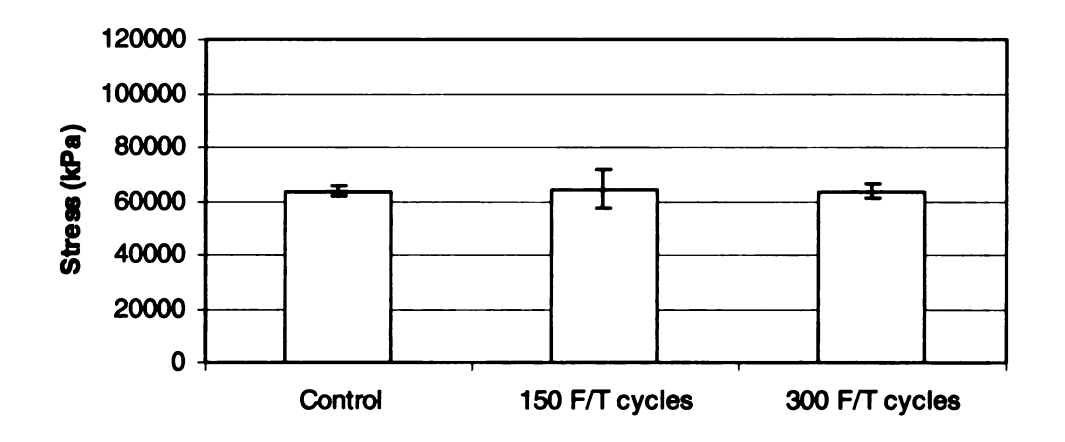


Fig 3.40 Average compressive strength of square glass-wrapped specimens

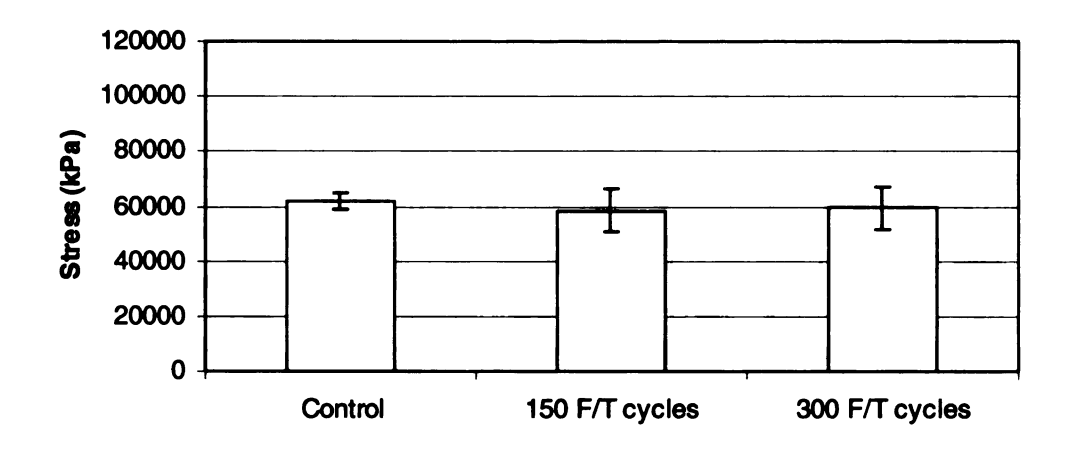


Fig 3.41 Average compressive strength of square carbon-wrapped specimens

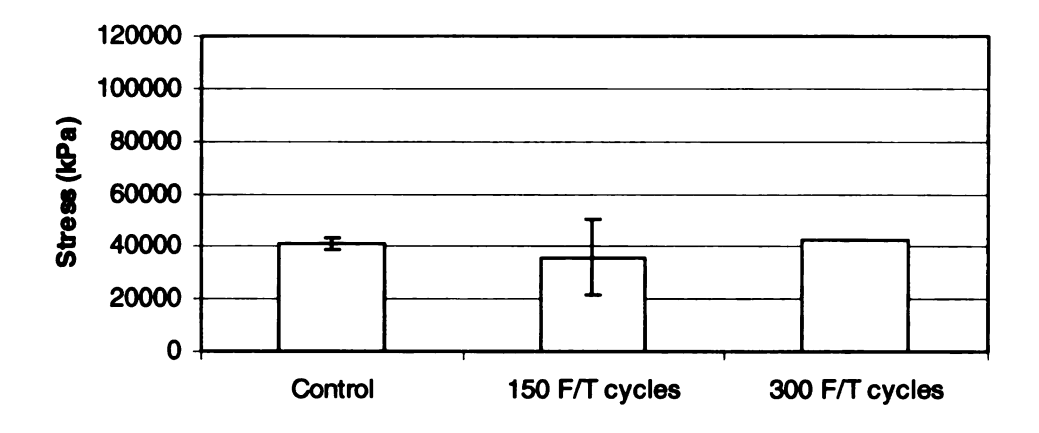


Fig 3.42 Average compressive strength of round plain specimens

3.2.4 Effect of Sustained Loads on Freeze-Thaw Durability of Wraps

Bristar was used in the wrapped specimens to investigate the durability of glass and carbon wraps under sustained load subjected to freeze-thaw cycling. The sustained load simulated the load generated in wrapped columns by corrosion products.

The compression strength of wrapped specimens subjected to freeze-thaw cycling was not significantly different than that of wrapped control specimens. This indicates that the wraps did not sustain any significant damage due to freeze-thaw cycling under sustained load.

3.2.5 Comparison of Measured and Predicted Confined Compression Strength

Equations for predicting the confined compression strength of wrapped circular and rectangular columns are outlined in Section 1.3.6. Here the confined compression strengths predicted by Eq. 1.1 and 1.5 are compared to the measured strengths. Measured FRP panel properties in Tables 2.1 and 3.1 were used in the predictions for unconditioned and conditioned specimens, respectively. The observed and predicted compression strengths are shown in Table 3.5.

Table 3.5 Comparison of measured and predicted confined compression strength

No. of F/T	Chana	Wasan Tama	Predicted	Measured	Predicted/
Cycles	Shape	Wrap Type	Strength (kPa)	Strength (kPa)	Measured
	Round	Glass	127,707	109,910	1.16
0	Round	Carbon	90,542	92,577	0.98
	Square	Glass	87,614	63,601	1.38
	Square	Carbon	67,649	61,924	1.09
	Round	Glass	108,224	108,370	1.00
300	Round	Carbon	85,131	84,714	1.00
300	Square	Glass	77,147	63,761	1.21
	Square	Carbon	64,742	59,384	1.09

Table 3.5 indicates that the Restrepol-DeVino model for rectangular sections over predicts the measured strengths of unconditioned specimens by about 38% and 9% for glass and carbon wrapped specimens, respectively. For unconditioned round glass and round carbon wrapped specimens, the Richart model over predicts the observed strength by about 16% and 2%, respectively. For conditioned specimens, the Restrepol-DeVino model for rectangular sections over predicts the measured strengths by about 21% and 9% for glass and carbon wrapped specimens, respectively. For conditioned round glass and round carbon wrapped specimens, the predicted and the measured strength are almost the same.

3.3 Accelerated Corrosion

3.3.1 Mass Loss Results

Corrosion specimens were removed from the corrosion tank in two phases and measurements of corrosion-induced mass loss were determined. Mass loss data and corrosion depths for the first batch (exposed to 130 days of accelerated corrosion) and the

second batch (exposed to 190 days of accelerated corrosion) is given in Tables 3.6 and 3.7, respectively. The standard deviation and 95% confidence margin for the corrosion depth also are provided. The corrosion depth for each individual bar varied significantly over the length of the bar. The depth reported in Tables 3.6 and 3.7 is the average depth calculated from the total mass loss for each bar. The average corrosion depth over the entire bar can be calculated from the fractional mass loss (FML) of the bar.

$$FML = \frac{w_i - w_f}{w_i}$$

where

 w_i = initial weight of bar

 $w_f = \text{final weight of bar}$

Note that

$$FML = \frac{\rho \pi r_i^2 - \rho \pi r_f^2}{\rho \pi r_i^2} = \frac{r_i^2 - r_f^2}{r_i^2}$$

where ρ is the density.

$$\therefore r_f = r_i \sqrt{1 - FML}$$

Average corrosion depth = $r_i - r_f$

$$= r_i \left(1 - \sqrt{1 - FML} \right)$$

The average corrosion depths for all categories and 95% confidence intervals are displayed in Fig. 3.43.

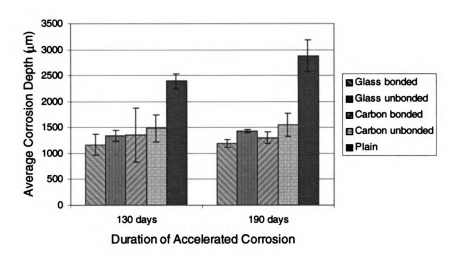


Fig. 3.43 Average corrosion depths due to accelerated corrosion

The following observations are made:

- Corrosion depths for reinforcement in specimens with unbonded wraps were
 approximately 20% more than those in specimens with bonded wraps after 190 days
 of testing. This may be due to water seepage between the concrete and the plastic
 sheet used to create the unbonded condition.
- 2. Wrapping reduced the corrosion depth by 46% 59% after 190 days of testing. It should be noted that the specimens removed after 130 days had corrosion levels of "medium" to "severe" prior to wrapping. The specimens removed after 190 days, on the other hand, had a "low" corrosion level prior to wrapping. This accounts for the higher variability in the corrosion mass loss in the specimens removed after 130 days.

Table 3.6 Mass loss and average corrosion depth for specimens exposed to 130 days of accelerated corrosion

					Aver	age Corros	Average Corrosion Depth (um)	Ê
Specimen	Corrosion Level	14.20	Original	Mass Loss	Individual	1	Standard	95% Conf.
Туре	Before Wrapping		Mass (g)	(6)	Specimens	Mean	Deviation	Margin
	Modium	6	289.0	82.5	982			
	Medicili	11	288.4	81.0	965			
Glass	,	98	281.0	93.0	1156	4460	Ç	ç
pepuoq	FOM	88	286.0	101.5	1250	8	2	3
	Sign 7	45	289.5	119.5	1484			
	Severe	47	288.6	96.4	1168			
	Country	62	289.2	103.2	1257			
Glass	Savaia	64	286.0	110.7	1378	1242	4	7107
pepuoqun	Modium	20	288.7	108.0	1326	245	8	<u>\$</u>
	Medicili	25	289.1	113.8	1405			
	Modium	29	289.3	88.4	1058			
Carbon	Medicili	31	288.0	136.0	1737	1251	330	1524
pepuoq	Colors	20	288.6	121.1	1512	2	676	1702
	Severe	72	288.8	91.2	1097			
	Covoro	54	288.8	121.5	1517			
Carbon	Severe	26	288.9	120.7	1505	1400	161	3301
pepuoqun	Modium	8	286.7	102.5	1260	70+	5	3
	Medicili	92	281.4	127.0	1646			
	Coron	99	286.0	187.0	2614			
	COVOIG	68	289.0	175.5	2370			
	770	38	289.0	176.0	2379			
O Ciclo		40	289.5	190.5	2637	2207	160	4140
3	Modium	2	290.3	181.5	2463	667	3	7
		4	289.4	172.5	2314			
	7110	13	289.4	169.2	2258			
		15	289.3	162.3	2143			

Table 3.7 Mass loss and average corrosion depth for specimens exposed to 190 days of accelerated corrosion

					AVE	age Corrosi	Average Corrosion Depth (µm)	Ê
Specimen	Corrosion Level	Bar No	Original	Mass Loss	Individual	Moon	Standard	95% Conf.
Туре	Before Wrapping	Dal NO.	Mass (g)	(6)	Specimens	MODIL	Deviation	Margin
	1 000	47	289.7	626	1156			
	LOW	19	288.7	98.5	1195			
Glass	,,,,,	25	289.5	101.3	1230	**	62	7.2
ponded	FO#	69	286.5	87.9	1063	- - -	2	H
		82	286.9	103.4	1271			
	8	2	280.9	98.2	1229			
		25	285.8	113.8	1424			
Glass	*	27	289.2	116.3	1439	7071	7	76.
pepuoqun	1	42	290.0	117.8	1456	<u> </u>	-	À
	* 01	44	288.6	114.5	1418			
	, , ,	33	289.2	100.0	1214			
Carbon	LOW.	32	286.4	102.7	1265	1001	6	1440
ponded	1	<i>11</i>	286.6	109.8	1362	/63	2	7
	LOW	62	285.9	108.6	1349			
	1 000	22	289.9	115.2	1420			
Carbon	LOW	54	288.7	116.3	1442	4550	770	ccc
pepuoqun		63	280.4	125.8	1635	200	<u>}</u>	777
	LOW	<u> </u>	280.9	130.3	1701			
	700	9	288.7	187.7	2594			
O ricio	LOW	2	285.8	204.0	2951	Oggc	103	702
B) out	23	288.4	208.8	3014	2007	2	2
		22	289.7	207.2	2961			

3.3.2 Statistical analysis

The following hypotheses are tested for the specimens exposed to 190 days of accelerated corrosion.

Null hypothesis (H_o): There is no significant difference between the mean corrosion depth for bonded and unbonded specimens with the same type of wrap.
 i.e., H_o: μ bonded = μ unbonded
 Alternate hypothesis (H_a): There is a significant difference between the mean

corrosion depth for bonded and unbonded specimens with the same type of wrap.

- i.e., . H_a: µ bonded ≠ µ unbonded
- 2. Null hypothesis (H₀): There is no significant difference between the mean corrosion depth for carbon bonded and glass bonded specimens or between carbon unbonded and glass unbonded specimens, i.e, H₀: μ carbon = μ glass Alternate hypothesis (Hₐ): There is a significant difference between the mean corrosion depth for carbon bonded and glass bonded specimens or carbon unbonded and glass unbonded specimens, i.e., Hₐ: μ carbon ≠ μ glass

Sample calculations

Comparing results for carbon wrapped bonded specimens and carbon wrapped unbonded specimens, for the former

$$\bar{x}_1 = 1297 \,\mu\text{m}, S_1 = 70 \,\mu\text{m}, n_1 = 4$$
, and for the latter

$$\bar{x}_2 = 1550 \,\mu\text{m}, S_2 = 140 \,\mu\text{m}, n_2 = 4$$

where \bar{x} , S, and n are sample average, standard deviation, and size, respectively.

A conservative degree-of-freedom is

d.o.f.= smaller of
$$n_1$$
 - 1 or n_2 - 1 = 4-1=3 \Rightarrow t* = 3.182 (2 tail test)

The 95% confidence interval for μ_{bonded} - $\mu_{unbonded}$, using a 2-sample t is

$$\mu_{\text{bonded}} - \mu_{\text{unbonded}} = \overline{x_1} - \overline{x_2} \pm t^* \sqrt{\frac{s_1^2}{n_1} + \frac{s_2^2}{n_2}}$$
 where μ is population mean

$$= -252 \pm 3.182 (78) = (-500, -3.4)$$

Since this confidence interval does not span zero, the means are significantly different and H_o is rejected.

The results of the hypothesis tests for the various comparisons are given in Table 3.8. The standard deviations and number of samples for each case are given in Table 3.7. The value of t* was 3.182 for all comparisons.

Table 3.8 Results of hypothesis tests (95%) on specimens exposed to accelerated corrosion

Wrap Type	C.I. for μ_{bonded} - $\mu_{unbonded}$ (μm)	Outcome of Test
Glass	(-343, -144)	Reject H _o
Carbon	(-300, -3.4)	Reject H _o
FRP/Concrete Adhesion	C.I. for μ_{carbon} - μ_{glass} (μm)	Outcome of Test
Bonded	(-41, 253)	Don't reject H _o
Unbonded	(-108, 340)	Don't reject H _o

The following observations are made:

• The mean corrosion depths for bonded and unbonded specimens are different at the 95% significance level. The bonded wrap is more effective in reducing the rate of corrosion than the unbonded wrap.

The mean corrosion depths for specimens with glass and carbon wraps for
either the bonded or unbonded conditions are not significantly different. Both
wrap systems, glass and carbon, are equally effective in reducing the
corrosion rate.

3.3.3 Strain Measurements for Accelerated Corrosion Test

The wrapped corrosion specimens were fitted with strain gages. Two gages oriented in the circumferential direction were mounted at mid-height were mounted on each specimen. On some specimens, the strain gages were installed near the anodes, the site of corrosion and subsequent volume expansion. For others, strain gages were installed between the anode and cathode. The purpose of this arrangement was to investigate the variation in strain gage readings with respect to the site of corrosion. The observations below are for the specimens exposed to 190 days of accelerated corrosion:

- For glass bonded specimens (Figure 3.44), it is evident that the strain reading is considerably higher for specimen 7 (approximately 4200 micro strain) for which the gages are located at the anodes. For other specimens the gages (installed between the anodes and cathodes) are consistent at about 900 micro strain. Based on the average strains developed at gages not located at the anodes, the confining pressure is estimated to be about 950 kPa away from the anodes, but much higher near the anodes.
- For glass unbonded specimens (Figure 3.45), all strain gage readings are about 1500 micro strain regardless of the gage location. This yields a confining pressure of about 1600 kPa (scaled directly from Table 2.5 as 5644.9 x 1500/5310). The unbonded

condition, created by a plastic sheet located between the wrap and the specimens, allows the wrap to expand more freely instead of concentrating the strains near the anode as in the bonded wraps.

- For carbon bonded specimens (Figure 3.46), the results are similar to those for the glass bonded specimens. The strains developed for specimen 13 (for which the gages are located at the anodes) are higher than the gage readings for the other specimens (for which gages are located between the anodes and the cathodes) and is approximately 1800 micro strain. The average strain value where gages are located between the anodes and the cathodes is about 1300 micro strain, and yields a confining pressure of about 1150 kPa.
- For carbon unbonded specimens (Figure 3.47), all strain gage readings are about the same regardless of the gage location and approximately 1300 micro strain. This yields a confining pressure of about 1150 kPa.

Figures 3.44 to 3.47 indicates that wrap strains for bonded specimens with both types of wraps tend to level off with time. One explanation could be that the stress concentration near the anodes in the bonded wraps is more effective in containing the corrosion-induced crack and reducing the corrosion rate. The slip of unbonded wraps and the resulting redistribution of strain along the entire wrap may be less effective at containing the large corrosion-induced crack near the anodes.

Figure 3.48 shows strains at gages placed on the anodes, and indicates the following:

• Even though the corrosion rate for the bonded specimens is lower than that for the unbonded specimens, hoop strains developed near the anodes for specimens with

bonded wraps are higher than those developed with unbonded wraps. In the case of unbonded specimens, the entire wrap (to some degree) absorbs the volume expansion associated with corrosion of the reinforcement, while for bonded wraps the strain is localized near the corrosion-induced crack at the anode.

corrosion of reinforcement seems to have a more direct effect on strain values generated in glass bonded wraps compared to those with carbon bonded wraps. The maximum strain for glass bonded wraps is approximately 4000 micro strain compared to 1800 micro strain for carbon bonded wraps. It should be noted that variations in strain readings also could be influenced by initial wrap tightness around the specimens and by crack width and direction. Although the wrap strain near the anode is large, there is no danger of stress rupture in the glass since the stress rupture limit (with a safety factor of 1.67) is about 0.2 ε_u = 4000 micro strain. Further, in real columns the strain near corroding bars will be significantly smaller because of the larger column diameter and concrete cover.

Note that the wrap strains measured in the accelerated corrosion test away from the anodes are lower than the wrap strains generated by Bristar in the freeze-thaw test.

Thus the internal expansive force used in the freeze-thaw test was very conservative.

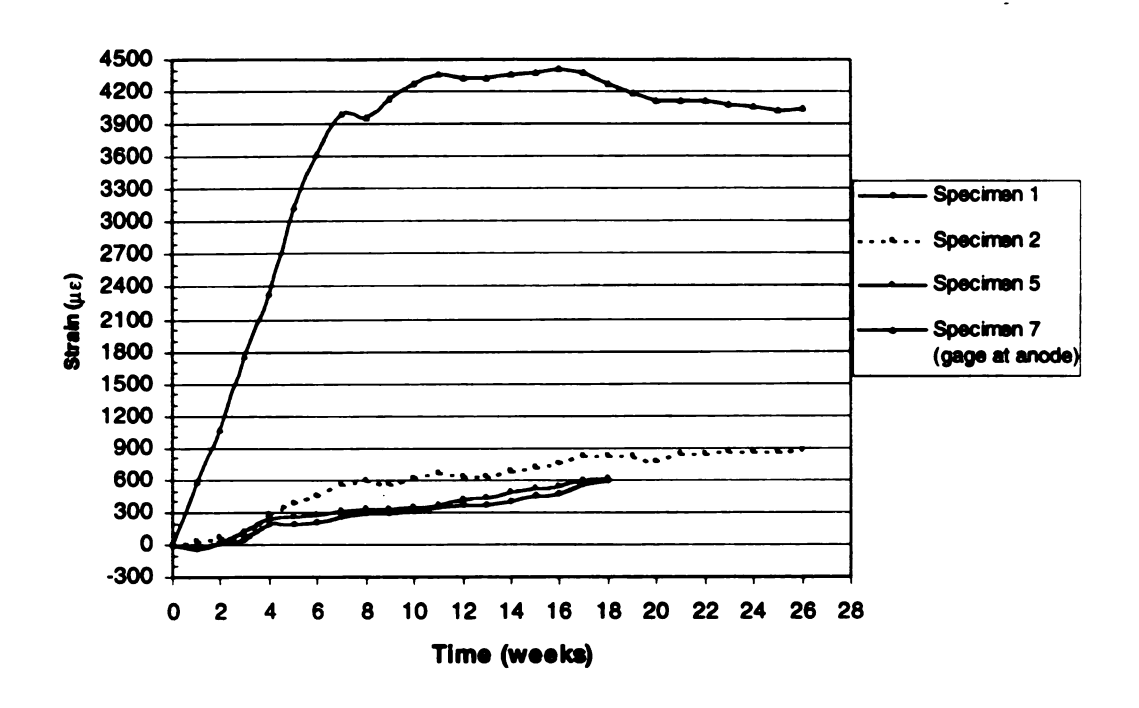


Fig. 3.44 Hoop strains in bonded, glass-wrapped specimens

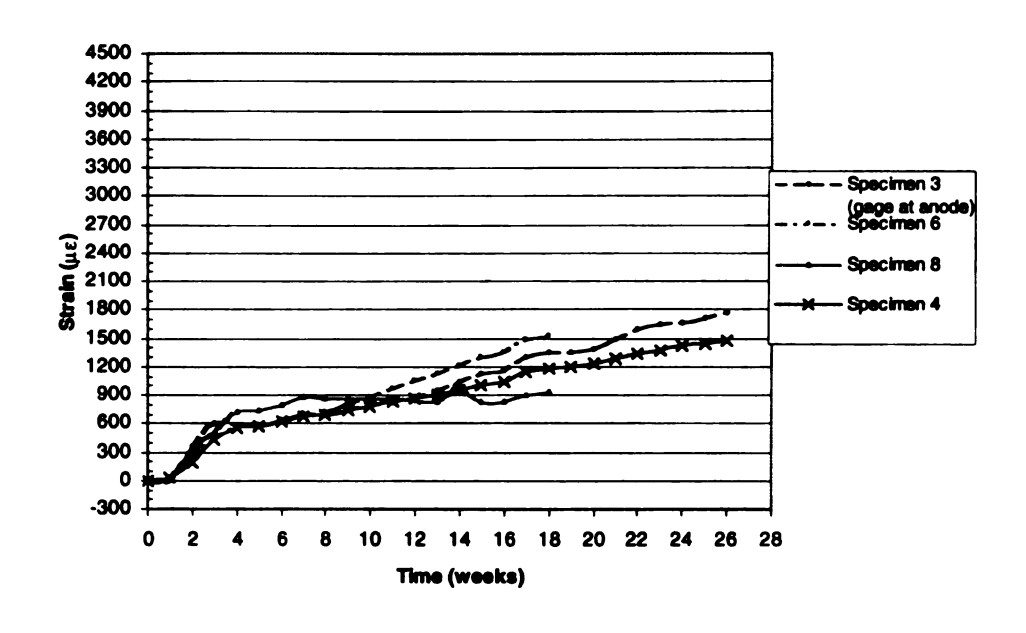


Fig. 3.45 Hoop strains in unbonded, glass-wrapped specimens

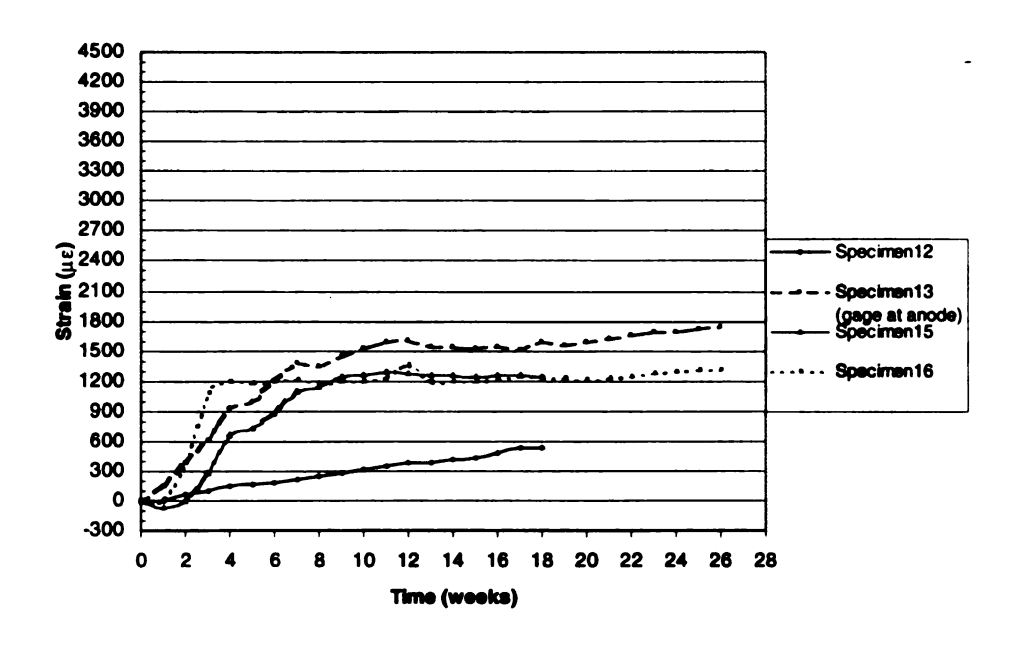


Fig. 3.46 Hoop strains in bonded, carbon-wrapped specimens

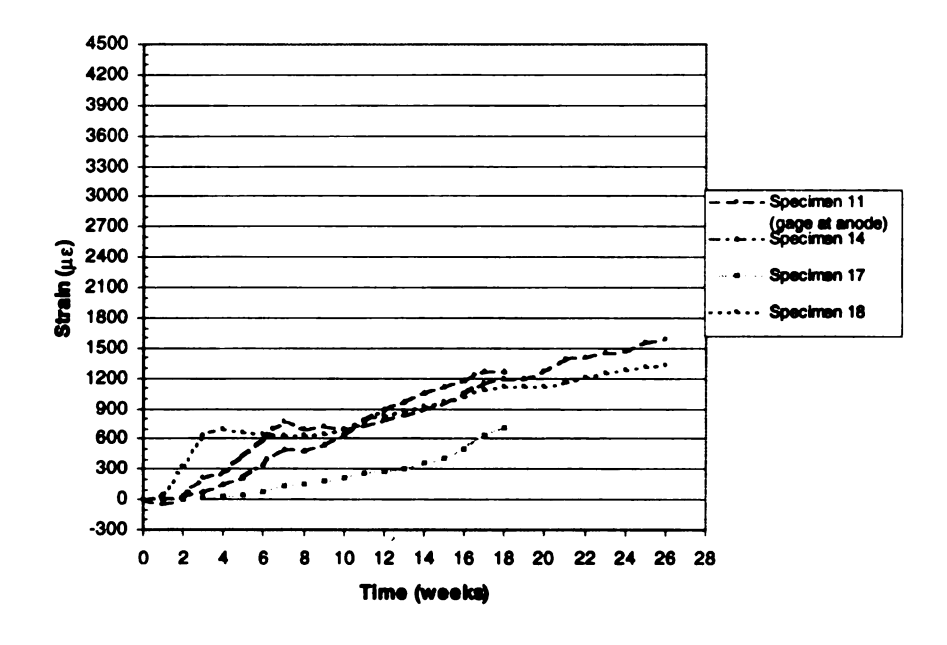


Fig. 3.47 Hoop strains in unbonded, carbon-wrapped specimens

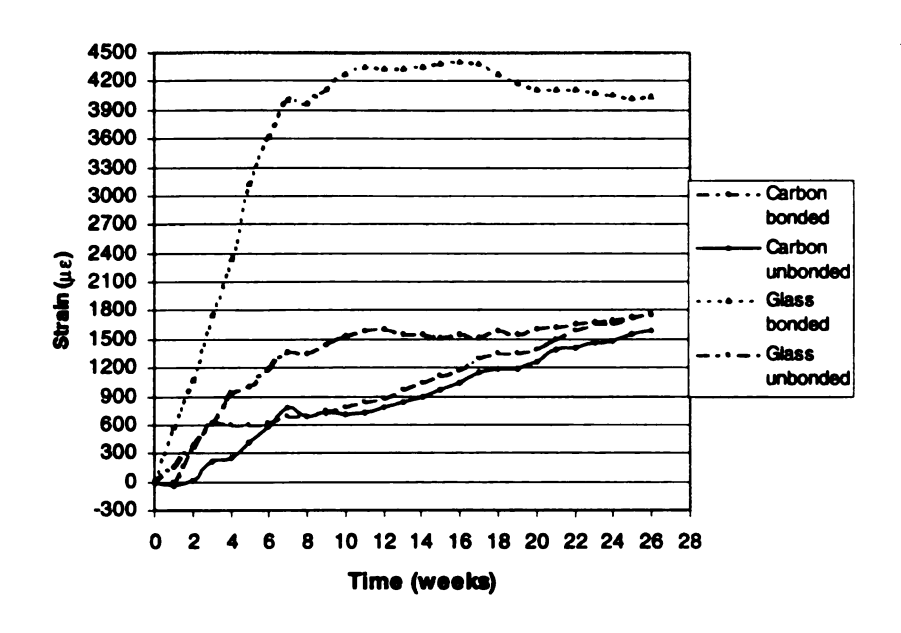


Fig. 3.48 Hoop strains in glass and carbon-wrapped specimens, gages at the anodes

Chapter 4 Summary, Conclusions and Recommendations

Experiments were conducted to assess the effects of using glass and carbon FRP wraps in rehabilitating corrosion-damaged columns. Issues that were explored are: (1) effect of freeze-thaw and wet-dry cycles on the properties of FRP panels; (2) freeze-thaw durability of concrete square and cylindrical specimens wrapped with glass and carbon FRP and subjected to an internal expansive force; and (3) effect of wrapping on the rate of corrosion in an accelerated corrosion test.

4.1 Freeze-Thaw Test

Strength and durability tests were carried out on wrapped circular (diameter of 152 mm by 305 mm high) and square cylinders (152 mm by 152 mm by 305 mm high). The primary purpose of the tests was to determine the endurance of the jackets under simulated cyclic environmental conditions. Creation of an internal bursting force similar to that produced by corroding steel was attempted. This was done by fabricating specimens with a hole in the longitudinal direction and filling it with an expanding cement known as Bristar (used for silent demolition). Chloride was impregnated into the cylinders during casting in order to simulate deteriorated concrete. Compression strength tests were carried out on plain control cylinders as well as wrapped test specimens after 150 and 300 cycles of freeze-thaw conditioning. A total of sixty specimens were utilized

in the freeze-thaw test. The strength of FRP panels subjected to 300 freeze-thaw cycles also was investigated.

Bristar was used in the wrapped specimens to investigate the durability of glass and carbon wraps under sustained load and subjected to freeze-thaw cycling. The sustained load simulated the load generated in wrapped columns by corrosion products. The means of the compressive strength of freeze thaw specimens are not significantly different from those of control specimens at the 95% confidence level. This holds both for carbon and glass wraps, and for specimens with round and square cross sections. It should be noted that a reduction in mean compressive strength was observed for carbon-wrapped specimens after freeze-thaw conditioning. Based on our sample size and statistical analysis, this difference is not significant. The results indicate that the wraps did not sustain significant damage due to freeze-thaw cycling under sustained load.

The square wrapped specimens had lower compressive strength compared to the round specimens, even though the cross sectional area of the square prisms is higher than that of the round cylinders. This is due to the reduced confinement provided by the wraps for square cross sections and stress concentrations that develop at the corners. Wrapped square prisms always failed by rupture of the wrap at a corner. A reduction of approximately 30% to 40% in the failure strength was observed for the square specimens compared to the round specimens. This loss of strength due to reduced confinement in square specimens is reasonably accounted for by Restrepo and Devino's (1996) model of confinement. Richart's model of confinement (1928) predicts the strength of round wrapped specimens reasonably well.

Compression strength of wrapped specimens is 1.4 to 2.6 times larger than the strength of unwrapped specimens for square and round sections, respectively. Ductility of wrapped specimens under compression is 4 to 9 times larger than that of unwrapped specimens for square and round sections, respectively.

4.2 Accelerated Corrosion Test

Tests were conducted on twenty-four 152 mm x 305 mm concrete cylindrical specimens. A water/cement ratio of 0.6 and 2% Cl⁻ ion by weight of cement (intended to simulate chloride contaminated columns) were used in the mix. Initially all specimens were partially submerged in 3% NaCl solution and subjected to electrically induced corrosion until cracks were visible on the exterior surfaces. After the initial corrosion stage, specimens were wrapped with glass and carbon FRP. Specimens were then placed in a tub and soaked in 3% NaCl solution for one hour each day while the electrically induced accelerated corrosion continued for several weeks. Some specimens were removed after 130 days and others after 190 days. The merit of using unbonded wraps to minimize localized wrap strains near reinforcing bars was investigated. The ASTM G1 mass loss test was performed to determine the total corrosion of reinforcement in unwrapped and wrapped specimens. The strength of FRP panels exposed to 190 wet-dry cycles with salt water also was determined.

The mean corrosion depths for glass and carbon wraps are not significantly different for either the bonded or unbonded conditions. Both wrap systems, glass and carbon, are equally effective in reducing the corrosion rate. Wrapping reduced the corrosion depth by 46% - 59% after 190 days of testing.

The mean corrosion depths for bonded and unbonded specimens are significantly different after 190 days of accelerated corrosion. The bonded wrap is more effective in reducing the rate of corrosion than the unbonded wrap. Corrosion depths for reinforcement in specimens with unbonded wraps were approximately 20% more than those in specimens with bonded wraps after 190 days of testing. This may be due to water seepage between the concrete and the plastic sheet used to create the unbonded condition.

Wrap strains for bonded specimens with both types of wraps tend to level off with time. One explanation could be that the stress concentration near the anodes in the bonded wraps is more effective in containing the corrosion-induced crack and reducing the corrosion rate. The slip of unbonded wraps and the resulting redistribution of strain along the entire wrap may be less effective at containing the large corrosion-induced crack near the anodes.

4.3 Recommendation for Field Installation

It is evident from the experimental study conducted that both carbon and glass wrap systems are equally resistant to freeze-thaw cycles and reduce the corrosion rate by about the same rate. Therefore, three layers of glass wrap or two layers of carbon wrap may be used to repair Michigan bridge columns. Reducing the number of layers may also be feasible, but it is not possible to provide any recommendation about this without additional studies.

The preferred wrap system will most likely depend on the material and installation cost rather than performance issues. However, it should be noted that many studies indicate strength degradation of glass FRP in an alkaline and/or humid

environment under elevated temperature. Thus in regions with long periods of hot and humid conditions, carbon FRP may be preferable to glass FRP.

It is also recommended that a non-destructive technique or coring be used every ten years to monitor the condition of the concrete inside the wrap.

4.4 Cost Saving of using FRP Wraps

The estimated cost for the conventional chip and patch repair technique that is currently used by the MDOT is approximately \$500-\$725/m² of repaired column surface. The estimated cost of the glass and carbon wrap systems used in this research study as provided be the respective suppliers is provided in Table 4.1.

Table 4.1 Estimated material and installation cost for Tyfo-S glass and MBrace carbon wrap systems

Wrap Type	Material Cost /m²/layer	Installation Cost /m ² /layer	No. of Layers	*Surface Prep./ m ²	Total Cost/ m ²
Glass	\$54	\$54	3	\$101	\$425
Carbon	\$75	\$54	2	\$101	\$360

^{*} Estimated cost of surface preparation prior to wrap installation was provided by MDOT

Another cost factor that should be considered in this analysis is the expected life span of the repair. It is estimated that the conventional chip and patch repair currently used has a lifetime of approximately five years. The FRP wrap system on the other hand, should last at least twice as long.

Factoring in life expectancy and assuming an inflation rate of 3% per year for materials and labor, Table 4.2 provides total costs estimated for conventional repair (chip and patch) and FRP wraps systems (glass and carbon) over a ten-year period beginning

now. Assuming 10 m² of repaired surface area for a typical bridge column, the cost saving over ten years by using an FRP wrap is estimated to be between \$6,550 and \$12,050 per column. With the large number of bridge columns in need of repair in Michigan, this cost saving clearly justifies the use of FRP wraps for the repair.

Table 4.2 Estimated total cost of different repair techniques over ten years

Conventional Repair	\$1080-\$1565/ m ²
Glass FRP Wrap (3 layers)	\$425/ m ²
Carbon FRP Wrap (2 layers)	\$360/ m ²

Chapter 5 Field Installation and Future Studies

5.1 Field Instrumentation

5.1.1 Corrosion Monitoring of Field Columns

Six corrosion probes were installed on six corrosion damaged field columns in the summer of 1999. These columns had considerable surface spalling and reinforcement was exposed at several locations. Each column was also fitted with two pre-weighed #13 reinforcing steel bars approximately 305 mm long to measure mass loss. The corrosion probes and the steel bars were located at the same level of the existing column reinforcement steel and about two meters above the roadway surface. The initial weights of the bars are given in Table 5.1. These columns are located on Lansing Road in Lansing, Michigan under the I-96 overpass (Bridge ID S09&S10 of 23 (52)). Columns one through three are located under the westbound overpass while columns four through six are located under the eastbound overpass. After superficially repairing the column surface spalls by patching (chloride was added to the patch to match existing chloride content of the column), two columns were wrapped with two layers of carbon fiber sheets, two were wrapped with three layers of glass fiber sheets and two were left unwrapped.

Table 5.1 Initial weight of corrosion bars installed in field columns

Column No.	Column 1 Glass wrapped		ł	Column 2 Carbon wrapped		mn 3 itrol
Bar No.	1	2	3	4	5	6
Bar Wt. (g)	252.09	276.14	270.70	263.80	263.58	271.13
Column No.		mn 4 itrol	Column 5 Glass wrapped			mn 6 wrapped
Bar No.	7	8	0	10	11	10
Dai 110.	,	•	9	10	11	12

The corrosion probes manufactured by Rohrback Cosasco Systems, Inc. (Santa Fe Springs, California) are based on an electrical resistance measurement system. This system is simple to install, directly measures the total corrosion, does not need regular measurements, is smaller, easy to transport, and costs about \$5,500 for six probes and the readout measurement device.

Corrosion data is being collected about twice a month. Due to the short duration since the corrosion probes were installed, the data is not significantly different from the initial readings. Corrosion monitoring is scheduled to continue for about 10 years. At that time, the reinforcing bars installed to monitor mass loss will be cleaned and mass loss analysis will be conducted.

Figs. 5.1 and 5.2 show a column condition before and after minor surface repairs, respectively. Fig. 5.3 shows a corrosion probe and pre-weighed reinforcing bars used for monitoring mass loss. Figs. 5.4 and 5.5 show the field installation of glass and carbon wraps, respectively. Fig. 5.6 shows columns after repairs were completed. The carbon wrapped column (nearest to camera) is yet to be painted while the glass wrapped column (middle one) has been painted.



Figs. 5.1 Column condition before surface repairs



Figs. 5.2 Column condition after surface repairs



Fig. 5.3 Corrosion probe and reinforcing bars for monitoring mass loss



Fig. 5.4 Field installation of glass wrap to selected columns



Fig. 5.5 Field installation of carbon wrap to selected columns



Fig. 5.6 Completed installation of glass and carbon wraps (glass wrapped column in the background with top coat and final paint layers applied).

Appendix D provides provisions for field installation as recommended by the wrap manufacturers — glass wrap system by Tyfo-S and carbon wrap system by Master Builders.

5.1.2 Results of Field Monitoring

Wrapped and unwrapped columns in the field have been monitored for 10 months using corrosion probes. So far no significant corrosion activity has been detected.

5.1.2.1 Calculation of Corrosion Rate

The corrosion rate for the concrete monitoring corrosion probes manufactured by Rohrback Cosasco is calculated as follows:

Corrosion Rate (mils/year) =
$$\frac{\Delta Dial \text{ Re } ading}{\Delta Time(Days)} \times 0.365 \times \text{Span}$$

The corrosion probe used in the filed columns (Model 650-0-T50) has a span of 25 mils.

References

ACI (2000). "Guide for the Design and Construction of Externally Bonded FRP Systems for Strengthening Concrete Structures." ACI Committee 440 R.

Alampalli, S., O'Connor, J., and Yannotti, A. (1999). "Advancing Composites." *Journal of Civil Engineering*, December A1-A7.

Allen, M. L. (1995). "Probability of Corrosion Induced Cracking in Concrete." Cement and Concrete Research, Vol.25, No. 6, 1179-1190.

Almusallam, T. H., Al-Salloume, Y. A., and Alsayed, S. H. (2000). "Durability of Concrete Cylinders Wrapped with GFRP Sheets at Different Environmental Conditioning." Seventh Annual International Conference on Composites Engineering, 27-28.

Arya C. and Sa'id-Shawqi, Q. (1996). "Factors Influencing Electrochemical Removal of Chloride from Concrete." Cement and Concrete Research, Vol. 26, No. 6, 851-860.

ASTM, 1990. "Standard Practice for Preparing, Cleaning, and Evaluating Corrosion Test Specimens." ASTM Designation: G 1-90 (Reapproved 1994), 9-15.

Brockenbrough, R. L. and Gallagher, W. P. (1985). "Effect of Clamping Pressure and Joint Geometry on Corrosion Induced Bowing and Distortion of Bolted Joints in Weathering Steel." *Journal of Construction Steel Research*, 213-238.

Chajes, Mertz, Thomson, and Farschman (1994). "Durability of Composite Material Reinforcement." Proceedings, Third Material Engineering Conference, ASCE, 598-605.

De Wilde, W.P. (1988). Proceedings of the International Conference on Computer Aided Design in Composite Material Technology. Computational Mechanics Publication, Springer-Verlag Berlin Heidelberg.

Debaiky, A. and Green, G., and Hope, B., (1999). "FRP Rehabilitation of Corrosion-Damaged Concrete Structures." *Proceedings of the 44th International SAMPE Symposium*, May 23-27.

Demers, M. et al. (1996). "The Strengthening of Structural Concrete with an Aramid Woven fiber/Epoxy Resin Composites", *Proceedings of the 2nd* International Conference, ACMBS, Montreal, PQ, Canada, pp.435-442.

Detwiler, R., Kjellsen K., and Gjorv, O. (1991). "Resistance to Chloride Intrusion of Concrete Cured at Different Temperatures." ACI Materials Journal, Vol. 88, 19-24.

Fyfe, E. R., Watson, R. J. and Watson, S. C. (1996). "Long-Term Durability of Composites Based on Field Performance and Laboratory Testing." *Proceedings of the ICCI'96 Conference*, Tucson, Arizona, 982-995.

Gomez, J., and Casto, B. (1996). "Freeze Thaw Durability of Composite Materials." *Proceedings of the ICCI'96 Conference*, Tucson, Arizona, 947-955.

Guttman, H. and Sereda, P.J. (1968). "Measurement of Atmospheric Factors Affecting the Corrosion of Metals." Metal Corrosion in the Atmosphere, ASTM STP 435, ASTM.

Halstead, O'Connor, Alampalli, and Minser. (2000). "Evaluating FRP Wrap with NDT Methods." *Proceedings of the NDT Conference*.

Hyun, A. (1995). "Fire Endurance and Hose Stream Tests of Three 48" high by 56" Wide Non-Symmetrical Walls." Technical Report, Inchape Testing Services of Warnock Hersey, Inc., Pittsburgh, CA.

Kenneth, W. N. and Labossiere, P. "Fiber Composite Sheets in Cold Climate Rehab." *Concrete International*, V. 20, No. 6, June 1998, pp. 22-24.

Kestner, Harries, Pessiki, Sause, and Ricles (1997). "Rehabilitation of Reinforced Concrete Columns using Fiber Reinforced Polymer Composite Jackets." Report No. 97-07. Advanced Technology for Large Structural Systems, Lehigh University, Bethlehem, PA.

Lee, C. (1998). "Accelerated Corrosion and Repair of Reinforced Concrete Columns Using CFRP Sheets", M. Eng. Thesis, Department of Civil Eng., University of Toronto, Toronto, ON, Canada, 106 p.

Lopez-Anido, R. (1993). "Influence of Temperature on the Service Life of Rebars." Cement and Concrete Research, Vol.23, No. 5, 1130-1190.

Malek, A. and Saadatmanesh H. (1996). "Physical and Mechanical Properties of Typical Fibers and Resins." *Proceedings of the ICCI'96* Conference, Tucson, Arizona, 68-79.

Mallick, P. K. (1993). Fiber Reinforced Composites-Materials, Manufacturing and Design. Second Edition, Marcel Dekker Inc., New York, 326-327.

Mander, J. B., Priestley, M. J. N., and Park R. (1988). "Theoretical Stress-Strain Model for Confined Concrete." *Journal of Structural Engineering*, ACSE, Vol. 114, No. 8, 1804-1826.

Martin, H. and Schieles, P. (1969). "The Influence of Time and Environmental Condition on Corrosion of Deformed Bars in Cracked Concrete." *Preliminary Report of RILEM International Symposium on Durability of Concrete*, Vol. II, Prague.

Martin, H. and Schieles, P. (1969). "The Influence of Cracks on Corrosion of Steel in Concrete." *Preliminary Report of RILEM International Symposium on Durability of Concrete*, Vol. II, Prague.

McCrum, R. (1994). MDOT office memorandum to Sonny Jadun, June 22.

Mehta, P., and Monteiro, J. (1993). Concrete, structure, properties, and materials. Second Edition, Prentice-Hall, Englewood Cliffs, 160-164.

Meier, U. (1996). "Composites for structural repair and retrofitting." *Proceedings, ICCI'96 Conference*, Tucson, Arizona, 1202-1216.

Michniewicz, J. (1996). "Repair and Rehabilitation of Reinforced Concrete Columns with Fiber-Reinforced Plastics", *M. Eng. Thesis*, Department of Civil Eng., University of Toronto, Toronto, ON, Canada, 97 p.

Murphy, K., Zhang, S., and Karbhari, V. M. (1999). "Effect of Concrete Based Alkaline Solutions on Short Term Response of Composites." *Proceeding of the 44th International SAMPE Symposium*, May 23-27.

Neter, J., Wasserman, W., and Whitmore, G.A. (1992). Applied Statistics, 4th Edition, Allyn and Bacon, Boston, MA.

Nilson A. and Winter G. (1991). *Design of Concrete Structures*. Eleventh Edition, McGraw-Hill, New York, New York.

Pantazopolou et al. (1996). "Repair of Corrosion-Damaged Concrete Using ACM", *Proceedings of the 2nd International Conference, ACMBE*, Montreal, PQ, Canada, pp.287-298.

Picher, F., Rochette, P., and Labossiere, P. (1996). "Confinement of Concrete Cylinders with CFRP." *Proceedings of the ICCI'96 Conference*, Tucson, Arizona, 829-841.

Pigeon, M. and Pleau, R.(1998). *Durability of Concrete in Cold Climates*. Modern Concrete Technology Series. E & FN Spon, London, UK, 1-5.

Restrepol, J. and DeVino, B. (1996). "Enhancement of the Axial Load Carrying Capacity of Reinforced Concrete Columns by means Fiberglass Epoxy-Jackets." *Proceedings of Advanced Composite Materials in Bridges and Structures II*, Montreal, August, 547-553.

Richart F. E., Brandtzaeg A, and Brown R. L. (1928). "A Study of the Failure of Concrete under Combined Compressive Stresses." University of ILL. Eng Exp. Stn. Bull 185.

Rivera, J. and Karbhari, V. (1999). Effects of Extended Freeze-Thaw exposure on Composite Wrapped Concrete Cylinders." *Proceedings of the 44th SAMPE Symposium*, May 23-27.

Rochette, P. and Labossiere, P. (1996). "A Plasticity Approach for Concrete Columns Confined with Composite Materials". *Proceedings of the 2nd International Conference, ACMBS*, Montreal, PQ, Canada, pp.359-366.

Sen, R., Mariscal, D., and Shahaway M. (1993). "Durability of Fiberglass Pretensioned Beams." ACI Structural Journal, Vol. 90, 525-533.

Sen, R., Mariscal, D., and Shahaway M. (1993). "Investigations of S_2 Glass Epoxy Strands in Concrete." Proceedings of the FRP Components Structures, International Symposium, 15-33.

Steckel, G. (2000). Personal Communication, The Aerospace Corporation, El Segundo, CA.

Tarricone P. (1995). "Composite Sketch." Civil Engineering Magazine, May, 52-55.

Toutanji, H. and Balaguru, P. (1998). "Durability Characteristics of Concrete Columns Wrapped with FRP Tow Sheets." *Journal of Materials in Civil Engineering*, February, 52-57.

Wrobel, P. (1994). "Laboratory Measurements of Corrosion Activity of Steel Reinforcement in Concrete using Simple Equipment." *Cement, Concrete, and Aggregates, CCAGPD*, Vol. 16, No. 2, Dec. 1994, 100-103.

www.corrosionsource.com (2000).

Yamato, T., Emoto, Y., and Soeda, M. (1987). "Freezing and Thawing Resistance of Concrete Containing Chloride." *Concrete Durability*, ACI SP100-50, Vol. 1, 901-917.

Appendix A

Aerospace Corporation's FRP Panel Environmental Durability Data

Fyfe Company E-Glass/Epoxy SEH 51/Tyfo S Epoxy

				O ZPONJ			
ENVIRONMENTAL EXPOSURE	YOUNG'S MODULUS, msi	TENSILE STRENGTH, ksi	FAILURE STRAIN, %	SHORT BEAM SHEAR STRENGTH, ksi	GLASS TRANSITION TEMP., °C	HARDNESS, SHORE D	WEIGHT CHANGE, %
CONTROL	3.96 ± 0.13	80.5 ± 5.1	2.10 ± 0.18	5.9 ± 0.5	65, 64, 68, 68	83 ± 3	
100% HUMIDITY/38°C							
1000 Hour	4.04 ± 0.13	71.6 ± 2.8	1.82 ± 0.08	6.0 ± 0.4	72	83 ± 2	0.56
3000 Hour	3.94 <u>+</u> 0.10	67.9 ± 1.9	1.77 ± 0.05	5.8 ± 0.3	73	84 ± 2	0.82
10,000 Hour	3.93 ± 0.18	51.4 ± 2.1	1.31 ± 0.08	4.5 ± 0.3	73	82 ± 2	1.09
SALT WATER							
1000 Hour	4.03 ± 0.09	80.8 ± 2.2	2.07 ± 0.06	6.0 ± 0.9	65	85 ± 2	0.46
3000 Hour	4.02 ± 0.04	81.7 ± 1.2	2.09 ± 0.03	5.6 ± 0.2	63	84 ± 3	0.57
10,000 Hour	4.09 ± 0.07	66.0 ± 1.9	1.64 ± 0.04	4.6 ± 0.2	63	82 ± 2	0.91
pH 9.5 CaCO ₃ SOLUTION							
1000 Hour	3.85 ± 0.03	83.2 ± 2.8	2.25 ± 0.11	5.9 ± 0.3	65	83 ± 2	0.36
3000 Hour	4.00 ± 0.13	80.8 ± 4.1	2.11 <u>+</u> 0.11	6.0 ± 0.3	61	85 ± 2	0.53
10,000 Hour	3.88 ± 0.06	62.4 ± 2.5	1.63 ± 0.08	5.1 ± 0.3	64	84 ± 2	0.88
DRY HEAT AT 60°C							
1000 Hour	3.89 ± 0.06	82.0 ± 1.7	2.17 ± 0.08	6.4 ± 0.4	95	85 ± 2	-0.33
3000 Hour	4.05 ± 0.06	84.8 ± 2.4	2.16 ± 0.09	6.7 ± 0.8	87	85 ± 2	-0.44
20 FREEZE/THAW CYCLES	4.02 ± 0.06	78.0 ± 2.1	2.00 ± 0.06	5.2 ± 0.3	68	82 ± 3	0.59
UV/CONDENSAT ION, 100 CYCLES	4.03 ± 0.08	84.0 ± 3.1	2.18 ± 0.11	6.5 ± 0.2	86	83 ± 3	-0.42
DIESEL FUEL, 4 Hour	4.01 ± 0.06	83.4 ± 2.6	2.16 <u>+</u> 0.06	5.9 ± 0.2	67	81 ± 2	

Master Builders "MBRACE" Carbon/Epoxy CF-130/MBI Epoxy

ENVIRONMENTAL EXPOSURE	YOUNG'S MODULUS , msi	TENSILE STRENGTH, ksi	FAILURE STRAIN, %	SHORT BEAM SHEAR STRENGTH, ksi	GLASS TRANSITION TEMP., °C	HARDNESS, SHORE D	WEIGHT CHANGE, % (2 PLY/6 PLY)
CONTROL	32.8 ± 1.8	636 ± 27	1.75 <u>+</u> 0.09	7.8 ± 0.3	67, 67, 67, 70	92 ± 2	
100 <i>%</i> HUMIDITY/3 8° C							
1000 Hour	34.0 ± 1.4	591 ± 25	1.59 ± 0.08	7.6 ± 0.1	75	91 <u>+</u> 1	1.13/0.95
3000 Hour	33.2 ± 0.4	540 ± 17	1.51 ± 0.06	7.2 ± 0.1	74	92 ± 1	1.41/1.03
10,000 Hour	33.1 ± 0.8	596 ± 22	1.67 ± 0.07	6.9 ± 0.2	70	93 ± 2	1.51/1.46
SALT WATER							
1000 Hour	33.6 ± 0.5	619 ± 25	1.70 ± 0.05	7.5 ± 0.2	65	90 ± 3	1.14/0.65
3000 Hour	33.9 <u>+</u> 1.1	623 ± 23	1.74 <u>+</u> 0.07	7.6 ± 0.4	65	91 <u>+</u> 2	1.24/0.88
10,000 Hour	32.1 ± 1.6	610 ± 23	1.75 ± 0.08	6.8 ± 0.1	63	91 ± 3	1.48/1.37
pH 9.5 CaCO ₃ SOLUTION							
1000 Hour	32.9 ± 1.3	597 ± 27	1.70 ± 0.11	7.6 ± 0.1	65	92 ± 1	1.24/0.44
3000 Hour	31.8 ± 0.8	585 ± 35	1.70 ± 0.09	7.2 ± 0.6	67	91 ± 2	1.27/1.02
10,000 Hour	33.1 ± 1.5	615 ± 39	1.70 ± 0.12	6.7 ± 0.2	62	92 ± 1	1.31/0.78
DRY HEAT AT 60°C							
1000 Hour	33.4 ± 1.2	637 ± 23	1.73 ± 0.08	9.5 ± 0.2	84	94 ± 1	-0.47/-0.20
3000 Hour	32.6 ± 0.9	582 <u>+</u> 12	1.67 <u>+</u> 0.05	8.6 ± 0.4	85	93 ± 1	- /-0.33
20 FREEZE/THAW CYCLES	33.3 ± 1.7	561 ± 29	1.57 ± 0.06	7.5 ± 0.1	72	91 ± 1	1.32/0.97
UV/CONDENSAT ION, 100 CYCLES	33.6 ± 1.2	644 ± 37	1.76 ± 0.09	8.4 ± 0.3	79	91 ± 2	-0.63/-0.33
DIESEL FUEL, 4 Hour	34.1 ± 1.5	589 ± 9	1.61 ± 0.08	8.2 ± 0.1	66	93 ± 3	0.02/0.00

Appendix B: Calculation Details

B.1 Strain in Column Wrap After 10 years

1. Geometric and Material Properties

Column diameter, D = 91.44 cmColumn area, $A_c = 6563.60 \text{ cm}^2$ Initial volume of col. = A_c (100 cm) = 656360 cm³ Core diameter = $d_c = 80.01 \text{ cm}$ Longitudinal steel Ratio, $\rho = 2\%$ Steel area, $A_s = \rho$ $A_c = 131.27 \text{ cm}^2$ Tie steel diameter, d = 1.27 cm

Tie steel diameter, d = 1.27 cm Tie steel cross sectional area: $A_{sp} = \frac{\pi d^2}{4} = 1.266$ cm² Tie Spacing = 30.48 cm

Volume of rust / volume of corroded steel = 6

2. Rust Volume

Corrosion rate for steel rebar (deformed) = 5% Corroded steel area, $A_{crd s} = 0.05 A_s = 6.56 \text{ cm}^2$ Rust area, $A_{rust} = 6 A_{crd s} = 39.38 \text{ cm}^2$ Rust Volume, $V_{rust} = A_{rust}$ (100 cm) = 3938 cm³ Corroded rate for ties (smooth steel) = 20% Corroded tie steel area, $A_{crd,tie} = 0.2 A_{sp} = 0.2532 \text{ cm}^2$ Rust area spiral steel, $A_{rust,tie} = 6A_{crd,tie} = 6 (0.2532) = 1.519 \text{ cm}^2$ Rust volume tie steel, $V_{rust,tie} = A_{rust,tie}$ (length of tie) = 1.519 πd_c 100/30.48 = 1252.0 cm³

3. Strain in Wrap

Change of volume in vertical steel: Chg. $V_{st} = \frac{5}{6}V_{rust} = \frac{5}{6}(3938) = 3281.66 \text{ cm}^3$

Change of volume in tie steel: Chg. $V_{sp} = \frac{5}{6}V_{rust-tie} = \frac{5}{6}(1252) = 1043.33 \text{ cm}^3$

Final column volume: Final V = Initial column volume +Chg. V_{st} +Chg. V_{sp} = 656360 + 3281.66 + 1043.33 = 660684.99 cm³

Final column diameter: $V_{final} = \frac{\pi (D_{final})^2}{4} 100$ $D_{final} = 91.74 \text{ cm}$

Strain generated in wrap:

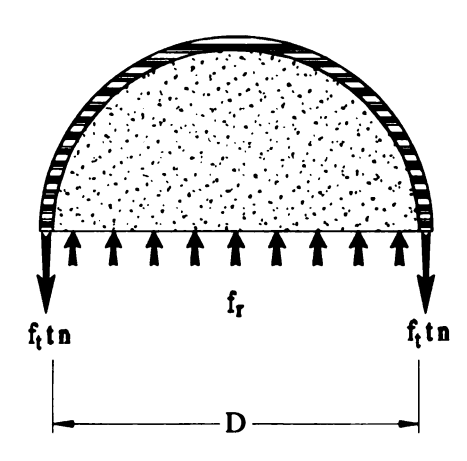
Strain =
$$\frac{D_{final} - D_{initial}}{D_{initial}} \approx .327 \%$$

B.2 Confining Pressure and Strain in Steel Jacket

Confining Pressure

From mechanics of thin walled cylinders, the confining pressure can be determined to be equal to:

$$f_r = 2 (f_t t n) / D = 2 (E \varepsilon_t t n) / D$$



For glass FRP,

$$f_r = 2 (22011 \times 0.00531 \times 0.1227 \times 3) / 15.24 =$$
5.645 MPa

where:

t =the thickness of the wrap per layer = 0.127 cm

 f_t = the circumferential stress of wrap

n = number of wrap layers = 3

D = the dia. of the concrete cylindrical column = 15.24 cm

E = modulus of elasticity of the wrap (glass/epoxy) = 22011 MPa

 ε_i = wrap strain = 0.531

Strain in Steel Jacket

$$f_r D = 2 f_{st} t_{st}$$

$$f_{st} = (f_r D) / (2 t_{st})$$

$$\varepsilon_{st} = f_{st} / E_{st} = (f_r D) / (2 t_{st} E_{st})$$

$$= (5.645 \times 15.24) / (2 \times 0.477 \times 200100) = 0.045\%$$

where

```
f_r = the confining pressure generating the strain in the jacket = 5.645 MPa d = diameter of steel jacket = 15.24 cm f_{st} = stress in steel jacket E_{st} = modulus of elasticity of steel jacket = 200100 MPa t_{st} = thickness of steel jacket =0.477 cm \varepsilon_{st} = strain in steel jacket
```

Appendix C: Spacimen, Bar and Gage Numbering

Table C.1 Specimen and gage numbering for freeze-thaw test

Freeze Thaw						
Spe	cimen Ty	ре	Specimen Number	Gogo Number		
Shape	Wrap	Cycle	Specimen Number	Gage Number		
		300	1	1		
				2		
- o			300	2	3	
5				· · · · · · · · · · · · · · · · · · ·	4	
Round	0	3	5 6			
				7		
<u>%</u>	300	4	8			
	Glass			9		
9	300	5	10			
				11		
<u>g</u>		300	6	12		
Square			7	13		
		0	7	14		
		300	8	15		
		300	0	16		
		300	9	17		
	Round	000		18		
Round		300 10	19			
			20			
		0 11		21		
				22		
	ç	300	12	23		
	မို့ ၂	_		24		
	Carbon	300	13	25		
	_			26		
உ		300	14	27		
Square				28 29		
Š		0	15	30		
				31		
		300	16	32		
Round	Plain	300	17, 18, 19	-		
Round	Glass	150	20, 21, 22	_		
Square	Glass	150	23, 34, 25	-		
Round	Carbon	150	26, 27, 28	-		
Square	Carbon	150	29, 30, 31	-		
Round	Plain	150	32, 33, 34	-		
Round	Glass	0	3, 35, 36, 37, 38, 39	-		
Square	Glass	0	7, 40, 41, 42, 43, 44	-		
Round	Carbon	0	11, 45, 46, 47, 48, 49	-		
Square	Carbon	0	15, 50, 51, 52, 53, 54	-		
Round	Plain	0	55, 56, 57, 58, 59, 60	-		

Table C.2 Specimen, bar and gage numbering for accelerated corrosion test

Specim	en Type	Specimen Number	Bar Number [†]	Gage Number
Wrap	Bonded	Specimen Number		
	Yes	1	9	1
			11	2
	Yes	2	17	3
		<u> </u>	19	4
	No	3	25	5*
	140		27	6*
	No	4	42	7
	110	-	44	8
(0	Yes	5	45	9
Glass	100		47	10
<u> </u>	No	6	50	11
_	140		52	12
	Yes	7	57	13*
	168	,	59	14*
,	No	8	62	15
	NO	•	64	16
	Vaa	9	82	•
	Yes	9	84	-
	Yee	40	86	-
	Yes	10	88	-
		44	22	17*
	No	11	24	18*
		40	29	19
	Yes	12	31	20
	.,	40	33	21*
	Yes	13	35	22*
_		4.4	54	23
<u> </u>	No	14	56	24
Carbon			70	25
ü	Yes	15	72	26
			77	27
	Yes	16	79	28
			90	29
	No	17	92	30
			93	31
	No	18	95	32
			2	•
	-	19	4	•
			5	-
	-	20	7	•
			13	-
.⊑		21	15	-
Plain			38	-
<u> </u>		22	40	-
	 		66	-
		23	68	
			73	
	•	24	75	
T C-41 1	ere also num	l hanad		

Cathodes were also numbered

^{*} Gage located on the anode-others are located in between anode and cathode

Appendix D FIELD INSTALLATION OF FIBER REINFORCED PLASTIC (FRP) WRAPS ON CONCRETE COLUMNS

Materials.-The following is a list of material required for each type of composite system:

1. TYFO SHE-51 composite system (glass):

Vendor: FYFE Co.

6044 Cornerstone Court West, Suite C

San Diego, CA 92121-4730

Tel: 619-642-0694

Local Rep.: Kurt Baron

Tel: 847-706-9230

Fabric: Tyfo SEH-51

Epoxy: Tyfo-S, parts A & B Top coat: Tyfo-WS, parts A&B

Paint: Tyfo A (acrylic), or Tyfo U (polyurethane). Color:

Concrete gray

2. MBrace composite system (carbon):

Vendor: Master Builders, Inc.

23700 Chagrin Boulevard Cleveland, OH 44122 Tel: 800-MBT-9990

Local Rep.: Brad Costello

Tel: 248-683-3554

Fabric: MBrace CF130

Primer: MBrace Primer, parts A&B
Saturant: Mbrace Saturant, parts A&B
Filler: Mbrace Putty, parts A&B

Top Coat: Mbrace Top Coat. Color: Concrete gray

Construction Methods.-

Do not apply when ambient temperatures are lower than 4°C. Do not apply to wet surface or when rainfall is anticipated. Do not apply when dew point is within 3°C of the concrete surface temperature.

Do not apply when humidity is 90% or higher.

Manufacturer's representative shall be on site for initial placement. Directions of the manufacturer's representative shall be followed.

1. TYFO SEH composite system:

- A. Remove loose concrete from the column surface and fill all voids to a smooth surface using Type S-F or Type S-M patching mixture, depending on the depth of the patch. The area of the patch shall be blown out with oil-free compressed air. The cleaned area for patching shall be flushed out with clean water under pressure immediately prior to application of the patching mixture. Forming methods used to retain the patching mixture shall not leave holes in the concrete surface. The patch shall cure for at least three days prior to application of wrap. Uneven surfaces, protrusions, and sharp edges shall be ground smooth. Dust from surface grinding shall be removed by using an oil-free air blower or other suitable means.
- B. Pre-cut desired number of layers of fabric to a length exceeding the column perimeter by at least 150 mm. Off site labor shall be used where possible. An overlap of 150 mm shall be provided in the fiber direction when terminating the wrap.
- C. Round or bevel corners by grinding to a radius of at least 20 mm.
- D. The concrete surface shall be free of any moisture at the time of application.
- E. Mix parts A and B of Tyfo-S epoxy at a ratio of 100:42 by volume (or 100:34.5 by weight) with a tolerance of 10%. Stir with a mechanical mixer, typically 5 minutes at 400 to 600 rpm until uniformly blended. Pot life is 3 hours at 20°C and 45 minutes at 38°C.
- F. Apply one coat of Tyfo-S epoxy by brush or roller to prime the surface. Volume to be applied may vary depending on the porosity of the concrete surface. Wait 2 to 4 hours and then apply wrap (as described below) while primer is still tacky.
- G. Tyfo-S epoxy shall be applied to TYFO fabric as follows:

- (1) Place dry fabric sheets in a saturation bath and add epoxy. Work epoxy into fabric using gloved hands, a paint roller, or similar tool. Alternatively, an automatic saturating machine may be used.
- (2) After the fabric has been completely saturated (both sides), remove excess epoxy by squeegying it out with a plastic trowel or by blotting the excess resin with the next dry fabric to be saturated.
- (3) Use a PVC pipe to spool the saturated fabric prior to wrapping column.
- H. The fabric shall be placed on the column entirely by hand assuring a smooth, uniform, mat finish. The (white) glass fibers shall be oriented horizontally. The (yellow) Kevlar fibers will then be oriented vertically. Pull the layer so that it is taut and free of bubbles. A lap length of at least 150 mm is required in the fiber longitudinal direction when terminating the layer.
- I. Apply additional layers while the wrapped column surface is still tacky to the touch, ensuring that overlaps are staggered.
- J. Mix parts A and B of Tyfo-WS epoxy at ratio of 100:42 by volume (or 100:34.5 by weight) with a tolerance of 10%.
- K. Apply final coat of Tyfo-WS top coat with a minimum thickness of 0.4 mm. Epoxy shall be tacky to touch before final coat is applied.
- L. The system shall be protected from damage, debris, and moisture during the initial curing period of 24 hours. Final curing is completed in 72 hours.
- M. Apply finish of two coats of Tyfo A or Tyfo U paint with a minimum thickness of 0.1 mm per coat.

2. MBrace composite system

A. Remove loose concrete from the column surface and fill all voids to a smooth surface using Type S-F or Type S-M patching mixture, depending on the depth of the patch. The area of the patch shall be blown out with oil-free compressed air. The cleaned area for patching shall be flushed out with clean water under pressure immediately prior to application of the patching mixture. Forming methods used to retain the patching mixture shall not leave holes in the concrete surface. Uneven surfaces to receive FRP shall be filled with Type S-F mixture or other approved material. Surface irregularities must be rounded and smoothed to less than 1 mm using a grinder. Dust from surface grinding shall be removed by using an oil free air blower or other

suitable means.

- B. Pre-cut desired number of layers of fabric to a length exceeding the column perimeter by at least 100 mm. Off site labor shall be used where possible. An overlap of 100 mm shall be provided in the fiber direction when terminating the wrap. The length of the carbon sheet should preferably be less than 3 m for manageability.
- C. Round or bevel corners by grinding to a radius of at least 13 mm.
- D. The concrete surface shall be free of any moisture at the time of application.
- E. Mix parts A and B of the primer at a ratio of 3:1 by volume (or 100:30 by weight). Stir with a mechanical mixer for at least 3 minutes at 400 to 600 rpm until uniformly blended. Pot life of the epoxy is approximately one-half to one hour after mixing.
- F. Prime the concrete surface with the primer using a brush or a roller at a rate of 0.25 to 0.4 kg/m². Volume to be applied may vary depending on the porosity of the concrete surface.
- G. Mix parts A and B of the filler at a ratio of 3:1 by volume (or 100:30 by weight).
- H. Apply filler to primed surface preferably within 1 or 2 days of, and no more than one week after, applying the primer. The filler may be applied immediately after applying the primer. Applying the filler is optional.
- I. Wait 2 to 4 hours before mixing and applying the saturant. The surface must be tacky to touch when applying the saturant, otherwise it must be roughened using sandpaper. If sandpaper is used, then the surface shall be cleaned using an air blower before applying the saturant.
- J. Mix parts A and B of the saturant at a ratio of 3:1 by volume (or 100:34 by weight). Pot life of the saturant is approximately one-half to one hour.
- K. Apply one coat of the saturant to primed surface using a medium nap (9.5 mm) roller at a rate of 0.25 to 0.4 kg/m².
- L. Place carbon sheet on a flat horizontal surface so that the backing paper is on top, smooth down by hand and peel away backing paper, and then wrap the sheet around the column. The surface that originally

contained the backing paper shall be placed against the column and the fibers shall be oriented horizontally (i.e., the corners containing the obtuse angles of the diamond stitch pattern shall be aligned horizontally).

- M. Squeeze the surface of adhered carbon sheet in the fiber direction in order to impregnate the saturant into the sheet. Remove excess epoxy by squeegying it out with a plastic trowel (without sharp edges) and roll out bubbles.
- N. Apply additional saturant over the bonded carbon sheet at the overlap.
- O. Wait a minimum of 30 minutes and then roll on an overcoat of saturant. (This is done for each layer.)
- P. Repeat saturant mixing and rolling for consecutive carbon sheets, waiting 1 to 2 hours after applying each layer. Apply while previous coat of saturant is tacky to touch and stagger wrap overlaps for each layer.
- Q. The system shall be protected from damage, debris, and moisture during the curing period of not less than 24 hours.
- R. Apply finish of two coats of Mbrace Top Coat using a 10 mm nap roller at a rate of 4.9 m²/liter per coat.

